EVALUATION OF STRATEGIES FOR ESTIMATING RESIDUAL NEUTRAL-ATMOSPHERE PROPAGATION DELAY IN HIGH PRECISION GLOBAL POSITIONING SYSTEM DATA ANALYSIS

A. D. VAN DER WAL

November 1995

EVALUATION OF STRATEGIES FOR ESTIMATING RESIDUAL NEUTRAL-ATMOSPHERE PROPAGATION DELAY IN HIGH PRECISION GLOBAL POSITIONING SYSTEM DATA ANALYSIS

Anthony D. van der Wal

Department of Geodesy and Geomatics Engineering
University of New Brunswick
P.O. Box 4400
Fredericton, N.B.
Canada
E3B 5A3

November 1995

PREFACE

In order to make our extensive series of technical reports more readily available, we have scanned the old master copies and produced electronic versions in Portable Document Format. The quality of the images varies depending on the quality of the originals. The images have not been converted to searchable text.

PREFACE

This technical report is a reproduction of a thesis submitted in partial fulfillment of the requirements for the degree of Master of Science in Engineering in the Department of Geodesy and Geomatics Engineering, September 1995. The research was supervised by Dr. Richard B. Langley, and funding was provided partially by the Natural Sciences and Engineering Research Council of Canada, and partially by the University of New Brunswick.

As with any copyrighted material, permission to reprint or quote extensively from this report must be received from the author. The citation to this work should appear as follows:

ABSTRACT

The research described in this thesis compares and evaluates techniques for the estimation of residual neutral-atmosphere propagation delay of Global Positioning System (GPS) measurements in high precision geodetic relative positioning applications. Three techniques were analysed: (1) a conventional weighted least squares adjustment, (2) a sequential weighted least squares adjustment, and (3) Kalman filtering.

The University of New Brunswick's DIfferential POsitioning Program (DIPOP) package was extensively modified to estimate residual neutral-atmosphere delay parameters for the three techniques under investigation. A data set of five baselines of regional length, 50 to 700 km, was analysed with the new DIPOP software. Ten days of data were analysed to determine the sensitivity of baseline component estimates to a priori constraints, and to provide an estimate of the precision and accuracy of the three techniques. Short-term repeatability of estimated baseline components was investigated as a gauge of precision. As a gauge of accuracy, estimated baseline components were compared with the International Earth Rotation Service (IERS) Terrestrial Reference Frame of 1993 (ITRF93). Particular attention was given to the vertical component of the baselines, since the vertical component of a GPS geodetic baseline is up to three times more sensitive to residual neutral-atmosphere delay than the horizontal components.

Mapping the repeatability of the estimated baseline components against a priori constraints showed that baseline component estimates are significantly sensitive to the initial constraints placed on the estimated residual delay parameters. The three techniques are capable of estimating geodetic parameters at approximately the same level of accuracy and precision. The sequential weighted least squares approach was found to be equivalent to the Kalman filtering approach for estimating residual delays when the random walk model was used to characterise the delay variability. However, the

equivalence breaks down when a stochastic process with time correlated states is used in the sequential weighted least squares technique.

The precision analysis revealed: (1) baseline component estimates are significantly sensitive to the a priori constraints placed on the estimated delay parameters; (2) the three techniques are capable of operating at the same level of precision; (3) empirical determination (sensitivity testing) of the stochastic process coefficients and constraints for the least squares residual delay parameters is necessary due to a lack of correlation between optimal residual delay parameter coefficients and baseline vector components; (4) precision for the conventional weighted least squares case ranged in magnitude from 5.6 mm to 13.0 mm in the height component, and 2.4 mm to 9.5 mm in the length component; (5) precision for the Kalman filter Gauss-Markov case ranged in magnitude from 5.8 mm to 9.8 mm in the height component, and 2.4 mm to 9.0 mm in the length component; and (6) precision for the Kalman filter random walk case ranged in magnitude from 5.9 mm to 10.1 mm in the height component, and 2.4 mm to 9.6 mm in the length component. The accuracy assessment revealed: (1) the three techniques are capable of estimating baseline components at approximately the same level of accuracy; (2) two of the five estimated baseline vectors agree well (within a factor of 2 times their short-term repeatability) in terms of height and length with the ITRF93 coordinates; (3) three of the five baseline vectors showed large height discrepancies (of the order of 4 to 9 cm); however, they agree well in the length component estimates.

TABLE OF CONTENTS

LIST OF TABLES

LIST OF FIGURES

ACKNOWLEDGEMENTS

CHAPTER 1

INTRODUCTION

The research discussed in this thesis evaluates the precision and accuracy of three estimation techniques for the reduction of residual neutral-atmosphere delay in Global Positioning System (GPS) measurements used in the determination of high precision geodetic baseline components. Residual neutral-atmosphere delay is one of the dominant error sources in high precision GPS geodetic baseline estimation of regional scale (50 to 1000 km). Neutral-atmosphere delay of GPS signals is a non-dispersive phenomenon arising from the delay and bending of GPS radio waves due to the non-ionised, or electrically-neutral, atmosphere. The term "troposphere" is commonly used in the space geodetic community as a substitute for the "electrically-neutral-atmosphere" which consists mainly of the troposphere and stratosphere; this is due to the troposphere contributing the bulk of the delay induced by the electrically-neutral-atmosphere. Of the total neutral-atmosphere delay the troposphere accounts for up to approximately 75% of the delay, the stratosphere for approximately 25% of the delay, and the atmosphere above the stratosphere for less than 0.01% of the delay (figures are based on standard atmosphere pressures from the *U.S. Standard Atmosphere, 1976*", tropopause height of 10 km, and no water vapour above the tropopause).

The neutral-atmosphere is one of the dominating sources of residual error in high precision relative GPS positioning [Delikaraoglou, 1989; Dixon, 1991; and Blewitt, 1993]. The neutral-atmosphere delay consists of two components: (1) a wet delay component, which is dependent on water vapour, and has an influence on signal propagation at the 10 cm level in the observer's zenith; and (2) a hydrostatic delay component, which is dependent mainly on surface air pressure, and has an influence on signal propagation at the 2.3 m level in the observer's zenith. The hydrostatic component has a smooth, slowly time-varying characteristic due to its dependence on variations in surface air pressure (weather cells). The wet component delay has a random, relatively rapidly varying characteristic due to its dependence

on water vapour pressure which is strongly influenced by small to large scale turbulence. The delays need to be removed with a high degree of certainty in high precision relative GPS positioning, due to the strong influence of errors due to the neutral atmosphere especially on the vertical component of baselines [Blewitt, 1993; Yunck, 1993].

There are three methods for reducing the detrimental effects of neutral-atmosphere delay on GPS measurements: (1) prediction, where theoretical models that predict the delay are used; (2) calibration, where equipment such as water vapour radiometers (WVRs) are used to independently determine the wet delay; and (3) estimation, where the total, or residual, delay is estimated along with geodetic parameters in an adjustment of GPS observations. The theoretical models are not at the level of precision or accuracy required for high precision relative positioning activities of regional extent. WVRs are complex and expensive to operate. This thesis focuses on the estimation of the delay -- a relatively accurate, precise, and inexpensive method. The effect of estimating residual neutral-atmosphere delay on GPS post-fit observation residuals is depicted in Figure 1.1. Low elevation angle observations are most subject to inaccuracies in prediction models and mapping functions; hence, in the top panel of Figure 1.1 the residuals show systematic trends towards the ends of the observation segments. In the lower two panels, where the residual neutral-atmosphere delay has been estimated, the systematic trends are reduced. Ignoring estimation significantly increases the magnitude of post-fit observation residual scatter by up to 50% .

Three estimation methods have been investigated in this research; they are: (1) conventional weighted least squares, (2) sequential weighted least squares, and (3) Kalman filtering. The conventional weighted least squares approach uses one or more neutral-atmosphere delay parameters per site and observation session to mimic the spatial and temporal variations of the delay. The sequential weighted least squares method models the delay parameters as stochastic processes by adding process

2

noise to the system of equations being solved. The Kalman filter approach also models the delay

parameters as stochastic processes.
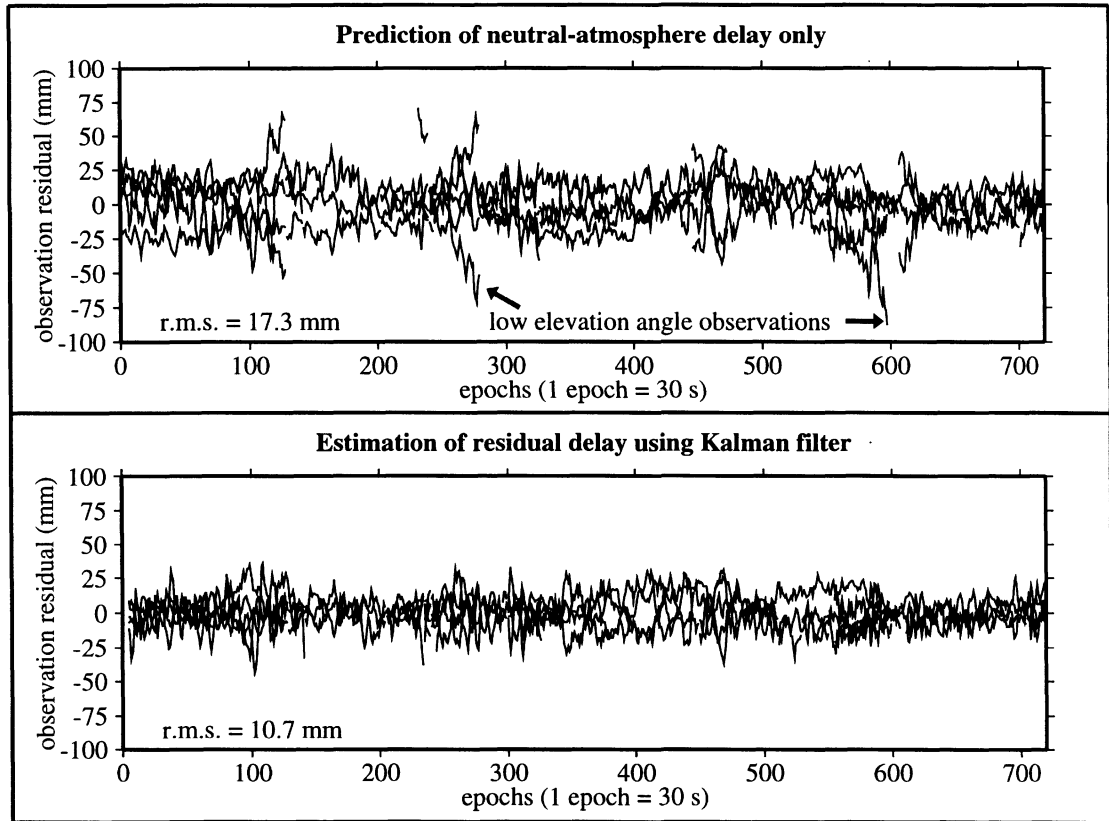
Figure 1.1 -- Post-fit observation residuals showing the effect of ignoring (top panel) and estimating residual neutral-atmosphere delay parameters (lower panel). An approximately 50% decrease in the scatter of the residuals is evident for the estimation case.

Figure 1.2 compares, in a graphical way, the conventional weighted least squares and filtering

approaches to estimating the residual neutral-atmosphere delay. For the conventional weighted least

squares case, the delay is modelled with three individual parameters whereas the filter uses a single

stochastic state at each station. Of interest in this diagram is the effect of constraints on the residual

delay parameters, in this case the a priori constraints were at the 10 mm level. Notice how within the

first approximately 100 epochs the estimates of residual delay have not reached a steady value. These

two contrasting methods, piecewise constant and smoothly varying, of estimating the residual delay
have been evaluated in this research.
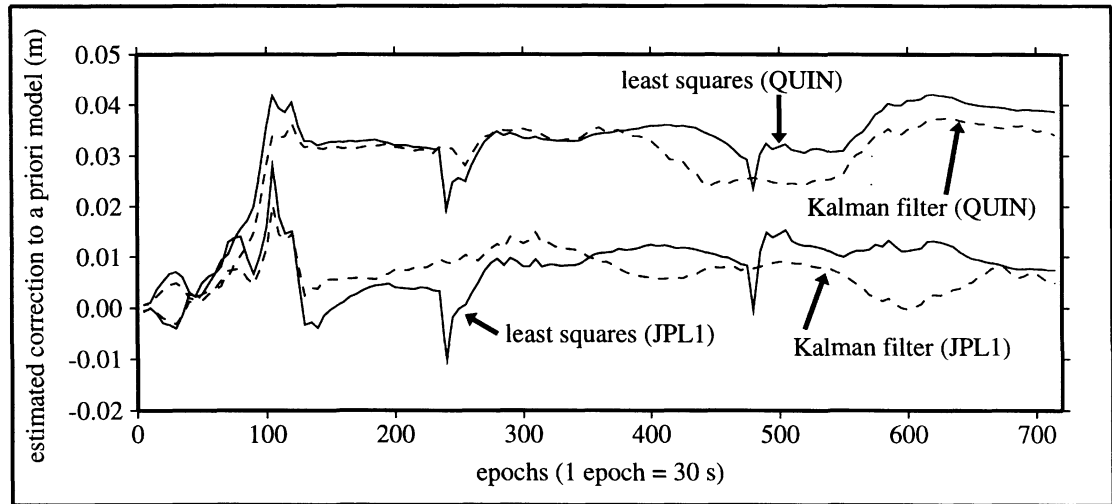
Figure 1.2--Time series (for sites JPL1 and QUIN) showing a conventional weighted least squares and Kalman filtering estimation of residual neutral-atmosphere delay. The time series are estimated neutral-atmosphere delay corrections to model predictions. Three delay parameters were estimated in the conventional weighted least squares approach.

1.1 Motivation

The role of GPS has changed from auxiliary geodetic equipment to an almost indispensable geodetic tool in recent times. One of the main reasons for this change in status of GPS is the improvement in precision of geodetic baseline estimates. Approximately three orders of magnitude improvement in the precision of estimated baseline components has been witnessed in the last decade [Blewitt, 1993]. Many of the advances have been made in the area of GPS observation error models. One of the dominant limiting factors to high precision baseline component estimation is the error modelling of residual neutral-atmosphere delay. This is a topic that still requires investigation to further improve the utility of GPS for high precision relative positioning.

The importance of estimating neutral-atmosphere delay for geodetic GPS observations is highlighted by residual neutral-atmosphere delay affecting mainly the vertical component of baseline estimates (see for example Yunck [1993]). For example, in the course of this research, estimating the residual neutral-atmosphere delay changed a height component estimate of a particular baseline by approximately 18 cm as compared to its estimate when using only prediction methods to account for the delay. Residual delay estimates can easily reach the 4 to 5 cm level, see for example Figure 1.2. Geodetic baseline estimates derived from GPS observations are, unfortunately, inherently weak in the vertical component due to the geometry of the trilateration used to determine position. The vertical component of baseline estimates is very important to many applications utilising GPS techniques (e.g. Bilham [1991]), such as: geodynamic studies of lithospheric plate motion, continuous monitoring of seismically active and hazardous regions, glacial rebound measurement, tide gauge establishment for monitoring global sea level, establishing precise orbits of earth orbiting space vehicles, and the establishment and densification of regional and national three-dimensional geodetic networks.

Theoretical neutral-atmosphere zenith delay models such as that of Saastamoinen [1973], are capable of predicting the neutral-atmosphere delay at the 2 to 3 cm level for observations in the zenith [Mendes and Langley, 1995]. When this error is propagated to observations at low elevation angles, say 15°, the prediction error can increase to approximately 8 to 12 cm. This fails to meet the stringent requirements for some geodetic and geodynamic applications. Certain applications require position rate uncertainties at the 1 to 5 mm/yr level [Dixon, 1991]. For example, monitoring lithospheric plates over thousands of kilometres with relative site velocities as small as a few centimetres per year would require longer project times given poor quality relative position estimates. Following the reasoning of Coates et al. [1985], a five year project observing every year would provide rate uncertainties of 7 mm/yr for relative position uncertainties at the 3 cm level, and 1 mm/yr for relative position uncertainties at the 5 mm level. It would take approximately an additional fifteen years of observation to reduce the rate uncertainty of the 3 cm relative position uncertainty from 7 mm/yr to 1 mm/yr.

WVRs provide reliable estimates of neutral-atmosphere delay for use in GPS relative positioning (e.g. de Jong [1991], Solheim [1993]). Estimation of neutral-atmosphere delay correction parameters has shown to be comparable in precision to WVRs (for example see Dixon et al. [1991]). However, WVRs have their limitations: they require additional equipment, and specialised analysis techniques.

Given the above background, the motivation for this research is clear. An investigation into estimation techniques for reducing the residual neutral-atmosphere delay error in high precision GPS geodetic applications will assist in providing a better understanding of their advantages, pitfalls, strengths, and sensitivities. The remainder of this chapter is devoted to a review of previous studies related to this research; a summary of contributions of this research; and a description of the following chapters of the thesis.

1.2 Previous Studies

Literature of relevance to this research can be grouped in six categories: (1) GPS theory, covering the history and description of GPS; (2) neutral-atmosphere delay of GPS signals, covering the theory of the non-dispersive phenomenon of radio signal delay and bending in the neutral-atmosphere; (3) prediction and calibration methods - two methods used to reduce the effects of neutral-atmosphere delay; (4) estimation methods, covering the theory of estimating neutral-atmosphere delay correction parameters; (5) estimation experiments, covering projects that have utilised estimation strategies for reducing residual neutral-atmosphere delay effects; and (6) comparisons of neutral-atmosphere delay estimation techniques, covering the previous studies that have looked at more than one estimation strategy in a single study.

GPS theory is covered extensively in many texts and scientific papers. A short and very incomplete list for high precision relative positioning and general GPS background information contains: Wells et

al. [1986], Lichten [1990a], Bilham [1991], Dixon [1991], Blewitt [1993], Hofmann-Wellenhof et al. [1993], Seeber [1993], and Yunck [1993]. The interested reader is referred to these papers and texts for detailed information on GPS. Of particular note are the papers by Dixon [1991], Blewitt [1993], and Yunck [1993] who review current standards in high precision geodetic, geodynamic, and geological activities using GPS relative positioning.

Neutral-atmosphere refraction of GPS signals is covered in part and in full by many authors. Excellent reviews on the principles of neutral-atmosphere delay of radio signals are presented by: Brunner [1984], Delikaraoglou [1989], de Jong [1991], Dixon [1991], Elegered [1992], Langley [1992], Trehauft [1992], Blewitt [1993], Brunner and Welsch [1993], Hofmann-Wellenhof et al. [1993], Seeber [1993], and Solheim [1993]. Dixon [1991] gives an introduction to neutral-atmosphere delay of radio waves, highlighting the 1991 state-of-the-art for reducing residual neutral-atmosphere delay effects. Langley [1992] reviews effects that the earth's ionised and non-ionised atmosphere has on radio signals in space geodetic applications. Trehauft [1992] reviews neutral-atmosphere delay in very long baseline interferometry (VLBI), which applies similarly to GPS. Elegered [1992] gives a detailed account of neutral-atmosphere delay of radio waves.

Prediction and calibration methods for neutral-atmosphere delay of radio signals includes the use of surface meteorological measurements, theoretical zenith delay models, mapping functions, and WVR. Modelling atmosphere delays is reviewed by Herring [1992], who describes the separation of the neutral atmosphere into wet and hydrostatic components. Janes et al. [1991] compare several models and mapping functions with ray traced standard atmosphere conditions. They conclude that the Saastamoinen [1973] zenith delay model in conjunction with either the Davis [1986] or Goad and Goodman [1974] mapping functions are best suited for GPS relative positioning. Mendes and Langley [1994] comprehensively compare 15 geodetic quality mapping functions, determining that the Lanyi [1984], Herring [1992], Ifadis [1986], and Neill [1993a, 1993b] mapping functions are the most reliable

for high precision relative positioning applications. Solheim [1993] gives a detailed explanation of WVRs, in particular the use of WVRs in GPS relative positioning. Trehauft [1992] also describes the WVR. He believes problems associated with WVRs are fundamental: they are due to WVRs measurement of sky brightness temperature (see section 2.4.2) and not phase or delay; hence, requiring sophisticated modelling and assumptions to get delay from power.

Estimation methods literature covers estimating neutral-atmosphere delay parameters with conventional weighted least squares or Kalman filter algorithms. Reviews of various estimation techniques are covered in: Lichten and Border [1987], Dixon and Kornreich Wolf [1990], Herring et al. [1990], Lichten [1990a], Lichten [1990b], Tralli and Lichten [1990], Elgered et al. [1991], Rothacher [1992], and Blewitt [1993]. Blewitt [1993] reviews stochastic estimation of neutral-atmosphere delay. Lichten and Border [1987] give a review, describing in functional form, the modelling of neutral-atmosphere delay as a random walk or Gauss-Markov stochastic process. Rothacher [1992] reviews conventional weighted least squares and Kalman filter techniques of estimating neutral-atmosphere delay from GPS signals. According to Yunck [1993], an alternative to these empirical methods is a physical modelling approach proposed by Trehauft [1992] based on the assumption that the wet component of the delay varies in the form of Kolmogorov turbulence. It is anticipated that given the correct a priori information, this technique can reduce the precision of baseline estimates by a factor of 2 to 3 compared to the stochastic estimation techniques. However, the selection of the a priori constraints is subject to other approximations and limitations which may prove to keep the precision level at around that of stochastic estimation.

Dixon and Kornreich Wolf [1990] give an extensive review of stochastic estimation of neutral-atmosphere delay. They investigate the sensitivity of baseline component repeatability by altering the a priori stochastic process coefficients, concluding that the use of random walk or Gauss-Markov processes to characterise the neutral-atmosphere delay variability results in equivalent baseline

component estimates. Herring et al. [1990] outline Kalman filtering used to analyse VLBI data. They also conclude that the choice of stochastic model does not influence baseline component estimates. They conclude that the Kalman filter provides superior results to those obtained through conventional weighted least squares techniques. They see a problem with mathematical estimation techniques: they are not (currently) able to account for azimuthal asymmetry in the distribution of neutral-atmosphere constituents. They also provide a detailed description of the Kalman filter algorithm and stochastic processes. Elgered et al. [1991] compare Kalman filter and WVR-assisted estimates of VLBI baselines.

Lichten [1990a] gives a comprehensive review of the Kalman filter approach to stochastic estimation of neutral-atmosphere delay. Lichten [1990b] predicts stochastic estimation techniques will achieve better than 5 mm r.m.s. delay estimates by the mid 1990s. Elgered et al. [1991] show the comparison of VLBI and WVR derived zenith delay estimates that have 6 to 10 mm r.m.s. differences over a few days. Yunck [1993] shows a similar comparison of GPS and WVR derived zenith delay estimates where an r.m.s. of 3 mm of the difference between the two types of estimates is seen after 5 hrs. Rocken et al. [1995] indicate that zenith delay estimates from GPS are at the single millimetre r.m.s. level, based on a 100 day experiment they can reliably compute precipitable water vapour (PWV) at the 1 mm r.m.s. level. PWV is directly related to the zenith neutral-atmosphere delay by a scaling factor that has a 2% accuracy. Tralli and Lichten [1990] review stochastic estimation of neutral-atmosphere delay. They investigate the sensitivity of parameter estimates to changes in a priori stochastic process coefficients. They conclude that the random walk or Gauss-Markov stochastic processes provide equivalent estimates of residual zenith neutral-atmosphere delays. They predict that GPS has the potential to resolve, in near-real-time of the order of a few minutes, zenith delay fluctuations at the centimetre level. They estimate that stochastic techniques provide 5-10 mm level accuracy of the zenith path delay.

Estimation experiments literature reviews regional size experiments where stochastic estimation of neutral-atmosphere delay has been used to improve the precision and accuracy of baseline component

estimates. Lichten and Border [1987] find successful orbit determination strategies use stochastic estimation techniques for reducing neutral-atmosphere delay effects. They find that post-fit r.m.s. scatter of observation residuals is reduced by more than 50% when stochastic neutral-atmosphere delay estimation techniques are used. Tralli and Dixon [1988] use GPS relative positioning for a campaign in southern California with 350 to 650 km baseline lengths. They find that using WVR and stochastic estimation of neutral-atmosphere delays provides short-term repeatability at the few parts in 10^8 level. By comparison with WVR, they find accuracy at the few parts in 10^7 level. Dixon and Kornreich Wolf [1990] look at data from a South American campaign using WVRs and several stochastic estimation techniques. They conclude both approaches provide centimetre level precision, and equivalent estimates of wet neutral-atmosphere delay. Importantly, they conclude [Dixon and Kornreich Wolf, 1990; p. 203]: "...WVR calibration is not critical for obtaining high precision results with GPS in the CASA region..." when estimating the neutral-atmosphere delay as a random process. The Northern-Caribbean plate boundary was first surveyed using GPS in 1986 by Dixon et al. [1991]. Geodetic baselines, 170 to 1260 km in length, were analysed, resulting in short-term repeatability of baseline length of 8 mm plus 1.3 parts in 10^8. Larson and Agnew [1991] assessed precision and accuracy of GPS derived baselines in California, 50-450 km in length, over a three year period. Stochastic estimation of neutral-atmosphere delays using a random walk stochastic process was performed. They conclude that GPS is comparable in precision and rate (relative velocity of receiver locations) accuracy with VLBI.

Comparisons of neutral-atmosphere delay estimation techniques looks at experiments that have compared more than one neutral-atmosphere delay estimation strategy, or looked at more than one technique for using a particular estimation strategy. Lichten and Border [1987] compared various Kalman filter strategies using random walk and Gauss-Markov processes. They have assessed various a priori coefficient scenarios deciding upon the random walk process as the "...best as judged by baseline and orbit repeatability." [Lichten and Border, 1987, p. 12757]. Rothacher [1992] looked at simulated neutral-atmosphere effects on orbit determination. He also studied different approaches to neutral-

atmosphere delay estimation. He theorises that estimating one neutral-atmosphere correction term per epoch in a conventional weighted least squares adjustment is equivalent to the stochastic techniques. He questions the reality of neutral-atmosphere delay estimates, citing correlation between neutral-atmosphere delay estimates and changes in satellite sky distribution as being peculiar.

Lindqwister et al. [1990] searched for an optimal stochastic model and elevation mask angle by analysing data from a North American network of GPS receivers. They conclude that a 15° elevation data mask angle coupled with either a random walk or Gauss-Markov stochastic process provides optimum results. They report agreement with VLBI baseline estimates at the 1 to 2 cm level, and precision (short-term repeatability) of 5 mm vertically and 3 to 4 mm horizontally. Tralli and Lichten [1990] conclude that random walk and Gauss-Markov processes used to describe the time varying behaviour of neutral-atmosphere delays provide baseline component estimate repeatability at the few parts in 10^8 level. They suggest that surface meteorological values are not necessary when estimating neutral-atmosphere delays for non-extreme meteorological conditions. Dixon et al. [1991] compared stochastic estimation, constant parameter estimation, and no estimation of neutral-atmosphere delay. They showed, for two baselines, approximately 250 km in length, that stochastic techniques are up to 3 times more precise than the other methods.

Brunner and Tregoning [1994a] investigated inconclusively the estimation of different numbers of neutral-atmosphere delay parameters. Brunner and Tregoning [1994b] conclude that high quality surface meteorological observations are not necessary if stochastic estimation techniques are used for the neutral-atmosphere delay. Gurtner et al. [1994] compare stochastic estimation of neutral-atmosphere delay with surface meteorological measurements from the International GPS Service for Geodynamics (IGS) global network and also conclude that surface meteorological measurements do not improve GPS baseline estimates when stochastic estimation techniques are applied to the neutral-atmosphere delay.

As can be seen from the above review of current literature, there is sufficient need for a study on the use of estimating neutral-atmosphere delay parameters in high precision geodetic GPS applications. Many studies have been done on individual estimation techniques, such as those of Lichten and Border [1987], Dixon et al. [1991], Tralli and Lichten [1991], Lindqwister [1990], and Brunner and Tregoning [1994a, 1994b]; however, none have compared in a systematic manner the three techniques evaluated in this thesis. Rothacher [1992] evaluates more than one technique: Kalman filtering and conventional weighted least squares. However, his research was not specifically oriented towards this idea, and subsequently the evaluation was brief and fairly inconclusive on this topic.

It is apparent from the literature review that estimation, of any kind, of neutral-atmosphere delay is preferable to prediction for precision and accuracy, and preferable to calibration for cost and simplicity. It is also apparent that recording surface meteorological observations is apparently not advantageous when estimating neutral-atmosphere delay (e.g. Gurtner et al. [1994]; Brunner and Tregoning, [1994b]). These arguments give weight to the estimation of neutral-atmosphere delay as an indispensable method of reducing the detrimental effects of the neutral-atmosphere on high precision GPS observations.

1.3 Contributions of Thesis

The evaluation of three techniques used to estimate residual neutral-atmosphere delay in high precision GPS data has been accomplished. The three approaches, conventional weighted least squares, sequential weighted least squares, and Kalman filtering, had not previously been compared, in recent literature, in a systematic manner. The sequential weighted least squares method had not been evaluated previously in the literature. The three techniques were analysed with data from six continuously operating receivers in southern California.

Extensive modifications to the UNB DIPOP software were made to accommodate: (1) additional estimated parameters in the form of residual neutral-atmosphere delay offsets to a priori predictions, (2)

a sequential least squares algorithm for the estimation of stochastic parameters (see section 3.3.2), and (3) a Kalman filter algorithm for the estimation of stochastic parameters. Additionally, software for dealing with dual-frequency antenna phase centre offsets was included in the new version of DIPOP.

The main contribution of this research is therefore the systematic evaluation of residual neutral-atmosphere delay estimation techniques, and the upgrading of the UNB DIPOP software with sequential weighted least squares and Kalman filtering algorithms. As can be witnessed by the recommendations chapter, research on this topic is still incomplete.

1.4 Outline of Thesis

Chapter 1: Introduction -- sets the outline and direction of the thesis. The motivation of the research is discussed with emphasis on reasons for the research based on current literature. A literature review follows indicating further reading for history and background information on GPS and neutral-atmosphere delay. The literature review covers: prediction, calibration and estimation of neutral-atmosphere delay; projects that have involved a study of the estimation of neutral-atmosphere delay; and research that compares estimation techniques. A discussion of the contributions of the thesis follows.

Chapter 2: Neutral-atmosphere Effects on GPS Signals -- reviews background material pertinent to the research topic. A review of the basic physics of the neutral-atmosphere is presented, followed by a brief description of the GPS signals. The delay and bending of GPS signals in the neutral-atmosphere is outlined. Outlines of the three approaches to reducing effects of neutral-atmosphere delay is reviewed. Prediction of neutral-atmosphere delay is presented by discussing theoretical zenith delay models and mapping functions. Calibration of neutral-atmosphere delay with WVR equipment is described in brief, outlining strengths and weaknesses of the technique. Estimation techniques are detailed by describing the three techniques investigated in this research.

Chapter 3: Evaluation of Estimation Strategies -- describes the methodology used in the research. Short-term repeatability, the gauge of precision, is outlined. Error sources likely to affect the results, or their interpretation, are outlined in the context of the research. Software modifications to the DIPOP software suite are described.

Chapter 4: Southern California Test Array -- describes the data set analysed and presents results of the analysis of the estimation strategies. The parameter estimation strategy is tabulated. Results of the baseline component sensitivity to changes in a priori constraints are presented in the form of "short-term repeatability maps". A gauge of accuracy is provided by comparison with the IGS-ITRF93 coordinates for the array sites. A discussion of results that summarises and compares the outcome of the sensitivity analysis and accuracy assessment of this chapter is presented last.

Chapter 5: Conclusions and Recommendations -- highlights the contributions of the thesis, important findings, and makes recommendations for future research in this field.

CHAPTER 2

NEUTRAL-ATMOSPHERE EFFECTS ON GPS SIGNALS

Two atmospheric regions degrade the quality of GPS observations: the ionised atmosphere, and the non-ionised atmosphere. The ionised atmosphere, or ionosphere, contributes a dispersive (frequency-dependent) delay to propagating radio signals; hence, first-order ionospheric effects can be removed by linearly combining observations on two observed frequencies (see for example Hofmann-Wellenhof et al. [1993], and Seeber [1993]). The ionosphere is the region of the atmosphere where free electrons exist in numbers that significantly affect the propagation of radio waves. The non-ionised, or neutral-atmosphere effect is not dispersive; hence, it requires alternative treatments to reduce its effects. This chapter reviews: the neutral atmosphere, describing its composition and significance in GPS relative positioning; the GPS radio signals, describing code and carrier phase observables, and positioning capabilities; the refraction of GPS signals in the neutral atmosphere, describing delay and bending of radio signals; and prediction, calibration and estimation techniques, describing how they reduce the effects induced on GPS signals by the neutral atmosphere.

As it is the objective of this thesis to evaluate estimation techniques of residual neutral-atmosphere delay for high precision GPS relative positioning, only a brief review of the fundamentals of GPS, the neutral atmosphere, and methods for reducing the effects of the neutral atmosphere on GPS relative positioning estimates is given. Interested readers are referred to texts that more fully outline the fundamentals of GPS and the physics of the neutral atmosphere. See Remondi [1985], Wells et al. [1986], Lichten [1990a], Bagley and Lamons [1992], Hofmann-Wellenhof et al. [1993], and Seeber [1993] for GPS fundamentals. For fundamentals of the physics of the atmosphere see Dutton [1986], Lutgens and Tarbuck [1986], and Barry and Chorley [1987]. Information on prediction, calibration and estimation of neutral-atmosphere delay can be found in: Lichten and Border [1987], Herring et al. [1990], Lichten [1990a], Herring [1992], Trehauft [1992], and Solheim [1993].

2.1 Composition and Structure of the Neutral Atmosphere

The neutral atmosphere consists of three temperature-delineated regions: the troposphere, the stratosphere, and part of the mesosphere. The neutral atmosphere is often loosely referred to in the space geodetic community and wave propagation fields, as the troposphere. The troposphere ranges in altitude from approximately 9 km at the poles to approximately 16 km at the equator. The boundary separating the troposphere and stratosphere is called the tropopause. The tropopause is situated at the height where temperature begins to increase with altitude (excluding local temperature inversions) [Barry and Chorley, 1987]. Figure 2.1 describes the temperature profile of a standard atmosphere [Champion et al., 1985].

The earth's neutral atmosphere is comprised of dry air gases, water vapour, and suspended particles (aerosols). Dry air gases are mixed very consistently up to an altitude of approximately 80 km [Barry and Chorley, 1987]. Water vapour in the atmosphere is spatially and temporally variable. Water vapour exists mainly in the troposphere since water vapour is limited by the saturation vapour pressure (see Dutton [1986]). Variability of water vapour in the atmosphere is the cause for neutral-atmosphere delay being a dominant residual error source in high precision GPS relative positioning.

The delay effect of water vapour in the zenith direction is at the tens of centimetres level, which is much smaller than the 230 cm or so delay induced by the dry air gases. Its variability in space and time, with typical rates of change of 1 cm/hr, is still significant enough to hinder high precision activities. Dry air gases, and water vapour in hydrostatic equilibrium, are easily modelled theoretically with the ideal gas law and the hydrostatic equation. It is the usual convention, in space geodesy, to separate the constituents of the neutral atmosphere into hydrostatic and non-hydrostatic, or wet, components.

16

100 —

90 — Thermosphere

80 — ——Mesopause ——

70 —

60 — Mesosphere

Height
(km)

50 —

—— Stratopause ——

40 —

30 —

Stratosphere

20 —

——Tropopause ——

10 —

Troposphere

0 —

-100   -80   -60   -40   -20   0   20   40
Temperature (Celsius)
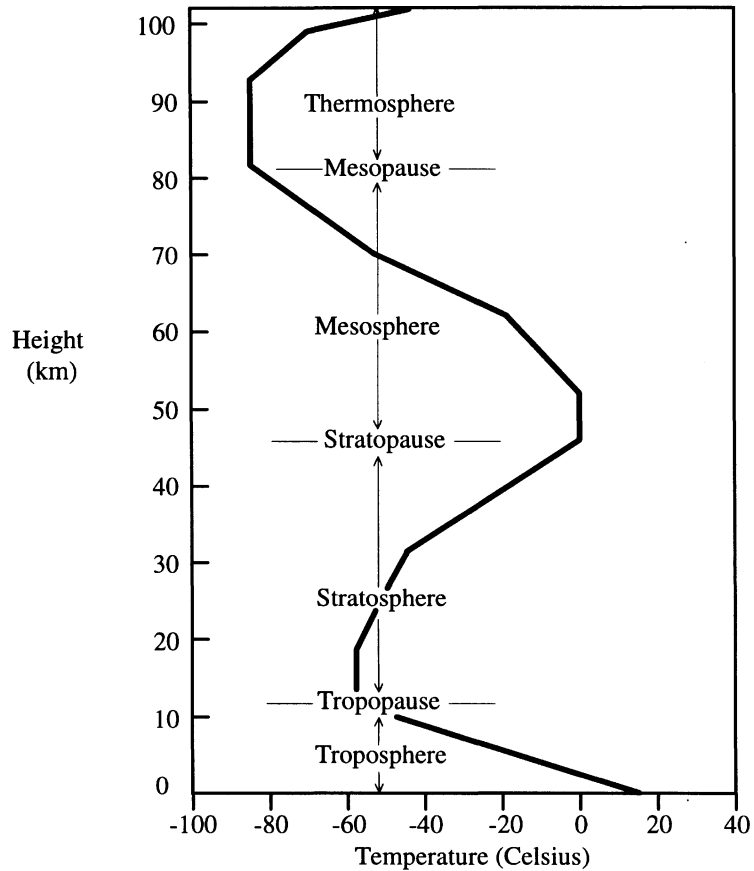
Figure 2.1 -- Thermal profile of atmosphere showing approximate altitudes of temperature regions.

2.2 GPS Signal

GPS is an all-weather space-based positioning system. GPS satellites transmit positioning signals on two L-band frequencies. A signal component that identifies the satellite and contains positioning and health status information is included. Ranging to GPS satellites is done by timing the propagation delay of signals sent from the GPS satellites. This section outlines the characteristics of the GPS signals, and the primary strategies used to derive receiver position from the measurement of range to GPS satellites.

Two L-band carrier signals, termed L1 and L2, are transmitted from GPS satellites. Pseudorandom noise codes are modulated onto the carrier signals. Table 2.1 lists the approximate specifications of the GPS code and carrier signals. The two codes are termed P-code (precision code) and C/A-code (coarse/acquisition code). The P-code is modulated onto both the L1 and L2 carriers. The C/A-code is modulated onto the L1 carrier. A low frequency, 50 Hz, data code is also modulated onto the L1 and L2 carriers. All timing and frequency control is derived from the atomic standards including code frequency and timing.

Table 2.1 -- Characteristics of the GPS carrier and code signals.

| | Carrier | | | Code | |
	L1	L2		P	C/A (L1 only)
frequency (carrier)	1.57542 GHz	1.2276 GHz	chipping rate (code)	10.23 MHz	1.023 MHz
wavelength (approx.)	19.0 cm	24.4 cm		30 m	300 m

Many observables can be recovered from GPS signals (see Langley [1993], and Wells et al. [1986]). Two basic observables are the pseudorange and carrier phase. The phase of the two L-band frequencies transmitted by the satellites is replicated in the receiver and differenced with the incoming, Doppler-shifted, signal to produce a beat frequency. This beat frequency can be observed with a very high precision, much higher than the pseudorange. It is the phase of this carrier beat frequency observation that geodetic relative positioning applications are based on.

The simplest positioning method involves one receiver and access to one of the codes from at least four simultaneously observed satellites. Three satellites define the receiver position and the fourth is needed to remove the receiver clock offset from GPS time. Satellite clock offsets from GPS time and satellite positions are broadcast in the navigation message. This type of positioning can provide 20 m accuracy horizontally (95% confidence) if the P-code is tracked; or up to 100 m accuracy horizontally

(95% confidence) if a degraded C/A-code is tracked. Code positioning accuracy is greatly increased, up

to two orders of magnitude, by employing relative or differential positioning techniques. Differencing

the observations between two simultaneously observing receivers, one with well determined position,

results in a relative position minus most of the error sources common to both receivers, such as satellite

position errors, satellite clock errors, and atmospheric delays, given atmospheric conditions are

correlated for both receivers. Differential code positioning can provide relative horizontal position

accuracy at the 2 to 10 m level (95% confidence) depending on the sophistication of the differencing

algorithm.

High precision relative positioning applications often require far more precise measurements than

code ranging techniques can provide (see for example Lichten [1990a], Bilham [1991], and Dixon

[1991]). Several techniques are currently capable of providing a few parts in 10^9 precision over receiver

separation distances of thousands of kilometres. The short wavelengths of the two GPS carriers (see

Table 2.1), and the fact that modern electronics can resolve the phase of a radio signal with a precision

of less than 1% of its wavelength, makes carrier phase relative positioning a potentially sub-millimetre

level precision positioning tool. For example, the Ashtech company claims its receivers can observe the

GPS carrier phase with an r.m.s. between 0.2 and 0.8% of the wavelength after 10 seconds of averaging

[Gourevitch et al., 1993]. Differencing carrier phase observations between simultaneously observing

receivers is thus a very precise means of relative positioning. One problem, overcome by estimation

techniques, is that the carrier phase observable has an initially ambiguous number of whole cycles

between satellite and receiver since only the fractional phase and number of whole cycles since initial

lock-on is observed.

2.3 Refraction of GPS Signals in the Neutral Atmosphere

The neutral atmosphere is a non-dispersive (frequency-independent) medium for radio frequencies

below approximately 30 GHz. There is no dual-frequency equivalent for the neutral-atmosphere effects

as there is for first-order ionospheric effects. Refraction of radio waves in the neutral atmosphere is dependent only upon the density of water vapour and dry air gases in the atmosphere. The hydrostatic component of refraction is easily and accurately modelled, at the 0.2% level, with surface pressure measurements. However, the wet component is modelled with a large degree of uncertainty since the spatial distribution of water vapour along the propagation path of a radio signal is hard to predict. An excellent reference for a discussion of refraction of radio signals in the atmosphere is Bean and Dutton [1966].

The behaviour of the hydrostatic component of the neutral atmosphere can be described with a few basic physical laws. Two laws are needed to describe the hydrostatic component: (1) the equation of state of gases; and (2) the hydrostatic equation. The equation of state for gases in the neutral atmosphere is given by the ideal gas law (e.g. Halliday and Resnick [1981]):

$$\frac{PV}{T} = \text{constant},\tag{2.1}$$

which describes the relationship between pressure (P), temperature (T), and volume (V) for gases in thermal equilibrium. Given that density (ρ) is mass (M) per unit volume, the ideal gas law can be written as:

$$\frac{P}{T} = \frac{\rho R}{M},\tag{2.2}$$

where R is the universal gas constant. The relationship between pressure and orthometric height is given by the hydrostatic equation (e.g. Halliday and Resnick [1981], and Dutton [1986]):

$$\frac{\partial P}{\partial z} = -g\rho,\tag{2.3}$$

where z represents the height of a parcel of air and g is the magnitude of acceleration of gravity at that height.

2.3.1 Delay

The change of speed of a transatmospheric radio signal in the neutral atmosphere is a result of the signal passing through regions of varying, generally increasing, refractive index. In the neutral atmosphere, the refractive index of radio waves is always greater than unity; hence, a range derived from a radio signal always measures longer after travelling through the neutral atmosphere than if it had travelled through a vacuum.

The range of a radio signal can be expressed as:

$$s = \int n \, ds, \tag{2.4}$$

where s is the measured range to the source of the radio signal, and n is the refractive index. The integral is evaluated along the path of the signal in the neutral atmosphere. The geometric range (s_0), the range that would be measured if the signal propagated in a vacuum, can be expressed by equating n to unity:

$$s_0 = \int ds_0. \tag{2.5}$$

The effect of neutral-atmosphere delay including bending is the difference between eqn. (2.4) and eqn. (2.5). Hence, the excess path length due to delay, neglecting ray bending, of radio signals in the neutral atmosphere is:

$$d_{na} = \int (n-1) \, ds. \tag{2.6}$$

The value of n differs little from unity in the neutral atmosphere. Hence, n is usually replaced by refractivity (N), which is defined as:

$$N = 10^6 (n-1). \tag{2.7}$$

After substituting refractivity, as given by eqn. (2.7), into the delay expression, eqn. (2.6), and splitting refractivity into hydrostatic (subscript hyd.) and wet (subscript w) components (e.g. Hopfield [1971]), radio signals propagating through the neutral atmosphere are delayed according to:

21

$$d_{na} = 10^{-6} \int N_{hyd.} \, ds + 10^{-6} \int N_w ds. \tag{2.8}$$

Hence, knowledge of the refractivity profile of a propagating signal can be used to evaluate delay. Equation (2.8) is evaluated along the signal path between the outer boundary of the neutral atmosphere and the receiving antenna.

A general form of refractivity of moist air for radio frequencies up to 20 GHz is given by Thayer [1974] as:

$$N = k_1 \frac{P_d}{T} Z_d^{-1} + [k_2 \frac{e}{T} + k_3 \frac{e}{T^2}] Z_w^{-1}, \tag{2.9}$$

where P_d is the partial pressure of dry air (mbar), T is the absolute temperature (K), e is the partial pressure of water vapour (mbar), Z_d^{-1} is the inverse compressibility factor for dry air constituents, Z_w^{-1} is the inverse compressibility factor for water vapour, and k_1, k_2, k_3 are empirically determined constants (K/mb, K/mb, K^2 / mb). Values for the empirical constants (k_i) can be found in Table 2.2 from the International Association of Geodesy [1963] as determined by Essen and Froome, and Thayer [1974]. Equation (2.9) can be expressed as the sum of a hydrostatic and wet component by making the first term of the equation dependent on the density of the total mass of the neutral atmosphere, as opposed to just the dry portion of it. According to Davis et al. [1985], Thayer's [1974] refractivity model can be expressed in the more convenient form of:

$$N = k_1 R_d \rho + [k_2 \frac{e}{T} + k_3 \frac{e}{T^2}] Z_w^{-1}, \tag{2.10}$$

which splits refractivity into hydrostatic and wet components. Where R_d is the gas constant for dry air, and ρ is the total density of the neutral atmosphere. It is more accurate to express the refractivity in terms of hydrostatic and wet components since the hydrostatic equation and the ideal gas law can not be applied to just the dry component of refractivity with full accuracy. The error induced in estimating refractivity assuming the "dry/wet" formalism instead of the "hydrostatic/wet" formalism depends on

the error in the assumption that the dry pressure is equal to the total pressure excluding the water vapour pressure. In the worst case where default atmosphere parameters are used (for example the default atmosphere parameters used in DIPOP of 15° C, 50% humidity, and 1013.25 mbar of total pressure, resulting in approximately 8 mbar of water vapour pressure) and the extreme case of say 30 mbar of water vapour present in the atmosphere, the dry pressure would be in error by 27 mbar based on the above assumption. This error represents about 2.5% of the dry pressure value, which is directly proportional to the effect this error would have on the prediction of the delay of a radio signal (approximately 60 mm in the observer's zenith).

Table 2.2 -- Refractivity model empirical constant values.

	k_1 (K / mb)	k_2 (K / mb)	k_3 (K^2 / mb)
IAG [1963]	77.624	64.7	3.719×10^5
Thayer [1974]	77.604	64.8	3.776×10^5

The neutral atmosphere delays and bends signals from GPS satellites. Bending and speed change are closely related and usually expressed, as the combination of the two effects, by the term refraction [Vanicek and Krakiwsky, 1986]. The refraction bias induced on a transatmospheric propagating radio signal due to the neutral atmosphere is:

$$d_{na} = \int_{r_s}^{r_a} [n(r) \csc E(r) - \csc \varepsilon(r)] \, dr, \tag{2.11}$$

where the refractive index (n) is along the signal propagation path, r is the geocentric radius, a and s refer to the altitude of the outer boundary of the neutral atmosphere and the receiver altitude respectively, E is the apparent (refracted) elevation angle of the signal source, and ε is the true (non-refracted) elevation angle of the signal source. Where the first part of the integral represents a signal propagating through a medium of varying density, i.e. the combined the effect of bending and speed change. The second part represents the ideal case of a signal propagating in a vacuum.

Delays at arbitrary elevation angles are determined from zenith delays and what is termed a "mapping function". Mapping functions have been developed for hydrostatic and wet components of the delay. Thus, the elevation angle dependent delay due to the neutral atmosphere is expressed as:

$$d_{na} = d_{hyd.}^{Z} \cdot m_{hyd.}(\varepsilon) + d_{w}^{Z} \cdot m_{w}(\varepsilon), \qquad (2.12)$$

where $d_{hyd.}^{Z}$ is the hydrostatic zenith delay, d_{w}^{Z} is the wet zenith delay, $m_{hyd.}$ is the hydrostatic mapping function, m_{w} is the wet mapping function, and ε is the non-refracted elevation angle. Approximate estimates of sea level zenith delay for radio signals would be within a few centimetres of 230 cm for the hydrostatic component, and 5-40 cm for the wet component. In extreme conditions, such as cyclonic, the hydrostatic delay may vary by up to 12 cm from the nominal value above. Figure 2.2 shows approximate typical magnitudes of total excess path length by mapping the zenith delay estimates into their elevation angle equivalents via a simplistic assumption that excess path length varies in elevation angle as a function of the cosecant of the elevation angle.
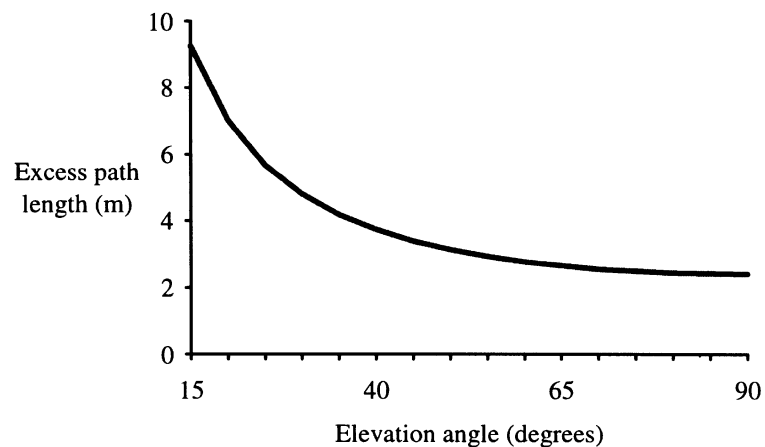
Figure 2.2 -- Approximate excess path length due to neutral-atmosphere delay (hydrostatic + wet).

2.3.2 Ray bending

Ray bending of radio signals propagating through the neutral atmosphere is quantified in eqn. (2.11) as the difference between curved and rectilinear signal paths. A radio signal propagating from an orbiting space vehicle to the earth encounters generally increasing densities of atmospheric constituents (increasing refractive index). According to Snell's law of refraction, a wave bends towards the denser medium. Details on ray bending of radio signals can be found in Bean and Dutton [1966], Brunner [1984], Dutton [1986], Vanicek and Krakiwsky [1986], Allnutt [1989], Hall and Barclay [1989], and de Jong [1991].

An empirical form of the contribution of ray bending to the delay of radio signals in the neutral atmosphere is given by Kouba [1979]:

$$rb(E) = \frac{1.92}{E^2 + 0.6},$$ (2.13)

where rb is the excess path length of the radio signal due to ray bending in metres, and E is the satellite elevation angle in degrees. Plotting this model, Figure 2.3, results in the conclusion that ray bending is significant at the centimetre level for observation elevation angles less than 15°. At 15° elevation angle, the ray bending effect would be considered significant for certain high precision applications.
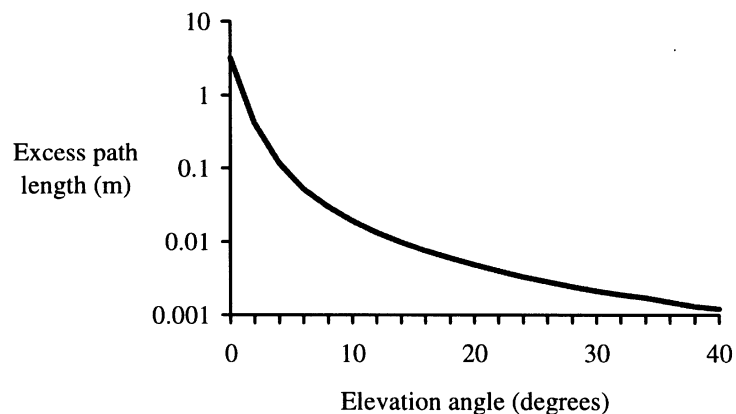
Figure 2.3 -- Empirical form of Excess path length due to ray bending according to Kouba [1979].

By comparing this equation with ray tracing results supplied by Mendes [1995], see Table 2.3, it is

obvious that the empirical form loses its generality at very low elevation angles. The ray tracing results

provide average delay due to bending based on one year of data collected at high-latitude (Alert,

Canada), mid-latitude (Nashville, USA), and low-latitude (San Juan, Puerto Rico) locations.

Table 2.3 -- Delay due to ray bending, comparison of ray tracing and empirical formula results.

Elevation angle	Alert	Nashville	San Juan
	ray trace - empirical	ray trace - empirical	ray trace - empirical
(degrees)	(m)	(m)	(m)
3	0.325	0.352	0.459
15	0.001	0.002	0.003
30	-0.001	-0.001	-0.001

2.4 Countering Neutral-atmosphere Effects

The GPS carrier phase observation equation can be written as [Wells et al., 1986]:

$$\Phi = \rho + c(dt - dT) + \lambda N - d_{ion} + d_{na} + d\Phi_m + \varepsilon_\Phi, \tag{2.14}$$

where Φ is the carrier phase range, ρ is the geometric range from receiver to satellite, c is the speed of

light in a vacuum, dt is the satellite clock error, dT is the receiver clock error, λ is the signal

wavelength, N is the carrier phase ambiguity term, d_{ion} is the ionospheric delay, d_{na} is the neutral-

atmosphere delay, $d\Phi_m$ is multipath induced error, and ε_Φ is a random error term. In this section

methods to reduce the effect of the neutral-atmosphere delay, d_{na}, are highlighted.

2.4.1 Prediction

Prediction of neutral-atmosphere delay involves applying theoretical functions to standard, or observed,

meteorological conditions. Models for predicting the delay are derived from regional or global data sets

and theoretical postulations. Most theoretical models provide zenith delay values which are used in

conjunction with mapping functions (section 2.4.1.2). Knowing the refractivity profile enables the

calculation of delay from eqn. (2.8). The Saastamoinen and Hopfield zenith delay models are described in the following section. The Saastamoinen model is derived from gas laws whereas the Hopfield model was developed from empirical fitting of global meteorological data. Many other models are available, see for example Janes et al. [1991], Gallini [1994], and Mendes and Langley [1995] for comparisons of some of the geodetic models used in practice. These two models emphasise the differences in the two main methods for predicting the neutral-atmosphere delay.

2.4.1.1 Zenith delay models

From the refractivity model of eqn. (2.10) the hydrostatic component of neutral-atmosphere delay is given by integrating the hydrostatic term on the right hand side of the equation in the observer's zenith:

$$d_{hyd.}(zenith) = 10^{-6} k_1 R_d \int \rho \, dz. \tag{2.15}$$

Surface pressure can be derived from the hydrostatic equation, eqn. (2.3), by integration as follows:

$$P_s = \int_h^\infty g(z)\rho(z) \, dz, \tag{2.16}$$

where P_s is the surface pressure (mbar), h is the height of the observer above the reference geoid (m), and g is gravity (m/s^2). Gravity can be replaced by an average value, g_0, along the integration path. The infinite limit of integration can be replaced with a finite one corresponding to the upper limit of the hydrostatic portion of the neutral atmosphere. By integrating over the hydrostatic region of the neutral atmosphere, the zenith delay in eqn. (2.15) can be written as:

$$d_{hyd.}(zenith) = 10^{-6} k_1 \frac{R_d P_s}{g_0}. \tag{2.17}$$

Equation (2.17) highlights that the hydrostatic component of the delay is essentially dependent only on surface pressure at the point of observation. In a possible worst case scenario where the observer is at an altitude of 5 km and near the earth's equator, eqn. (2.17) could be in error by up to 0.4% of the zenith delay due to the assumption of a constant gravity term.

27

The average gravity value in eqn. (2.17) is computed as the value at the centroid of a vertical column of atmosphere for the location. According to Saastamoinen [1973], the height (H) in metres for the centroid of this vertical column is given by:

$$H = 7.3 \text{x} 10^3 + 0.9 h. \tag{2.18}$$

The dependency of gravity on latitude and height is accounted for by Saastamoinen by replacing average gravity (g_0) with:

$$g = 9.784[1 + 2.6 \text{x} 10^{-3} \cos 2\phi + 2.8 \text{x} 10^{-7} h], \tag{2.19}$$

where ϕ is latitude, and h is height above sea level. In the Saastamoinen model the hydrostatic atmosphere consists of a troposphere ranging from the earth's surface to 11-12 km altitude depending on latitude and season, on top of which is an isothermal stratosphere extending approximately 60 km from the tropopause [Janes et al., 1991].

Hopfield's model [Hopfield, 1969], in contrast to Saastamoinen's model, uses empirical observations to determine a best fitting algorithm that describes the dry neutral-atmosphere delay. The Hopfield model is based on a single layer, ranging from the earth's surface to an altitude of approximately 40 km. The height of this layer (in metres) is given by:

$$h_d = 40136 + 148.72(T_s - 273.16), \tag{2.20}$$

where T_s is the surface temperature. The dry refractivity profile is modeled as a quartic function of height (h) above the earth's surface by:

$$N_d(h) = N_{d,s} \left[\frac{h_d - h}{h_d} \right]^4, \tag{2.21}$$

where subscript d refers to dry component, subscript s refers to the earth's surface.

Wet refractivity is much harder to model than dry refractivity due to the temporal and spatial variations in partial water vapour pressure. There have been many attempts to model the wet portion of

the neutral atmosphere. Different models reflect different interpretations and assumptions made about the water vapour content in the neutral atmosphere. The struggle to predict the wet component of neutral-atmosphere delay is probably best represented by Hopfield's explanation for modelling the wet delay as a quartic function similar to the dry delay function. She states [Hopfield, 1977, p. 207]: "The fourth-degree form of the profile is theoretically justified for dry air; it is used for water vapor also, for lack of a better expression."

Saastamoinen's derivation of wet delay is based on the hydrostatic/wet formalism of refractivity, eqn. (2.10), and five other assumptions: (1) the ideal gas law applies, (2) water vapour is located in the troposphere only, (3) temperature decreases as a linear function of height, (4) water vapour pressure is given by:

$$e(h) = e_s \left(\frac{T}{T_s}\right)^{\left[\frac{4gM}{R\alpha}\right]},$$

(2.22)

where e is water vapour pressure, h is height above the surface, subscript s refers to surface values, T is temperature, g is gravity, M is the molecular mass of air (hydrostatic plus wet components), R is the gas constant, α is the temperature lapse rate, and (5) gravity is constant along the integration path. As just mentioned Hopfield's model for the wet zenith delay uses the same form of model as for the dry delay term. The Hopfield model is based on a single layer, ranging from the earth's surface to a tropopause height (h_d) of 11 km.

2.4.1.2 Mapping functions

Equation (2.8) shows the dependence of neutral-atmosphere delay on the path of the signal. The delay is dependent on the density of dry air and water along the signal path. It is also evident from the derivations of section 2.4.1.1 that predicting neutral-atmosphere delay can be achieved by integrating refractivity in the observer's zenith. Hence, relating zenith delay predictions to elevation angle equivalents is performed with a mapping function. This is not always the case, for example the Wide

Area Augmentation System (WAAS) neutral-atmosphere delay model does not contain these two components explicitly. However, the two component method enables the neutral-atmosphere delay to be estimated (using least squares techniques) in the observer's zenith and not at the elevation angle of the incoming signal.

The mapping function of Hopfield's formulation is implicit in the elevation angle dependent form of her models. They are formulated by replacing heights in the refractivity model with radial distances (see Hopfield [1969]). Realising that Hopfield's original derivation can be improved [Janes et al., 1991; Mendes and Langley, 1994], some modified versions of her model have been made: Yionoulis [1970], Goad and Goodman [1974], Black [1978], and Black and Eisner [1984]. Saastamoinen [1973] accounts for elevation angle dependence using a truncated binomial series expansion of Snell's law for a spherical atmosphere.

Other mapping functions are based on the continued fraction form first developed by Marini [1972]. The general form of this type of mapping function is:

$$m(\varepsilon) = \cfrac{a}{\sin\varepsilon - \cfrac{b}{\sin\varepsilon + \cfrac{c}{\sin\varepsilon + \ldots}}}, \qquad (2.23)$$

where a, b, and c are empirical functions of parameters such as surface pressure, surface water vapour pressure, surface temperature, tropopause height, and temperature lapse rate, and ε is the unrefracted satellite elevation angle. The empirical coefficients are usually determined by fitting ray traced radiosonde profiles to the continued fraction function. Davis et al. [1985] took this form one step further by modifying the two term Chao mapping function. The CfA-2.2 mapping function [Davis et al., 1985] consists of three levels of fraction with the second sin ε in the above form replaced by a tan ε in order that m(zenith) be unity.

Mapping functions are based on the assumption that the constituents of the neutral atmosphere are uniformly distributed in azimuth around the observer, i.e. no horizontal gradients. Gardner [1976] shows that azimuthal asymmetry can lead to errors of up to 3 cm (r.m.s.) when mapping zenith delays to low elevation angles (< 10°). Tralli et al. [1988] estimate 2 cm bias in wet delay due to azimuthal asymmetry. Herring [1992] shows some significant results from using a "tilted" atmosphere assumption to estimate north-south and east-west gradients, improvements in baseline length repeatability of the order of 10% were reported.

2.4.2 Calibration

Large spatial and temporal variations of water vapour in the neutral atmosphere require that special consideration be given to estimating the wet delay component of neutral-atmosphere delay [de Jong, 1991; Seeber, 1993]. Surface measurements of water vapour content are mostly useless due to the large variations in water vapour content with height and inaccurate measuring techniques. Good estimates of the water vapour content along the signal propagation path are required to correctly determine the wet delay component if non-estimation techniques are used.

To measure water vapour content in the atmosphere a radiosonde (a balloon with meteorological measuring devices attached) can be used. It samples temperature, pressure and humidity nominally above the observer. The radiosonde has four flaws according to de Jong [1991]: (1) its ascent over the observing station is subject to wind strength and direction; thus, it profiles a portion of the atmosphere not directly in the observer's zenith; (2) data from the sensors is not continuous; (3) the ascent of the balloon takes approximately 1 to 1.5 hrs to cover the desired portion of the atmosphere; thus, the profile is not of the instantaneous conditions; and (4) relative humidity sensors are unreliable in the presence of liquid water (clouds) and at low temperatures. These four factors combine to give an accuracy of only 10% of the total wet component delay [de Jong, 1991].

31

A WVR is a passive ground based instrument that measures sky brightness temperature. Sky brightness temperature is a function of water vapour content in the atmosphere. Water vapour content in the atmosphere has a resonant molecular frequency of 22.235 GHz; hence, radiometers are operated at this frequency. Brightness temperature is also a function of liquid water in the atmosphere; hence, WVRs usually operate at two frequencies, the second frequency is used to separate the effects of liquid water, oxygen, background radiation (galactic sources) and water vapour [Elgered et al., 1991]. It is important to consider the liquid water content for WVR. It has little impact on refraction of microwaves; however, it significantly contributes to sky brightness temperature [de Jong, 1991]. Details of the mathematical model used to separate water vapour from liquid water can be found in Wu [1979].

The current accuracy level of WVR is at the 0.5 to 1 cm level for elevation angle observations greater than 10°, which implies an accuracy in the sky brightness temperature of 0.5 to 1.0 K [Janssen, 1985; de Jong, 1991]. Robinson [1988] expects that future accuracy for WVRs will be at the 0.15 K level (or about 0.1 cm in terms of wet delay).

2.4.3 Estimation

Offset, or scale, delay parameters can be included in a least squares based adjustment of GPS observations to account for inaccuracies of the theoretical delay prediction models. The offset parameters (offset is used in this research, as it allows, in the author's opinion, an easier interpretation of the delay magnitude) are related to the GPS observation model by their functional dependence on elevation angle through a mapping function. Using the form of eqn. (2.12), an offset parameter can be included in the definition of neutral-atmosphere delay as follows:

$$d_{na} = [d_{na}^Z + \upsilon_{na}] \cdot m_{na}(\varepsilon), \tag{2.24}$$

where υ_{na} is the offset to a priori predictions of the zenith neutral-atmosphere delay. A priori values are in the form of theoretical model predictions, WVR calibrations, radiosonde calibrations, or no a priori predictions/calibrations by having the offset term estimate all of the neutral-atmosphere delay.

Estimating one delay parameter per site and observation session can be accomplished in a conventional weighted least-squares algorithm. One drawback of only estimating a single delay parameter at each site is that the final baseline estimates may be degraded due to variations in the delay during the session that were ignored. Two solutions exist to remedy this situation: (1) estimate a sufficient number of delay parameters, separated in time, to account for significant variations in the delay rate of change; or (2) estimate stochastic, time varying, parameters characterised by a suitable random process, such as a random walk or first order Gauss-Markov random process. The multiple parameter method is accomplished with a conventional weighted least squares technique. The stochastic techniques include sequential weighted least squares and Kalman filtering. The conventional weighted least squares, sequential weighted least squares, and Kalman filtering techniques are outlined in the following sections.

2.4.3.1 Conventional weighted least squares

Estimated parameters in a conventional weighted least-squares adjustment are static; that is, they have no ability to change with respect to time. Thus, changes in the neutral-atmosphere delay are accounted for by estimating separate delay parameters every "n" observations. The design matrix for a system of equations that has delay parameters valid for "n" observations would contain a banded hyper-matrix of delay parameter coefficients. The general form of a parametric least squares adjustment is used [Vanicek and Krakiwsky, 1986; Krakiwsky and Gagnon, 1987]:

$$\hat{\underline{x}} = (\underline{A}^T \underline{P}_\ell \underline{A})^{-1} \underline{A}^T \underline{P}_\ell \underline{\ell}, \tag{2.25}$$

where $\underline{\hat{x}}$ is the least squares optimised vector of unknown parameters, $\underline{A}$ is the first design matrix, $\underline{P}_\ell$ is the observation weight matrix (inverse of the observation covariance matrix), and $\underline{\ell}$ is the vector of observations. The estimation strategy and algorithms for the conventional weighted least squares component of the DIPOP software are detailed in Vanicek et al. [1985].

2.4.3.2 Kalman filtering

Kalman filtering is the sequential estimation of states in a dynamic environment (see Schwarz [1987], and Brown and Hwang [1992]). The Kalman filter provides estimates of states based on past and present observations. A recursive algorithm is used: it updates the previous state and its covariance with the current observations. Key components of a Kalman filter include: the state vector, the dynamics model, the transition matrix, the update and prediction equations, and the gain factor. These components will be briefly explained below. For further details, see Brown and Hwang [1992].

The dynamic model expresses the change of state of parameters over time. Each new estimate is a new state whereas, in conventional weighted least squares, one parameter is estimated for all of the data. The observation model for a conventional weighted least-squares adjustment is modified to include a time dependence of all parameters in the Kalman filter equations. The Kalman filter observation model in linear form is given by:

$$\underline{\ell}(t) = \underline{A}(t)\underline{x}(t) + \underline{e}(t), \tag{2.26}$$

where $\underline{\ell}(t)$ is the observations vector at time t, $\underline{A}(t)$ is the design matrix at time t, $\underline{x}(t)$ is the unknown state vector at time t, and $\underline{e}(t)$ is the measurement noise vector at time t. Due to the discrete sampling nature of GPS measurements, eqn. (2.26) can be written as:

$$\underline{\ell}_k = \underline{A}_k \underline{x}_k + \underline{e}_k, \tag{2.27}$$

where the subscript k refers to time epoch k, and the covariance matrix of the measurement noise at epoch k is $\underline{C}_k^e$.

In filtering, the dynamic model is used to define the change in state of $\underline{x}_k$ from time t_k to t_{k+1}. The dynamic model is therefore written as:

$$\underline{x}_{k+1} = \underline{\Phi}_{k+1,k}\underline{x}_k + \underline{u}_{k+1,k},$$

(2.28)

where $\underline{\Phi}_{k+1,k}$ is the transition matrix, and $\underline{u}_{k+1,k}$ is the system noise vector. The system noise vector describes the uncertainty in the dynamic model, just as the measurement noise describes the uncertainty in the observation model. The determination of the system noise is usually performed by empirical methods since the analytical derivation of it is complicated and sometimes not possible (see for example Schwarz [1987]). In this study the system noise is determined empirically by optimising the precision of estimated geodetic components. The system noise has zero mean, $E[\underline{u}_{k+1,k}] = 0$ and its variance is given by $E[\underline{u}_{k+1,k}\,\underline{u}_{k+1,k}^T] = \underline{C}_{k+1,k}^u$, where $E[.]$ is the statistical expectation operator. The derivation of the transition matrix and the system noise covariance matrix is complex and will not be dealt with here. A detailed description of analytical and empirical methods for deriving the transition matrix and the system noise covariance matrix is given by Gelb [1974], Schwarz [1987], and Brown and Hwang [1992]. The transition matrix provides a means of obtaining an estimate, given only the previous state and its covariance matrix.

Combining eqn.s (2.27) and (2.28), an optimal estimate of $\underline{x}(t)$ at any time t_k is given. The optimisation is defined in the least squares sense. According to Schwarz [1987, p. 237] "...the resulting estimate is unbiased and the trace of the corresponding covariance matrix is minimum." Kalman filtering has two states of estimation: (1) prediction, and (2) update. The prediction equations are:

$$\underline{\hat{x}}_k(-) = \underline{\Phi}_{k,k-1}\underline{\hat{x}}_{k-1},$$

(2.29)

$$\underline{C}_k^x(-) = \underline{\Phi}_{k,k-1}\underline{C}_{k-1}^x\underline{\Phi}_{k,k-1}^T + \underline{C}_{k,k-1}^u,$$

(2.30)

35

where $(-)$ refers to the process of prediction, and $\underline{C}_k^x$ is the covariance matrix of the optimal estimate

$\underline{\hat{x}}_k$. The update equations are:

$$\underline{\hat{x}}(+) = \underline{\hat{x}}(-) + \underline{K}[\underline{\ell} - \underline{A}\underline{\hat{x}}(-)], \qquad (2.31)$$

$$\underline{C}^x(+) = [\underline{I} - \underline{KA}]\underline{C}^x(-), \qquad (2.32)$$

$$\underline{K} = \underline{C}^x(-)\underline{A}^T[\underline{A}\,\underline{C}^x(-)\underline{A}^T + \underline{C}^e]^{-1}, \qquad (2.33)$$

where $(+)$ refers to the process of updating (i.e. calculations based on a new measurement), $\underline{K}$ is the

Kalman gain matrix (weight matrix), $\underline{I}$ is the identity matrix, and $\underline{C}^e$ is the covariance matrix of the

measurement noise vector. Equations (2.31) to (2.33) are recursive; i.e., the optimal estimate of the state

vector is based on all measurements up to the current epoch. However, only the previous estimate, its

covariance matrix, and the update measurement are needed. Optimal estimates based on eqn.s (2.29) to

(2.33) are only optimal at their time of calculation; i.e., a new measurement can improve all previous

estimates.

Random walk and first-order Gauss-Markov random processes are used to characterise the neutral-

atmosphere delay variability since they are capable of modelling many non-deterministic signals [Gelb,

1974] including the delay variability and orbit solar radiation pressure coefficients. In its discrete form,

the random walk stochastic process is written as:

$$x_{k+1} = x_k + \omega_{rw}, \qquad (2.34)$$

where x is the model state, ω_{rw} is a random variable with the following characteristics,

$$E[\omega_{rw}] = 0, \qquad (2.35)$$

$$E[\omega_{rw}^2] = \sigma_{rw}^2\,\Delta t, \qquad (2.36)$$

36

where σ_{rw}^2 is the random walk process variance rate of change (length unit^2 / time unit), and t is time

(see Gelb [1974], Bierman [1977], Herring et al. [1990], and Tralli and Lichten [1990] for detailed

descriptions). The discrete form of the first-order Gauss-Markov stochastic process is written as:

$$x_{k+1} = m \cdot x_k + \omega_{GM}, \tag{2.37}$$

where x represents the model state, ω_{GM} is a random variable, and m is a measure of exponential

correlation between adjacent states:

$$m = \exp[\frac{-\Delta t}{\tau_{GM}}], \tag{2.38}$$

where τ_{GM} is the correlation time. The random variable ω_{GM} has the following properties:

$$E[\omega_{GM}] = 0, \tag{2.39}$$

$$E[\omega_{GM}^2] = \sigma_{GM}^2 (1 - m^2), \tag{2.40}$$

where σ_{GM}^2 is the steady state variance. Note that the Gauss-Markov process asymtotically approaches

the random walk process as $\tau_{GM} \to \infty$. Further detail can be found in Gelb [1974], Bierman [1977],

Herring et al. [1990], and Tralli and Lichten [1990].

The implementation of these processes into a system of filter equations occurs at two points: (1) the

transition matrix, and (2) the system noise variance matrix. The transition matrix elements

corresponding to the neutral-atmosphere delay parameters are unity for the random walk process and m,

eqn. (2.38), for the first order Gauss-Markov process. The system noise covariance elements for the

random walk process are given by eqn. (2.36) and eqn. (2.40) for the random walk and first order Gauss-

Markov processes respectively. The selection of values for σ_{rw}, σ_{GM}, and m will be discussed later.

Numerical instability can be a problem for the conventional Kalman algorithm. The problem arises

from the explicit differencing and inversion of data with a large dynamic range. This problem is

efficiently controlled (with minimal computational burden) by use of factorisation techniques. Bierman [1977] details the square root information filter (SRIF) and the U-D factorisation methods. Lichten [1990a] describes the use of the SRIF and U-D factorisation methods for applications of satellite orbit and geodetic parameter estimation using GPS.

2.4.3.2.1 A posteriori variance factor

The problem: defining the degree of freedom for a Kalman filter system of equations containing states with added system noise. Degree of freedom is used in the calculation of an estimated variance factor (also known as the variance of unit weight). The estimated variance factor $(\hat{\sigma}_0^2)$ is defined in conventional weighted least squares terminology as:

$$\hat{\sigma}_0^2 = \frac{\underline{r}^T \underline{P}_\ell \underline{r}}{n - u}, \tag{2.41}$$

where $\underline{r}$ is the vector of a posteriori measurement residuals, $\underline{P}_\ell$ is the weight matrix, n is the number of observations (measurements), and u is the number of estimated parameters. In the filtering domain, u is very hard to define when the state vector contains system noise added states, such as the residual neutral-atmosphere delays being estimated in this study. Comments from researchers in this field indicate this topic to be a complicated and unresolved one [Brown, 1994; Herring, 1994; Lichten, 1994; Muellerschoen, 1994]. The controversy of the situation revolves around the definition of a new system noise state variable and hence an increase in the number of unknown parameters (u). A new state is defined when the constraint between successive states is "weak". The definition of weak is very subjective. In the case of "strong" constraints between successive states, the successive state is considered to be the same state and hence u is not affected. An empirical study into the definition of strong and weak constraints is recommended for future analysis using a filtering technique with system noise parameters.

The argument essentially involves the calculation of the number of unknown states. In this study, where the number of observations far outweighs the number of estimated states, the effect of increasing or decreasing u is considered to be insignificant; however, for smaller data sets with fewer observations, this value may have an effect on the variance-covariance estimates. In this study, the maximum change in u would result in an approximately 5% difference in the estimated variance factor ($\hat{\sigma}_0^2$). The estimated variance factor is used to scale the a posteriori state variance matrix.

2.4.3.3 Sequential weighted least squares

Modelling the neutral-atmosphere delay in a sequential weighted least squares adjustment as a stochastic process has been outlined by Chen [1994]. The sequential weighted least squares adjustment is equivalent to the Kalman filter algorithm if the transition matrix is treated as an identity matrix, and the process noise matrix is treated as a null matrix (see Schwarz [1987] for derivation of the equivalence of the Kalman filter and sequential least squares). The sequential least squares algorithm used in this research is a Kalman filter algorithm (see section 2.4.3.2) with an identity transition matrix and a null process noise matrix.

For the first order Gauss-Markov random process, the design coefficients of the stochastic parameters in the system of equations being solved are multiplied by the exponential function in the random process definition:

$$a_k' = \exp[-\frac{t_k - t_{k-1}}{\tau}] \cdot a_k, \tag{2.42}$$

where a_k is the design matrix coefficient of the stochastic parameter; a_k' is the modified design matrix coefficient of the stochastic parameter; $(t_k - t_{k-1})$ is the observation, or batch, sample interval; and τ is the stochastic parameter's correlation time. The covariance of the stochastic parameters are updated by adding process noise, ω_{GM}, to them:

$$c'_k = c_k + \sigma^2_{GM} \cdot [1 - \exp(-2 \frac{t_k - t_{k-1}}{\tau})],$$ (2.43)

where c_k is the covariance matrix element for the stochastic parameter; c'_k is the modified covariance matrix element for the stochastic parameter, and σ^2_{GM} is the steady state variance of the Gauss-Markov process.

In the case of the random walk stochastic process ($\tau = \infty$) being used to model the neutral-atmosphere delay, the modifications to design matrix coefficients and covariance matrix elements are:

$$a'_k = a_k,$$ (2.44)

and

$$c'_k = c_k + \sigma^2_{rw} \cdot (t_k - t_{k-1}),$$ (2.45)

where σ^2_{rw} is the random walk process variance rate of change

CHAPTER 3

EVALUATION OF ESTIMATION STRATEGIES

Many applications of GPS, such as the study of crustal dynamics, are concerned with the accurate and precise determination of position over large distances and sometimes over considerable periods of time. Two tools are used in this research to analyse the precision and accuracy of the strategies being evaluated: (1) short-term repeatability as a gauge of precision, and (2) comparison with established ITRF93 coordinates, from the Scripps Institute of Oceanography (SIO) IGS data archives (denominated IGS-ITRF in this thesis), as a gauge of accuracy. The IGS-ITRF reference frame is defined by SIO through a combination of observations at Permanent GPS Geodetic Array (PGGA) stations and IGS core stations. To successfully evaluate estimation strategies for residual neutral-atmosphere delay, other error sources that can affect the interpretation of the analysis need to be realised and quantified. Detailed analysis of precision and accuracy in high precision GPS experiments have been put forward by Blewitt [1989 and 1993], Davis et al. [1989], Delikaraoglou [1989], Prescott et al. [1989], Dixon [1991], Larson and Agnew [1991], and Larson et al. [1991].

Generally, three methods are used to determine GPS geodetic baseline accuracy and precision [Blewitt, 1993]: (1) repeated measurements of the same quantity, the weighted r.m.s. scatter about the mean [see Larson and Agnew, 1991]; (2) comparison with not fully-independent techniques such as VLBI, SLR, or terrestrial geodetic methods; (3) formal error computation, derived from the variance-covariance matrix of the least squares estimation. These methods provide a consistent picture of GPS geodetic baseline estimation precision and accuracy given that good quality data is available and a sound estimation technique is employed.

The doubly differenced carrier phase observation is the basis of the DIPOP software. The receiver-satellite double difference observation equation is written as [Wells et al., 1986]:

$$\nabla\Delta\Phi_{AB}^{jk} = \nabla\Delta\rho_{AB}^{jk} + \nabla\Delta\lambda N_{AB}^{jk} - \nabla\Delta d_{ion\,AB}^{jk} + \nabla\Delta d_{na\,AB}^{jk} + \nabla\Delta d\Phi_{m\,AB}^{jk} + \nabla\Delta\varepsilon_{\Phi AB}^{jk}, \qquad (3.1)$$

where $\nabla\Delta$ is the double difference operator (see Wells et al. [1986]), $\nabla\Delta\Phi_{AB}^{jk}$ is the doubly differenced carrier phase observation to satellite pair jk from receiver pair AB, $\nabla\Delta\rho_{AB}^{jk}$ is the doubly differenced geometric range between receivers and satellites, λ is the carrier phase wavelength, $\nabla\Delta\lambda N_{AB}^{jk}$ is the doubly differenced carrier phase cycle ambiguity bias, $\nabla\Delta d_{ion\,AB}^{jk}$ is the doubly differenced ionospheric bias, $\nabla\Delta d_{na\,AB}^{jk}$ is the doubly differenced neutral-atmosphere bias, $\nabla\Delta d\Phi_{m\,AB}^{jk}$ is the doubly differenced carrier phase multipath bias, and $\nabla\Delta\varepsilon_{\Phi AB}^{jk}$ is the doubly differenced measurement noise error. Although the main thrust of the evaluation is comparative in nature, the accuracy and precision of the individual techniques is the tool by which the comparisons are made; thus, it is imperative that the majority of bias and error sources are minimised, and remaining errors and biases are quantified.

This chapter highlights the methodology used to assess the three estimation techniques. The gauges of accuracy and precision are outlined in the first two sections. Error sources affecting the estimation of baseline components are reviewed. The chapter closes with a brief outline of modifications to the UNB DIPOP software.

3.1 Short-term Repeatability

Short-term repeatability is often used, for projects of short duration, to assess the precision of a particular experiment. Some error sources have a degree of daily repetition. Multipath, neutral-atmosphere delay modelling error, and orbital force model error are sources of error likely to have a daily period [Bock, 1991; Blewitt, 1993]. Caution should be taken when dealing with extended observation periods on regional and global networks to account for relative site velocities. Plate motion models such as no-net-rotation-NUVEL-1 (NNR-NUVEL1) [Argus and Gordon, 1991] can be used to

transform site coordinates on a specific plate from an arbitrary epoch to the reference epoch. Repeatability is the criteria used to assess the success of experiments conducted by Bock and Murray [1988]; Davis et al. [1989]; Prescott et al. [1989]; and Larson and Agnew [1991]. Results from these experiments indicate, even with superseded 4 satellite receivers, repeatability for baselines up to 400 km in length are at the several millimetre level for north and east components, and at the few tens of millimetres level for the vertical component. The limited vertical precision is due to the fact that satellites are only visible above the viewer's horizon and hence sensitive to neutral-atmosphere delay calibration errors [Janes et al., 1991; Langley, 1992; Brunner and Welsch, 1993; Yunck, 1993], a factor of approximately three worse than north and east components [Dixon, 1991].

Dixon [1991] gives the weighted scatter about a mean value for components of regional size GPS baseline estimates as:

$$\text{STR} = \frac{\dfrac{n}{n-1} \sum_{i=1}^{n} \dfrac{(x_i - \bar{x})^2}{\sigma_i^2}}{\sum_{i=1}^{n} \dfrac{1}{\sigma_i^2}}, \tag{3.2}$$

where n is the number of observation sessions, x refers to the component under investigation (latitude, longitude, height, length), and σ^2 is the estimated formal variance of a particular component. Short-term repeatability will not take into account any long-term systematic errors that may be occurring; however, it provides a reliable tool to compare the precision of processing strategies.

3.2 Comparison with VLBI, SLR, and GPS

Repeatability is a good method for assessing precision; however, it is desirable to have some form of accuracy assessment. It is very difficult to assess the absolute accuracy of GPS determined baseline components, especially baselines of regional to global scale. A fully independent assessment of accuracy can not be guaranteed, since other techniques capable of producing the same information have

an uncertainty level approximately the same as GPS. One method of assessing the accuracy of GPS determined baselines is by comparison [Dixon, 1991]. Depending on the scale of the experiment, GPS can be compared to terrestrial techniques such as electro-optical distance meters (EDMs), or extra-terrestrial techniques such as VLBI and satellite laser ranging (SLR).

Comparison is currently the only method for estimating accuracy; although there may be some concern as to the independence of other techniques used in the comparison need to be defined. GPS is dependent on VLBI-derived coordinates for reference frame determination, i.e. earth orientation and rotation parameters used to define reference frames are primarily derived from VLBI observations; and, GPS and VLBI are both influenced in a similar fashion by residual neutral-atmosphere delays [Dixon, 1991]. When comparing GPS to VLBI and SLR it is essential that the vector between instrument reference points be adequately determined and accurately related to geodetic markers. Care should also be taken when considering the coordinates for which the comparisons are being made. Are the coordinates being compared at the same instance of time? Will station motion be significant? Davis et al. [1989] has demonstrated centimetre level agreement between GPS and VLBI determined geodetic baselines up to several hundred kilometres in length. Blewitt [1993] believes that comparison is perhaps the best available measure of accuracy.

3.3 Other Biases and Errors

To exploit the millimetre precision of GPS, it is necessary to observe the carrier phase of the GPS signals. To exploit the millimetre precision of the geodetic baseline estimation capability of GPS, it is necessary to eliminate, or greatly reduce, the biases and errors influencing the GPS observation equation. The major sources of error associated with high precision GPS geodetic baseline estimation are: clock biases in the receivers and satellites; atmospheric refraction in the ionosphere and neutral-atmosphere; satellite orbit estimates; carrier phase cycle ambiguities; multipath bias; and receiver noise error. The differencing of simultaneously observed signals, see eqn. (3.1), enables the elimination, or

reduction, of many of these errors and biases; however, residual amounts of error may remain which are significant in high precision baseline determination.

To eliminate receiver and satellite clock biases, excluding selective availability (SA) induced errors (see section 3.3.4), most analysis techniques employ double difference techniques. Doubly differenced observations are used in this research. Another option is to use undifferenced data to estimate the clock bias, rather than eliminate it by differencing. The clock bias estimation process uses a Kalman filter approach that models clock behaviour as a stochastic process. Stochastic models that have been used for estimation include: white noise; time-correlated coloured noise; polynomials; and combinations of the three [Blewitt, 1993]. Clock bias estimation by stochastic modelling has been successfully used in the GIPSY software for GPS orbit determination [Lichten and Border, 1987].

The following discussion highlights the significant sources of error in high precision GPS geodetic baseline estimation. Further information on GPS biases and errors can be found in: Kroger et al. [1986]; Wells et al. [1986]; Davis et al. [1989]; Delikaraoglou [1989]; King and Blewitt [1990]; Dixon [1991]; Larson et al. [1991]; and Blewitt [1993]. In this section, error sources that affect the GPS observation equation and analysis of geodetic baseline estimates, with the exception of the neutral-atmosphere, are reviewed.

3.3.1 Ionosphere

Changes in the velocity of propagation of GPS signals can be attributed to the refractive nature of the ionosphere and neutral atmosphere (see Kleusberg [1986]; Wells et al. [1986]; Coco [1991]; Janes et al. [1991]; Klobuchar [1991]; Langley [1992]; and Brunner and Welsch, [1993]). The presence of electrons in the ionosphere, the region of the earth's atmosphere located at an altitude of approximately 50 to 1000 km [Langley, 1992], is primarily due to solar ultraviolet radiation interacting with gaseous molecules to free outer-shell electrons. The electrons influence GPS signals by delaying the signal modulation (group

delay) and advancing the phase of the carrier (phase advance). The phase advance and group delay are frequency-dependent (dispersive) in the ionosphere, and are equal in magnitude, but of opposite sign, to a first-order approximation. The total delay is dependent on electron content along the signal path, solar activity, time of day, latitude, and elevation angle of observation [Dixon, 1991].

GPS ranging signals are transmitted on two frequencies. The two GPS carrier frequencies can be linearly combined to form an ionosphere-free combination [Wells et al., 1986, Seeber, 1993]:

$$\Phi(L_0) = \frac{1}{f_1^2 - f_2^2} [f_1^2 \Phi(L1) - f_2^2 \Phi(L2)], \tag{3.3}$$

where $\Phi(L_0)$ is the ionospheric-free phase observation, f_1 is the L1 carrier frequency, and f_2 is the L2 carrier frequency. If station separation is small (approximately less than 10 km), then ionospheric conditions are, under a quiescent ionosphere, sufficiently correlated that only single frequency measurements are necessary for reliable baseline estimates. This is due to the correlated ionospheric delay being greatly reduced by differencing. However, over longer distances correlation is weaker and dual frequency observation is essential.

3.3.2 Satellite orbits

High precision GPS relative positioning over long distances requires high precision GPS satellite orbit estimates. GPS orbit information comes from a variety of sources, such as the broadcast message and independent orbit estimations. GPS satellite orbits can be precisely determined by tracking the satellites from an extended network of ground stations with accurately known positions, e.g. VLBI or SLR sites where there is a co-located GPS receiver. Detailed discussions of GPS orbit estimation techniques are presented by Lichten and Border [1987]; Agrotis [1988]; Davis et al. [1989]; Delikaraoglou [1989]; Dong and Bock [1989]; Chen and Langley [1990]; King and Blewitt [1990]; Lichten [1990a, 1990b]; Dixon [1991]; Larson et al. [1991]; and Blewitt [1993].

A rule of thumb for estimating the influence of GPS orbit estimation uncertainty on a geodetic baseline is given by Lichten [1990a]:

$$\sigma_{bl} \approx (0.2)\sigma_{orb}L/h ,$$

(3.4)

where σ_{bl} is the uncertainty in the baseline component estimation, σ_{orb} is the uncertainty in the orbit estimation, L is the baseline length, and h is the satellite altitude. This approximation suggests that a more precise orbit than the broadcast ephemeris provides should be used when aiming for sub-centimetre level accuracy for baselines longer than 100 km, given that the broadcast ephemeris is accurate at approximately the 10 m level.

3.3.3 Receiver noise

Receiver noise is a random error source associated with GPS observations. Modern geodetic quality receivers have the ability to measure P-code pseudoranges on the L1 and L2 carriers, C/A-code pseudoranges on the L1 carrier, and full wavelength carrier phases on the L1 and L2 frequencies. In times of an encrypted P-code (see section 3.3.5) carrier phase tracking is done using code-less cross-correlating techniques (see for example: Meehan et al. [1992]; Ashjaee [1993]; and Trimble Navigation [1993]). Estimates of receiver noise levels are outlined in Table 3.1 for geodetic quality receivers.

Table 3.1 -- Approximate geodetic quality receiver noise levels.

Observable	Approximate signal wavelength	Approximate noise level
C/A-code	300 m	4 to 300 cm
P-code	30 m	1 to 30 cm
Carrier phase	20 cm	0.5 to 3 mm
Code-less carrier phase	20 cm	0.5 to 7 mm

Noise levels are dependent on the signal to noise ratio of the satellite signals at the receiver. A rule of thumb estimate suggests that receiver noise levels are at approximately 1% of the signal wavelength [Wells et al., 1986]. This rule is not true for the new generation of "super C/A-code" receivers that are

capable of tracking the C/A-code with a noise level of 4 cm [Wells et al., 1995] and the carrier phases with a noise level of 0.5 to 1.0 mm [Gourevitch et al., 1993].

3.3.4 Selective-availability

Selective availability (SA) is present in most Block II GPS satellites. Its presence can be described in two forms: (1) degradation of the ephemeris in the navigation message; and (2) frequency changes are introduced on the L1 and L2 signals. Considering data received is tagged at receive time, and SA is common at transmission time differencing will not completely eliminate the SA induced clock biases, particularly when station separations are large; however, Dixon [1991] estimates that the maximum error induced by form (2), at current levels of SA, would result in only millimetre level uncertainties on even the longest of baselines.

3.3.5 Anti-spoofing

Since January 1994 the GPS P-code has been encrypted with a classified algorithm for United States national security reasons. The resulting code is called the Y-code. Only authorised users (mainly military) will have access to the Y-code. The primary purpose of the encryption is to prevent the intentional falsification of GPS signals; thus, the term anti-spoofing (AS). Without the use of a precise pseudorange many high precision applications suffer. The use of cross-correlating receiver technology is one saving grace. Table 3.2 summarises the analysis of Zumberge [1994] who has estimated experimentally and theoretically the degradation of median daily repeatability due to the impact of AS for non-fiducial sites of the International GPS Service for Geodynamics (IGS) global GPS network. An approximately 30% increase in the magnitude of the median repeatability is observed for all components of the non-fiducial stations.

Table 3.2 -- Degradation of the median daily repeatability due to the impact of anti-spoofing for non-fiducial stations of the global IGS network (after Zumberge [1994]).

geodetic component	observed degradation	expected degradation
north	29%	25%
east	28%	26%
vertical	32%	53%

3.3.6 Multipath, scattering and phase centre variation

Electromagnetic signals observed by a GPS receiver's antenna are sensitive to the effect of signals reflected by nearby surfaces. The interference of one or more reflected signals with the direct signal is known as multipath. The resultant signal's amplitude and phase are altered by the interfering signal. For carrier phase observations this effect on range may reach up to 5 cm [Seeber, 1993]. The periodicity and amplitude of the multipath error is dependent on the geometry of the receivers, satellites and reflectors contributing to the error. The typical periodicity of multipath signatures is of the order of a few to tens of minutes [Muller et al., 1989]. Low elevation angle observations are more likely to produce multipath interference; hence, the use of elevation mask angles (nominally 10 to 15 degrees). The use of mask angles improves the reliability of observations by reducing exposure to (1) multipath effects; (2) prediction of neutral-atmosphere effects which are prone to break down at low elevation angles; and (3) high order ionospheric effects. Some "Band-Aid" solutions for reducing the effect of multipath are: use of antenna ground planes or radio frequency absorbent material, filtering of the repetitive multipath signal, and increasing observation periods to longer than the multipath signal period. A preventative solution to multipath is careful location of the antenna.

Another form of interference of GPS signals is known as scattering, i.e. the diffraction of signals by nearby objects that can interfere with the reception of the direct signal. Elósegui et al. [1994] and Niell et al. [1994] report on centimetre level discrepancies in estimated residual neutral-atmosphere delays and height estimates possibly due to scattering from a concrete pillar that supports the antenna.

A GPS receiver's antenna phase centre is not a stable reference point. Variations in the antenna phase centre position are dependent on the elevation angle and azimuth of the observed signal (see for example Tranquilla [1986]). According to anechoic chamber measurements of some common geodetic GPS antennae, Schupler et al. [1994] show variations in phase centre that could have potentially centimetre level effects on GPS relative positioning. Models to account for these elevation angle and azimuth dependencies can be incorporated in the processing of GPS observations, and have been used successfully in GPS relative positioning (see for example Braun et al. [1994]).

3.3.7 Carrier phase cycle ambiguities

Fixing the carrier phase cycle ambiguities to integer numbers can increase the precision and accuracy of the east and north geodetic baseline components, for baseline lengths up to 2000 km [Blewitt, 1989], by a factor of two to three. Ambiguity resolution techniques for regional to global scale networks are discussed in detail by: Dong and Bock [1989], and Blewitt [1989]. A brief outline of the requirements for resolving cycle ambiguities for long to very long baselines is given by Blewitt [1993]: a mixture of baseline lengths aids the resolution process; long baselines provide good parallax conditions for GPS satellite orbit estimation; solving ambiguity terms for short baselines improves the ambiguity term estimates for the longer baselines by utilising the correlation between ambiguity term parameters.

DIPOP, in its form used in this study, does not employ the full correlation of baseline components in a network adjustment; thus, the "bootstrapping" technique as outlined by Blewitt [1993] can not be used. The sequential fixing of ambiguities is an option to consider for future DIPOP improvements. However, this will require one of two additional improvements: (1) use of pseudorange observations, or (2) use of an ionospheric model. One of these two techniques will need to be implemented since the sequential ambiguity resolution schemes of Blewitt [1989] and Dong and Bock [1989] require the use of the wide-lane observable which is sensitive to ionospheric biases. Santos' [Santos, 1995b] DIPOP version for real-time GPS satellite orbit improvement includes the full mathematical correlation of baselines in a

network, and hence would be well suited to the implementation of a "bootstrapping" ambiguity resolution technique.

3.4 Software Development

DIPOP 1.0 (DIfferential POsitioning Program version 1.0) was developed in the early 1980s on the University of New Brunswick's (UNB) Department of Surveying Engineering's (now Department of Geodesy and Geomatics Engineering) HP 1000 mini-computer. Since then DIPOP has been modified many times by staff, graduate students, and post-doctoral researchers working on space geodetic activities. DIPOP now exists in many specific task oriented forms, such as DIPOP-E for orbit improvement studies, DIPOP-ERP for earth rotation parameter estimation, DIPOP 2.1 the distributed version for general GPS processing, the real-time orbit improvement version of DIPOP [Santos, 1995b], and the current DIPOP 3.0 which houses the modifications made for this research. The concept, creation and evolution of the DIPOP suite of programs are documented in Beutler et al. [1984]; Langley et al. [1984]; Vanicek et al. [1985]; Santerre et al. [1985]; Kleuberg et al. [1989]; Chen [1991]; and Li [1994].

The contributions of this research in terms of modifications to DIPOP (version 2.1 was used as the platform for modification) are (1) installation of the HISUB subroutine to account for different geodetic antennae phase centre locations (subroutine HISUB is from the GAMIT software suite and was provided courtesy of Yehuda Bock of the Scripps Institute of Oceanography, La Jolla, California); (2) addition of residual neutral-atmosphere delay parameters, with variable validity time, included in the weighted least squares adjustment of DIPOP 2.1; (3) implementation of a Kalman filtering algorithm, that doubles as a sequential least squares algorithm, for the stochastic estimation of residual neutral-atmosphere delays; and (4) additional vectors for the storage of post-fit observation residuals for multiple baselines, allowing the plotting of all baseline residual sets from a network solution.

51

CHAPTER 4

SOUTHERN CALIFORNIA ARRAY TEST

Evaluation of the estimation strategies was performed by analysis of data from the PGGA in California. Five baselines of regional length, 55 to 686 km, have been analysed. The range of baseline lengths is typical of regional size geodetic, geodynamic, and geophysical studies where accuracy, particularly rate accuracy, of geodetic monument positions is of the utmost importance. The object of the analysis of the test array was to determine the sensitivity to a priori constraints, and the achievable accuracy of each of the techniques outlined in Chapter 3. "A priori constraints" is defined in this chapter as being the constraints placed on the neutral-atmosphere delay estimates.

Considering that the a priori constraints being investigated relate to an essentially non-deterministic process, it is important that the user of these estimation techniques be aware of the consequences of an inappropriate choice of constraints. Hence, the study of the sensitivity of estimated baseline components, specifically height and length, to realistic variations in the constraints. A priori constraints imply stochastic coefficient values for the filtering strategies, and a priori weights and parameter validity times for the conventional adjustment strategy. In this way, an estimate of the best achievable precision for this data set is obtained for each of the methods under investigation.

For the conventional weighted least squares approach, varying the number of estimated neutral-atmosphere delay parameters and the a priori standard deviation of them allows the mapping of these two coefficients versus the estimated baseline component short-term repeatability as defined in section 3.1. In the case of the Kalman filtering and sequential weighted least squares techniques, two stochastic processes that characterise the neutral-atmosphere delay variability have been investigated: the first order Gauss-Markov and the random walk stochastic processes. The sensitivity of estimated baseline component short-term repeatability is investigated by varying the correlation time and steady state

standard deviation for the Gauss-Markov case and the process noise rate of change for the random walk case.

The accuracy assessment of the techniques is performed by method of comparison with the only feasible independent method available: a combined VLBI, SLR, and GPS coordinate set. The comparison coordinates are from the International Earth Rotation Service (IERS) Terrestrial Reference Frame of 1993 (ITRF93). The heights and lengths of the estimated baseline components are investigated. The height component is the most affected by residual neutral-atmosphere propagation delays. The baseline length estimates will show the combined affect on all three components (latitude, longitude, and height). Site locations were chosen in order to cover the range of baseline lengths that is typical of regional studies. The sites are all equipped with high precision dual-frequency geodetic quality receivers. Table 4.1 lists the sites, their location, receiver type, and approximate geodetic height in metres above the WGS84 ellipsoid. The heights are listed to emphasise the variety of interstation vertical separations. Since the main objective of eliminating residual neutral-atmosphere delay is to improve the precision and accuracy of the height determination, stations covering a range of vertical separations were analysed.

Table 4.1 -- California test array station summary.

Station name	Station location	Receiver type (frequency standard)	Approximate geodetic height (m)
JPL1	Pasadena, Ca.	Rogue SNR-8 (Rubidium)	424
DS10	Goldstone, Ca.	Rogue SNR-8 (Maser)	987
PIN1	Piñon Flats, Ca.	Ashtech Z-12 (Internal)	1256
PVEP	Palos Verdes, Ca.	Trimble 4000SST (Internal)	70
VNDP	Vandenberg AFB, Ca.	Rogue SNR-8 (Rubidium)	-11
QUIN	Quincy, Ca.	Rogue SNR-8000 (Internal)	1106

The interstation separation of the network provides a good variation of typical regional size baselines. The distribution of the test array stations is depicted in Figure 4.1. The network is in the seismically-active region of the San Andreas fault system. For this reason, the data covers a relatively short interval of time during which no major seismic activity occurred. One day after the last day of analysed data a major earth-quake shook the California district of Northridge. This quake significantly changed the relative separation of several of the test network sites at the few centimetre level. The IGS-ITRF93 coordinates for the test array sites were adjusted to the test epoch using site velocities provided with the coordinate set.
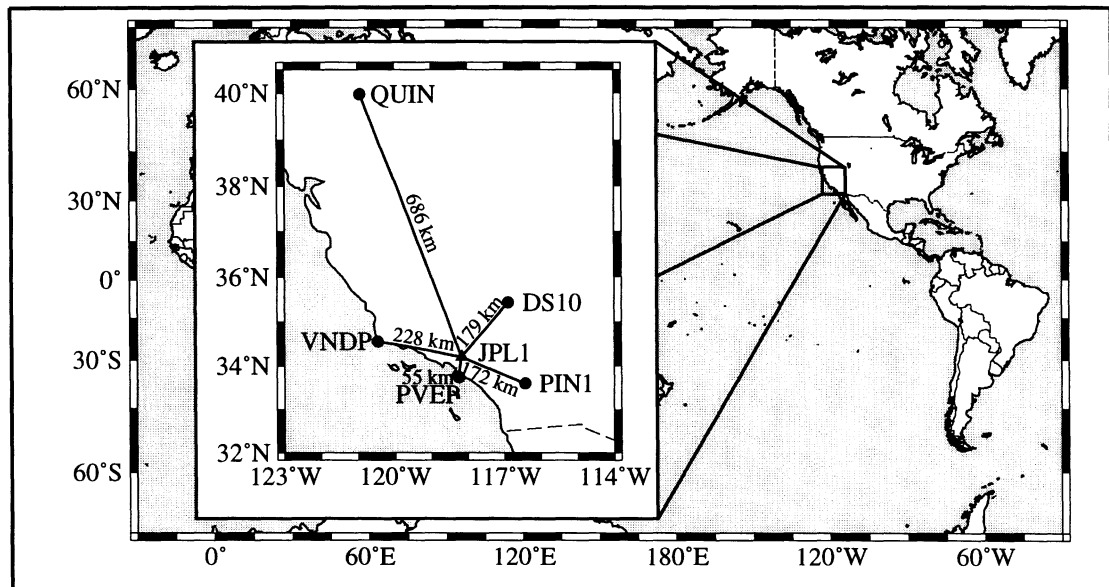
Figure 4.1 -- Location of test array stations.

Section 4.1 outlines the parameter estimation strategy and reviews the error and bias contributions likely to affect the analysis. Section 4.2 summarises the sensitivity analysis of the three estimation techniques. Section 4.3 summarises the coordinate comparison analysis results. Section 4.4 discusses the equivalence and similarities of the sequential weighted least squares and Kalman filtering

54

approaches. Section 4.5 is a general discussion of all results. It brings together the separate analysis

results and compares them to assess the strengths and weaknesses of each technique.

4.1 Parameter estimation strategy

The analysis strategy is driven by the need to: (1) minimise errors and biases likely to affect the

interpretation of results, and (2) maximise the ease of the evaluation process. The data set from the star

shaped test array equipped with high quality geodetic receivers facilitates both of these objectives. The

general parameter estimation and specific filter and adjustment strategies employed are outlined in

Table 4.2. The a priori neutral-atmosphere delay models are driven by default surface meteorological

values (1013.25 mbar pressure, 15° C temperature, and 50% relative humidity) for all sites.

Table 4.2 -- Parameter estimation strategy.

Strategy	Parameter	A priori value
General	Satellite positions	Fixed, post-fitted SIO orbits used
	Fixed station (JPLM)	Constrained to 0.1 mm
	Floating stations	Constrained to 0.1 m
	Carrier phase measurement noise	12 mm - Rogue receiver
		15 mm - Ashtech/Trimble receiver
	Neutral-atmosphere dry zenith delay	Saastamoinen
	Neutral-atmosphere wet zenith delay	Saastamoinen
	Neutral-atmosphere dry mapping function	Ifadis
	Neutral-atmosphere wet mapping function	Ifadis
	Solution type	Ionosphere-free linear combination of double difference phases
	Carrier phase cycle ambiguities	Estimated as real numbers
	Data elevation mask angle	15 degrees
Kalman filter	Treatment of Neutral-atmosphere	Estimate zenith correction to a priori model values for each station
	Neutral-atmosphere parameters	Gauss-Markov random variables
Least squares	Treatment of Neutral-atmosphere	Estimate zenith corrections to a priori model values for each station
	Neutral-atmosphere parameters	Constant variables, valid for variable time intervals

The dual-frequency combination of full wavelength carrier phase observations used in this analysis eliminates, up to a very good first-order approximation, ionospheric effects. Higher order terms are generally considered to be insignificant (few millimetre level) in most precise GPS geodetic surveys and positioning techniques using radio frequencies above 1 GHz, however they may have serious effects (few centimetre level) under certain conditions See Yunck [1993] for a review of high order ionospheric effects on high precision space geodetic techniques.

Post-fitted estimates of GPS satellite orbits from the Scripps Institute of Oceanography (SIO) IGS data processing/analysis centre have been used to minimise orbit uncertainty effects. From eqn. (3.4) the effect of orbit uncertainty on the estimated baseline components can be investigated. Assuming the SIO post-fitted orbits to be accurate to at least the 0.5 m level, which is a pessimistic estimate according to Santos [1995a], the effect on baseline component estimates for the range of baseline lengths in this study would be at the 0.3 to 3.4 mm level.

The high quality data supplied by the test array receivers ensures that the best available data for the analysis was used. However, the combination of L1 and L2 carrier phase observations to form the ionospheric-free observable results in an amplification of the observation noise level by a factor of approximately three. With the estimated noise levels of the L1 and L2 carrier phase observables at the 2 to 3 mm level (see Table 3.1), the resulting 6 to 9 mm noise level is what dominates the post-fit observation residuals; see for example the lower two panels of Figure 1.1 where the r.m.s. scatter of the residuals is at the 10 mm level.

Selective availability (SA) is an error source that cannot be directly reduced by non-authorised users (this includes geoscientists). Fortunately, its effect on baseline component estimates is, at most, at the single millimetre level [Dixon, 1991]. Anti-spoofing (AS) is another factor that prevents non-authorised users accessing the full accuracy of GPS. For this reason, the test array data set spanned a period of

time prior to the full-time encryption of Block II satellite P-codes. Had the experiment been pursued under AS conditions Zumberge [1994] estimates an approximately 30% increase in the uncertainty of all baseline component estimates. Since this study is an evaluation, and mainly a comparison, of three estimation techniques it was considered that the data set should be of optimum quality; hence the use of non-AS affected data.

The effect of multipath and its removal from space geodetic data is one of the current topics of ongoing research in the space geodetic community. As such, it is difficult to deal with multipath effects in ways other than the obvious, i.e. place receiver antennae in sites that are likely to be immune from multipath effects. Currently, mainly experimental empirical methods for reducing the multipath effects are being used (for example Bock [1991], and Genrich and Bock [1992]). The new generation of GPS receivers include design features that help to minimise multipath effects. The receiver locations used in this analysis show relatively low levels of multipath when analysed with the UNAVCO QC software [UNAVCO, 1994]. Considering that this evaluation is a comparative one and the data is investigated for ten days with a repeating satellite constellation, the effect of any multipath on the precision and accuracy comparisons will be minimal. However, any multipath effects present will affect the magnitude of precision and accuracy attained.

Carrier phase cycle ambiguity resolution for baselines of regional length can improve the accuracy and precision of baseline component estimates by up to a factor of three. However, correct resolution of carrier phase ambiguities for baseline lengths exceeding 20 km is difficult and requires the use of either pseudorange observations and/or a priori ionospheric calibration (see Blewitt [1989], and Dong and Bock [1989]). The DIPOP software does not currently have these options; hence, it is recommended for future studies in this area to include an ambiguity resolution scheme for long baselines as outlined in section 3.3. An investigation into the level of correlation between neutral-atmosphere delay and carrier

phase cycle ambiguity estimates revealed mathematical correlation at the sub 10% level. Hence it is anticipated for this study that the effect of not resolving carrier phase cycle ambiguities is minimal.

For the conventional weighted least squares analysis of the residual neutral-atmosphere delay the a priori standard deviation was varied between 0.5 and 80 mm and the number of epochs for which a delay parameter was valid was varied between 10 and 720 epochs (5 minutes and 6 hours respectively). In the case of the Kalman filter first-order Gauss-Markov stochastic process, a mesh of a priori constraints ranging from 1 to 20 hr correlation time and 0.5 to 80 mm steady state standard deviation was investigated. For the Kalman filter random walk investigation the range of random walk process noise rate of change was varied between 0 and 110×10^{-2} mm/$\sqrt{s}$. Table 4.3 details the investigated a priori coefficients.

Table 4.3 -- Strategy of the investigation of a priori constraints of the residual neutral-atmosphere delay.

Strategy	Type of constraint (units)	A priori constraints investigated
Conventional weighted least squares	a priori standard deviation (mm)	0.5, 1.5, 2.5, 5.0, 7.5, 10.0, 12.5, 20.0, 35.0, 50.0, 65.0, 80.0
	neutral-atmosphere parameter validity (min.)	10, 30, 60, 120, 180, 360, 720
Kalman filter Gauss-Markov	steady state standard deviation (mm)	0.5, 1.5, 2.5, 5.0, 7.5, 10.0, 12.5, 20.0, 35.0, 50.0, 65.0, 80.0
	correlation time (hr)	1.0, 2.5, 5.0, 7.5, 10.0, 12.5, 15.0, 17.5, 20.0
Kalman filter random walk	rate of change of process noise (10^{-2} mm/$\sqrt{s}$)	0.0, 0.5, 1.5, 2.5, 5.0, 7.5, 10.0, 12.5, 15.0 17.5, 20.0, 35.0, 50.0, 65.0, 80.0, 95.0, 110.0

According to Mendes and Langley [1994], the Ifadis mapping function represents one of the most accurate mapping functions down to 15° elevation angle. The Ifadis mapping function was used in this analysis for the prediction and estimation components of the adjustments and filtering of the data. According to Janes et al. [1991], the Saastamoinen zenith delay model provides the best prediction of neutral-atmosphere delays based on a ray-tracing comparison. The Saastamoinen zenith delay model is used in this analysis for the a priori prediction of the combined, wet plus hydrostatic, neutral-atmosphere delay.

4.2 Sensitivity to a priori constraints

The sensitivity of baseline component estimates, in the form of short-term repeatability, has been investigated. The results of this analysis are presented in this section and reveal the effects of varying the a priori constraints, as described in Table 4.3, on the conventional weighted least squares and Kalman filtering estimation strategies. Short-term repeatability is mapped as a function of (1) the neutral-atmosphere parameter estimation interval and a priori standard deviation for the conventional weighted least squares case (see section 4.2.1); (2) the correlation time and steady state standard deviation for the Kalman filter first order Gauss-Markov case (see section 4.2.2.1); and (3) the process noise rate of change for the Kalman filter random walk case (see section 4.2.2.2). A summary of the precision analysis is given in section 4.5 where the ranges and optimum precision values of the are presented.

4.2.1 Conventional weighted least squares

Figures 4.2 to 4.6 depict the height and length short-term repeatability of the five test baselines. The figures are ordered according to increasing length. The height component is significantly more sensitive than the length of the baselines to changes in a priori constraints. The level of short-term repeatability of the height component is generally a factor of 2 to 3 larger than the length (as expected from section 2.5). Variation in parameter estimation interval (est. int.) is approximately as sensitive in terms of short-

term repeatability as variation in a priori standard deviation. Significant variation in precision, when considering geodetic applications, is apparent for all baselines within the range of tested conditions. In certain cases, a factor of two improvement when using the correct constraints cán be achieved in short-term repeatability as compared to the worst cases.

Height -- JPLM to PVEP (55 km)

Length -- JPLM to PVEP (55 km)
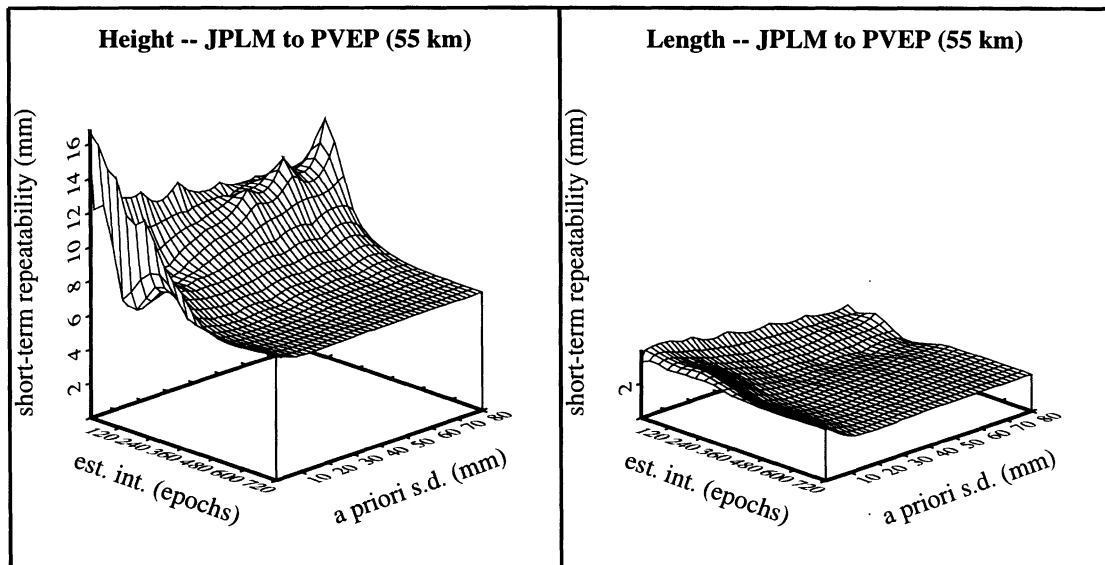
Figure 4.2(a)

Figure 4.2(b)

Figure 4.2(c)

Height -- JPLM to VNDP (228 km)   **Length -- JPLM to VNDP (228 km)**

Figure 4.2(d)

Height -- JPLM to QUIN (686 km)   **Length -- JPLM to QUIN (686 km)**
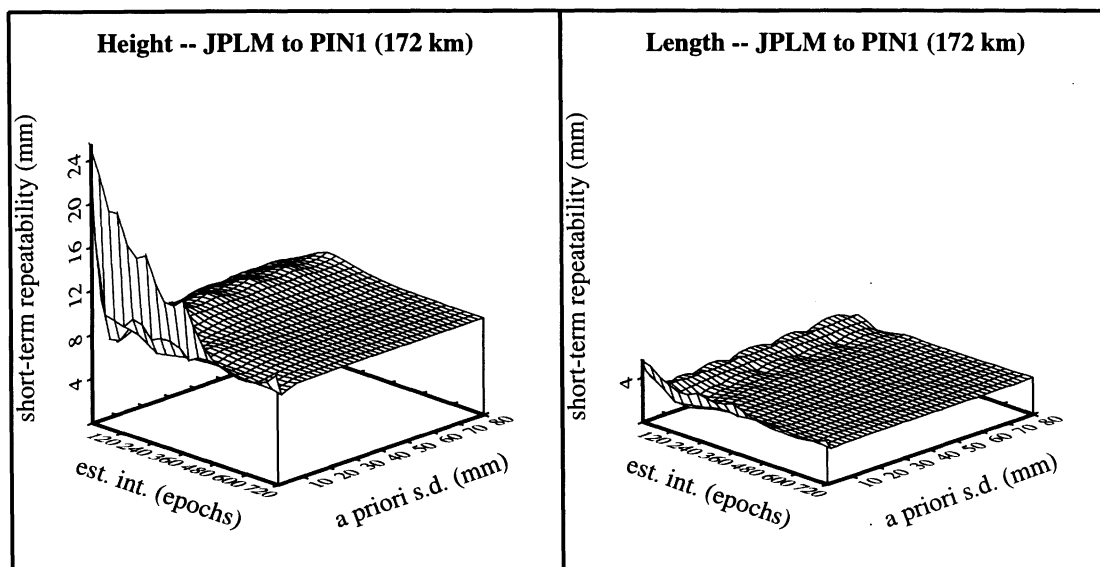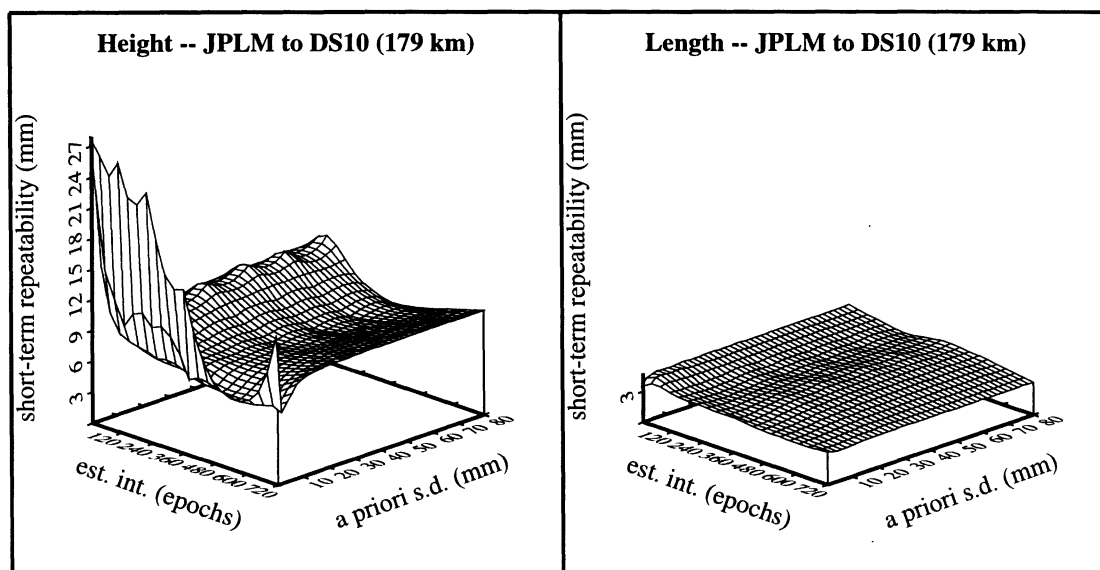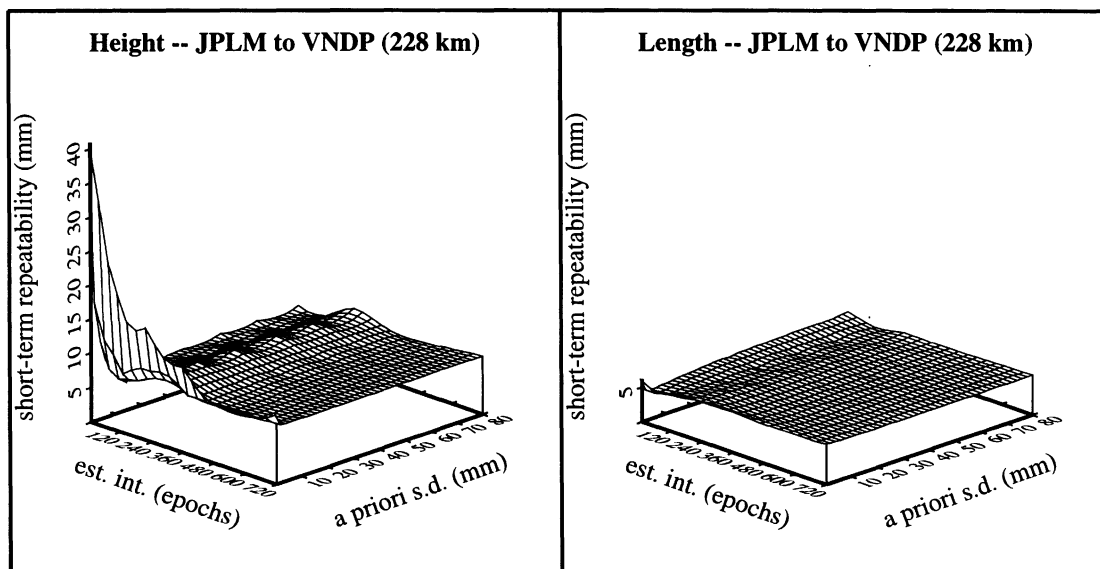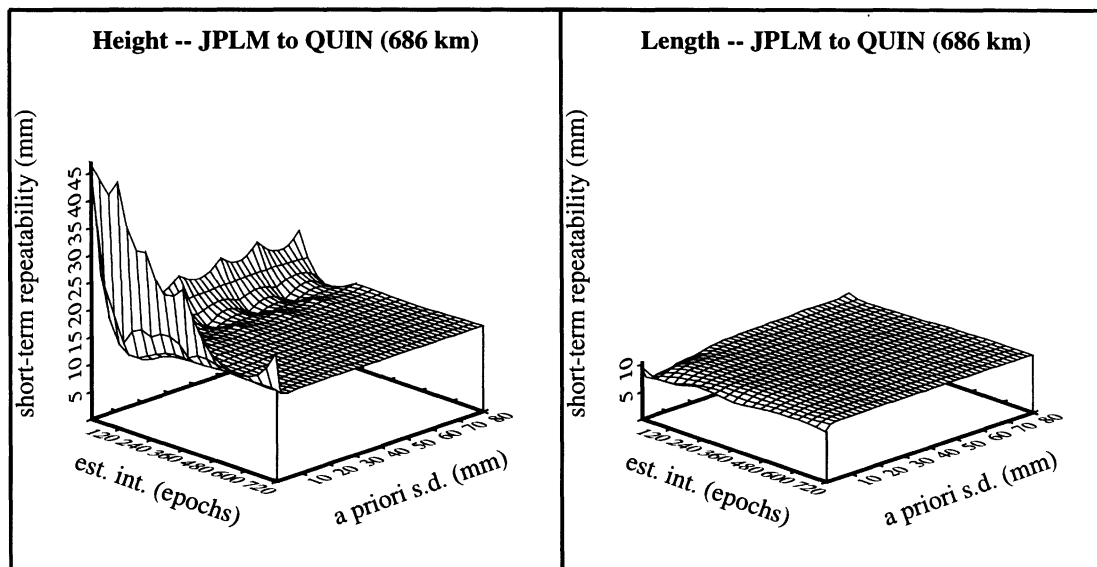
Figure 4.2(e) -- Estimating the residual neutral-atmosphere delay with a conventional weighted least squares algorithm. Short-term repeatability for height and length estimates of the baselines: (a) JPL1 to PVEP, (b) JPL1 to PIN1, (c) JPL1 to DS10, (d) JPL1 to VNDP, and (e) JPL1 to QUIN.

4.2.2 Kalman filtering

This section summarises the analysis of the Kalman filter with first order Gauss-Markov (section 4.2.2.1) and random walk (section 4.2.2.2) stochastic processes used to characterise the estimated residual neutral-atmosphere delay variability.

4.2.2.1 First-order Gauss-Markov stochastic process

Figures 4.7 to 4.11 show the height and length short-term repeatability for the case of estimating the residual neutral-atmosphere delay as a first order Gauss-Markov stochastic process. Height is more sensitive to variation in correlation time and steady state deviation than length. The level of short-term repeatability for height is approximately a factor of 2 to 3 larger than the length short-term repeatability. Variation in steady state deviation is more sensitive in terms of short-term repeatability than the correlation time for the a priori constraints investigated. An inappropriate choice of a priori conditions can result in a height precision degradation of a factor of 2 to 3.

Figure 4.3(a)

63
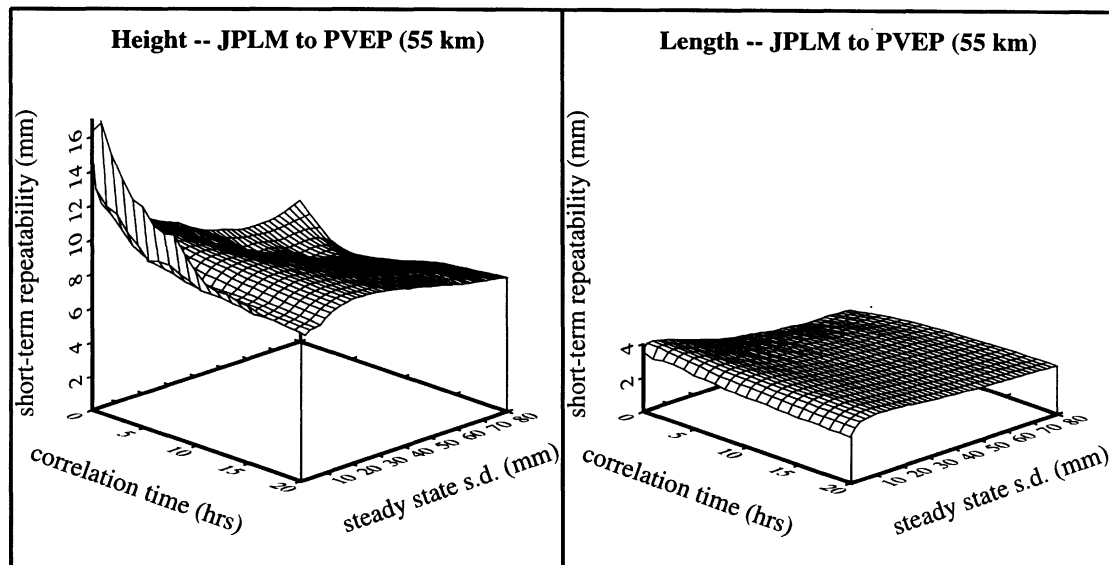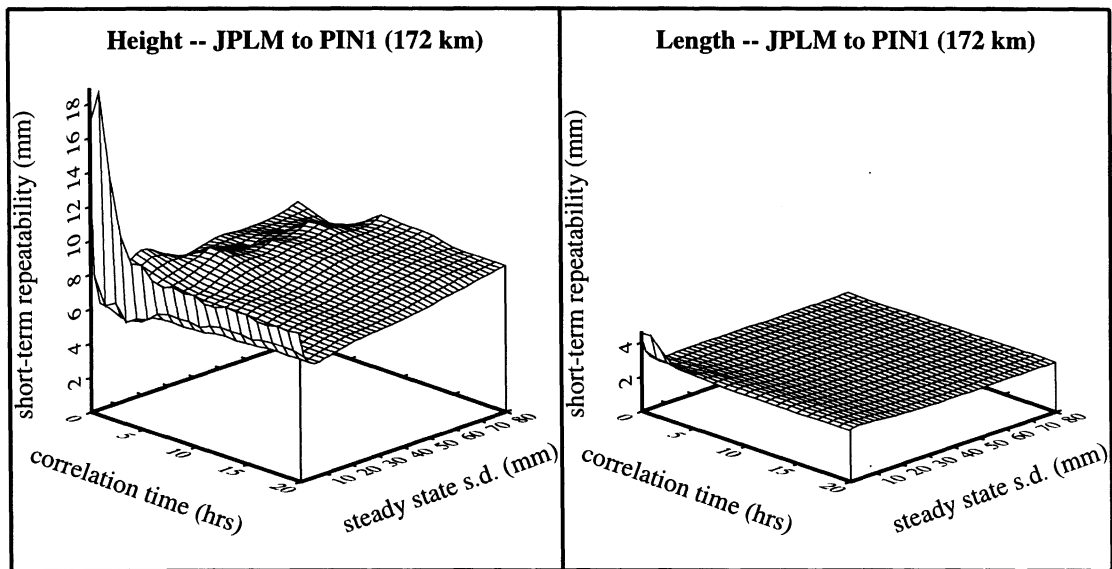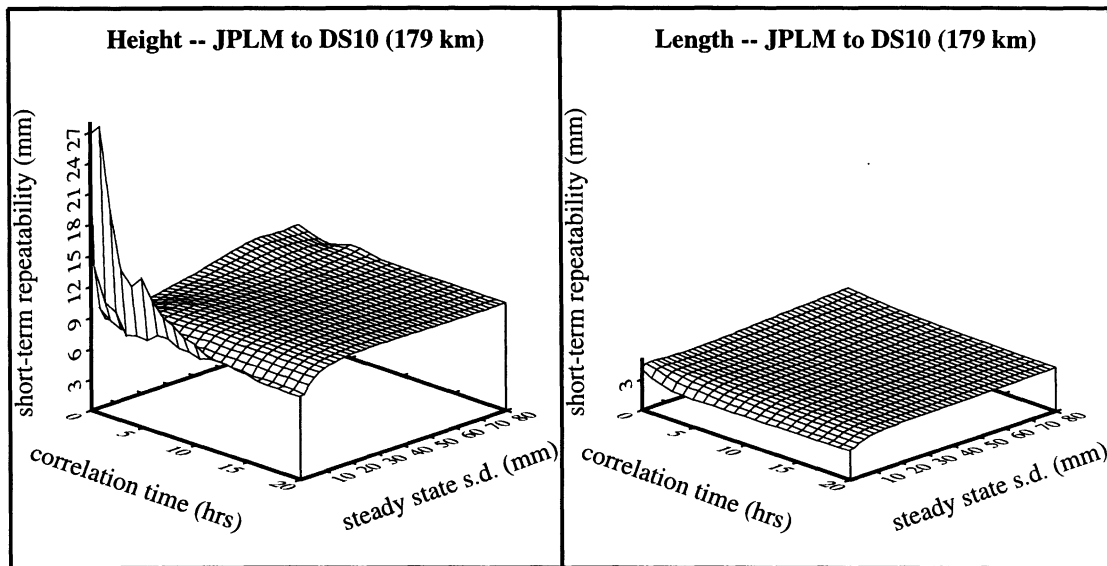
Figure 4.3(b)

Figure 4.3(c)
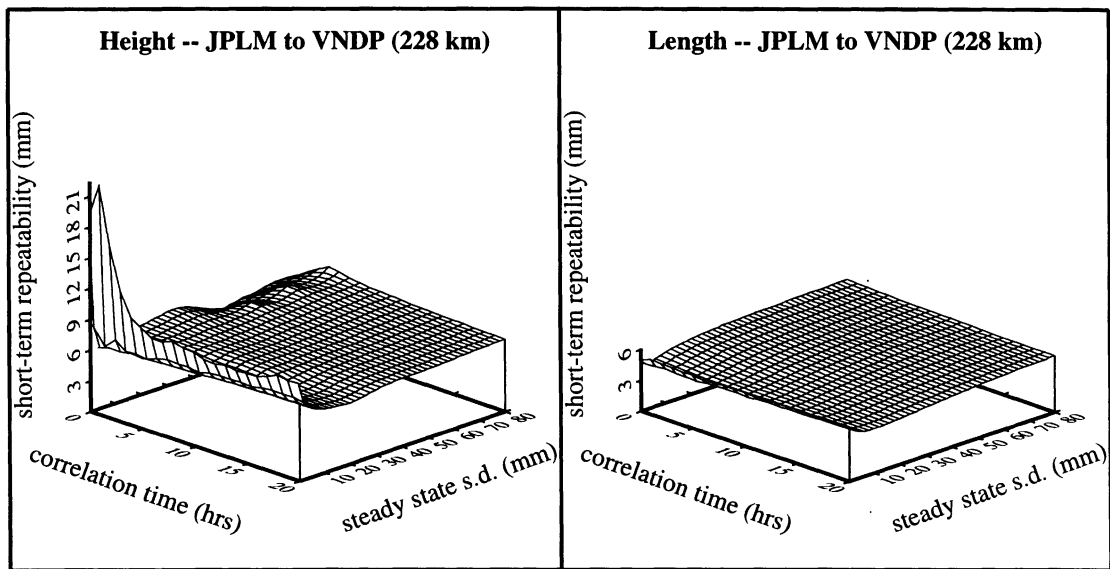
Figure 4.3(d)
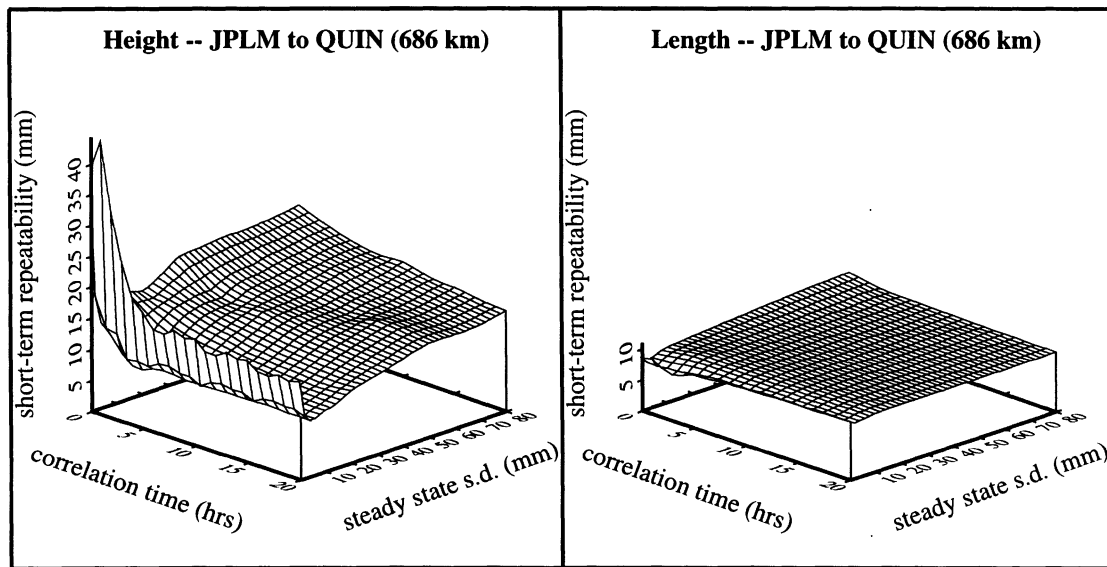
Figure 4.3(e) -- Estimating the residual neutral-atmosphere delay with a Kalman filter (Gauss-Markov) algorithm. Short-term repeatability for height and length estimates of the baselines: (a) JPL1 to PVEP, (b) JPL1 to PIN1, (c) JPL1 to DS10, (d) JPL1 to VNDP, and (e) JPL1 to QUIN.

4.2.2.2 Random walk stochastic process

Figures 4.12 to 4.16 summarise the short-term repeatability of height and length components when estimating the delay variability using a random walk stochastic process. Height is typically more sensitive to variation of process noise rate of change than the length. On the shortest baseline, the optimum short-term repeatability occurred for the case of estimating the delay with one constant parameter for the whole observation session (zero rate of change of the process noise). Height is a factor of 1.5 to 3 larger in short-term repeatability than length for the a priori conditions investigated. The minimum short-term repeatability appears to have no correlation with baseline length, or vertical separation, highlighting the non-deterministic nature of the residual delay.

JPL1 to PVEP (55 km)

y-axis: short-term repeatability (mm), values 0, 5, 10, 15
x-axis: standard deviation rate (mm/s$^{0.5}$ E-02), values 0, 50, 100
curves: height, length

Figure 4.4(a)

66

Figure 4.4(b)

Figure 4.4(c)

JPL1 to VNDP (228 km)

JPL1 to QUIN (686 km)
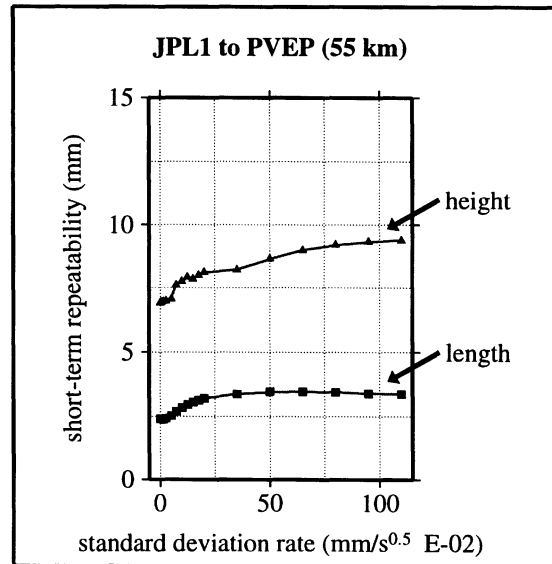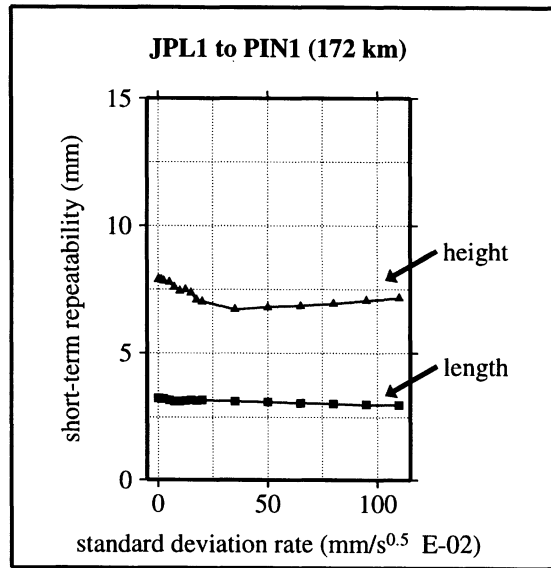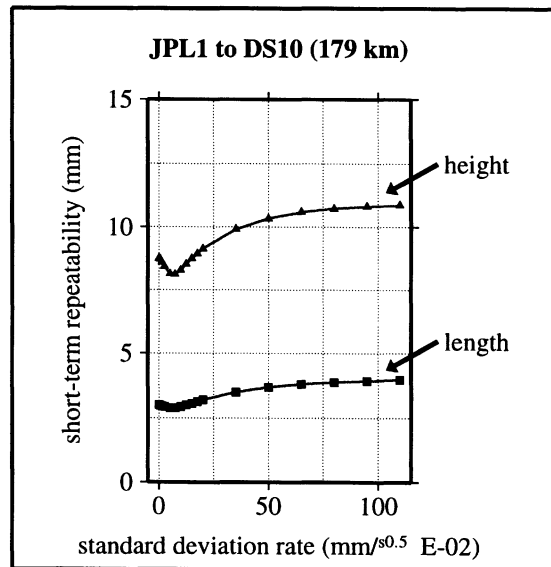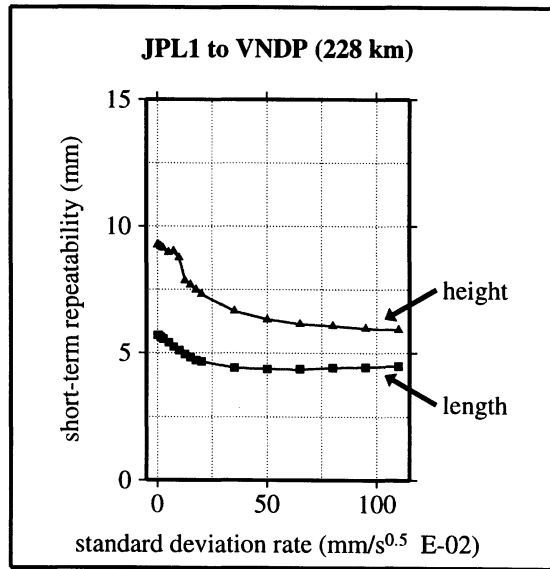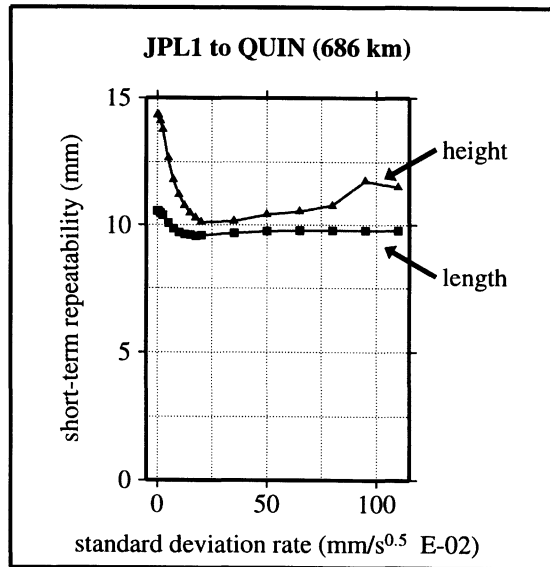
Figure 4.4(d)

Figure 4.4(e) -- Estimating the residual neutral-atmosphere delay with a Kalman filter (random walk) algorithm. Short-term repeatability for height and length estimates of the baselines: (a) JPL1 to PVEP, (b) JPL1 to PIN1, (c) JPL1 to DS10, (d) JPL1 to VNDP, and (e) JPL1 to QUIN

4.3 Comparison with IGS-ITRF coordinates

This section summarises the accuracy assessment component of the study. Coordinates of the IGS-ITRF93, adjusted to the experiment epoch, are compared with DIPOP 3.0 baseline component estimates. This comparison shows only the results from the 'best' solutions based on short-term repeatability. Additionally, section 4.2.1 highlights the effect of not estimating residual neutral-atmosphere delay parameters.

4.3.1 Ignoring residual neutral-atmosphere delay

The ionospheric-free solution for the five baselines is summarised in Figure 4.17. Error bars, the formal estimates of uncertainty, are plotted at the same scale as the displacements. Vertical and horizontal scales are the same for all plots. The vertical scale origin in each plot is shifted so that the 10 day mean displacement is near centre. DIPOP estimates of height vary by up to 14 cm from the IGS-ITRF93 values; whereas, the length estimates are typically within 1 cm of the IGS-ITRF93 derived lengths.

Figure 4.5 -- No residual neutral-atmosphere delay estimation discrepancy between DIPOP and IGS-ITRF93 estimates of height and length for the five test baselines. The dashed line represents the 10 day DIPOP solution mean value.

4.3.2 Conventional weighted least squares

The comparison of the conventional weighted least squares approach to residual neutral-atmosphere delay estimation with IGS-ITRF93 is summarised in this section. Figure 4.18 shows the discrepancy time-series for height and length of the five test baselines. The minimum height short-term repeatability solution was chosen for the accuracy analysis. The solution chosen is shown in the comparison plots as "e***sd***", where e*** is the estimation interval in epochs of the chosen solution, and sd*** is the a priori standard deviation of the residual delay parameters in millimetres of the chosen solution. The vertical and horizontal scales are the same. Error bars, showing the estimated formal uncertainty, are represented at the true scale. The vertical scale origins are shifted in each window so that the 10 day average estimate is near centre. Estimated uncertainties for the height components are generally a factor of 2 to 4 larger than their length estimate uncertainty counterparts. The DS10 and VNDP heights agree at the single centimetre level with the IGS-ITRF93 values. However, the other height estimates agree at the 4 to 7 cm level. Baseline lengths agree at the less than 2 cm level in all cases.

Height -- JPLM to PVEP (55 km)

ITRF93 - DIPOP (m)

e720 sd7.5

-0.06
-0.07
-0.08
-0.09

6 8 10 12 14 16 18
day of year (1994)

Length -- JPLM to PVEP (55 km)

ITRF93 - DIPOP (m)

e720 sd7.5

0.01
0.00
-0.01
-0.02

6 8 10 12 14 16 18
day of year (1994)

Height -- JPLM to PIN1 (172 km)

ITRF93 - DIPOP (m)

e30 sd5.0

-0.06
-0.07
-0.08
-0.09

6 8 10 12 14 16 18
day of year (1994)

Length -- JPLM to PIN1 (172 km)

ITRF93 - DIPOP (m)

e30 sd5.0

0.01
0.00
-0.01
-0.02

6 8 10 12 14 16 18
day of year (1994)

Height -- JPLM to DS10 (179 km)

ITRF93 - DIPOP (m)

e360 sd2.5

0.03
0.02
0.01
0.00

6 8 10 12 14 16 18
day of year (1994)

Length -- JPLM to DS10 (179 km)

ITRF93 - DIPOP (m)

e360 sd2.5

0.02
0.01
0.00
-0.01

6 8 10 12 14 16 18
day of year (1994)

Height -- JPLM to VNDP (228 km)

ITRF93 - DIPOP (m)

e10 sd20.0

0.01
0.00
-0.01
-0.02

6 8 10 12 14 16 18
day of year (1994)

Length -- JPLM to VNDP (228 km)

ITRF93 - DIPOP (m)

0.00
-0.01
-0.02
-0.03

e10 sd20.0

6 8 10 12 14 16 18
day of year (1994)

Height -- JPLM to QUIN (686 km)

ITRF93 - DIPOP (m)

e120 sd10.0

0.06
0.05
0.04
0.03

6 8 10 12 14 16 18
day of year (1994)

Length -- JPLM to QUIN (686 km)

ITRF93 - DIPOP (m)

e120 sd10.0

0.02
0.01
0.00
-0.01

6 8 10 12 14 16 18
day of year (1994)

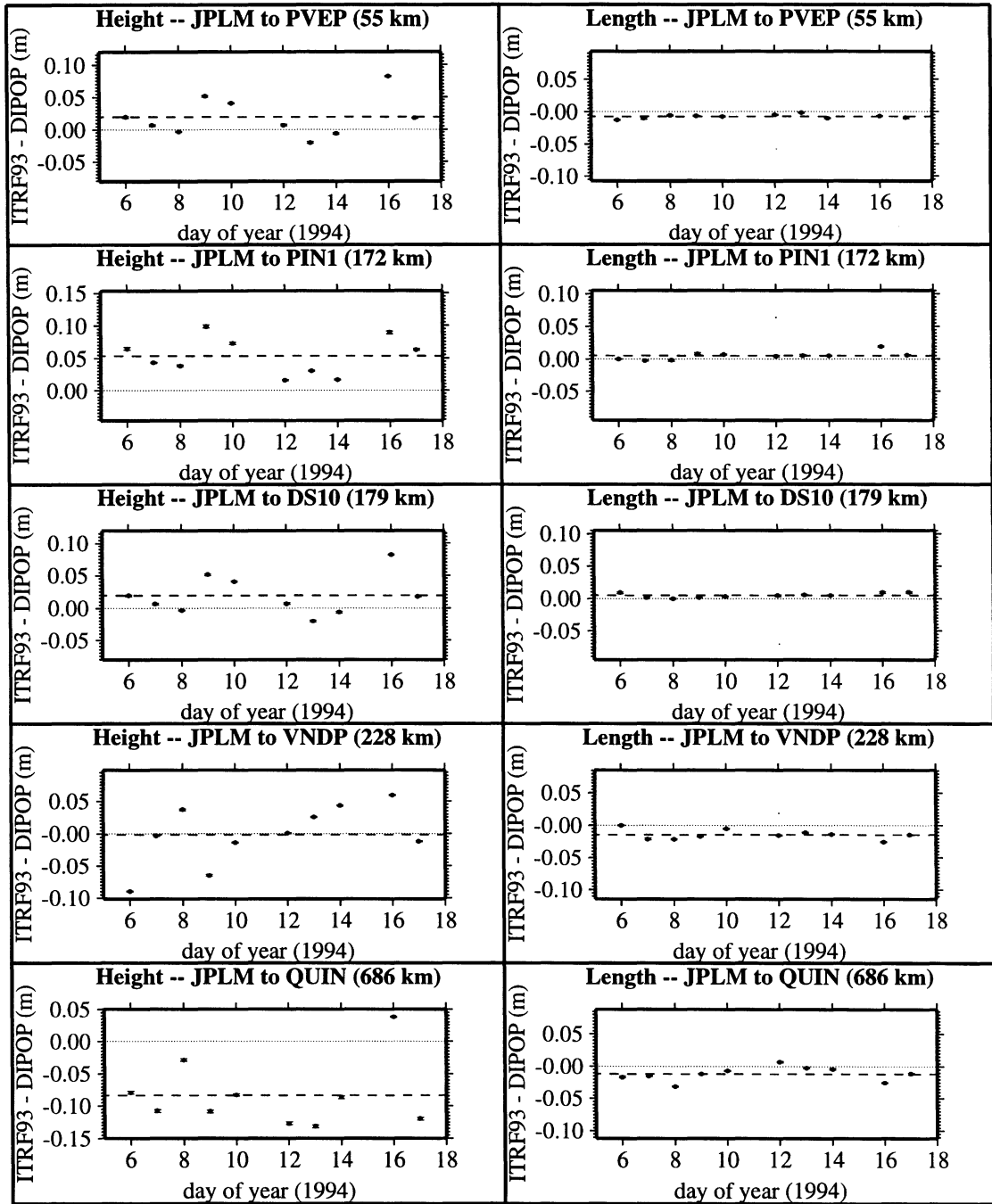**Figure 4.6** -- Conventional weighted least squares residual neutral-atmosphere delay estimation discrepancy between DIPOP and IGS-ITRF93 estimates of height and length for the five test baselines. The dashed line represents the 10 day DIPOP solution mean value.

4.3.3 Kalman filtering

This section outlines the results from the Kalman filter Gauss-Markov and random walk process investigations.

4.3.3.1 First order Gauss-Markov stochastic process

Figure 4.19 summarises the investigation of the first order Gauss-Markov stochastic process when used to characterise the residual neutral-atmosphere delay in the Kalman filter algorithm. Figure 4.19 shows difference between the IGS-ITRF93 and DIPOP solutions that possess the minimum height component short-term repeatability. The solution chosen is shown in the comparison plots as "ct***ss***", where ct*** is the correlation time in hours of the chosen solution, and ss*** is the a priori steady state standard deviation of the residual delay states in millimetres of the chosen solution. Vertical and horizontal scales are the same. Error bars, showing the estimated formal uncertainty, are represented at the true scale. The vertical scale origins are shifted in each window so that the 10 day average estimate is near centre. Estimated height uncertainties are typically a factor of 2 to 4 larger than the length uncertainties. The DS10 and VNDP height estimates agree at the single centimetre level; however, the other height estimates can differ by up to 8 cm. All length comparisons agree at the sub 2 cm level.
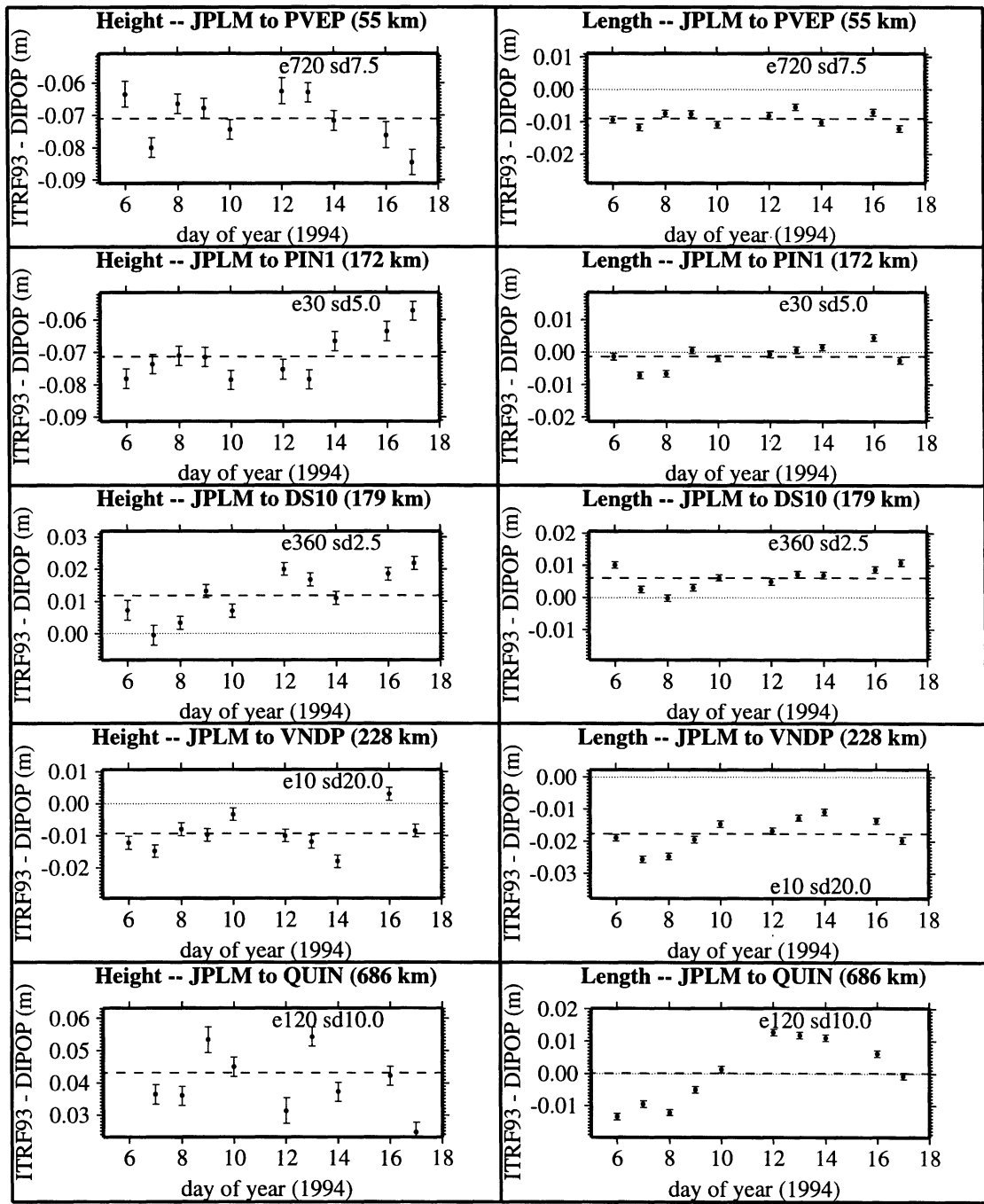
Figure 4.7 -- Kalman filter (Gauss-Markov) residual neutral-atmosphere delay estimation discrepancy between DIPOP and IGS-ITRF93 estimates of height and length for the five test baselines. The dashed line represents the 10 day DIPOP solution mean value.

4.3.3.2 Random walk stochastic process

Figure 4.20 summarises the investigation of the random walk stochastic process when used to characterise the residual neutral-atmosphere delay in the Kalman filter algorithm. Figure 4.20 shows the difference between the IGS-ITRF93 and DIPOP height and length solutions that possess the minimum height and length short-term repeatability respectively. Different height and length solutions for the components of each baseline were chosen for the comparison since there are significant differences in length repeatability for the minimum height repeatability for each baseline (see Figures 4.12 to 4.16) and between baselines. The solution chosen is shown in the comparison plots as "s.d. rate ***", where s.d. rate *** is the a priori standard deviation rate of change of the residual delay state of the chosen solution. The vertical and horizontal scales are the same for all graphs. Error bars, showing the estimated formal uncertainty, are represented at the true scale. The vertical scale origins are shifted in each window so that the 10 day average estimate is near centre. Estimated height uncertainties are typically a factor of 2 to 4 larger than the length uncertainties. The DS10 and VNDP height estimates agree at the single centimetre level; however, the other height estimates can differ by up to 9 cm. All length comparisons agree at the sub 2 cm level.

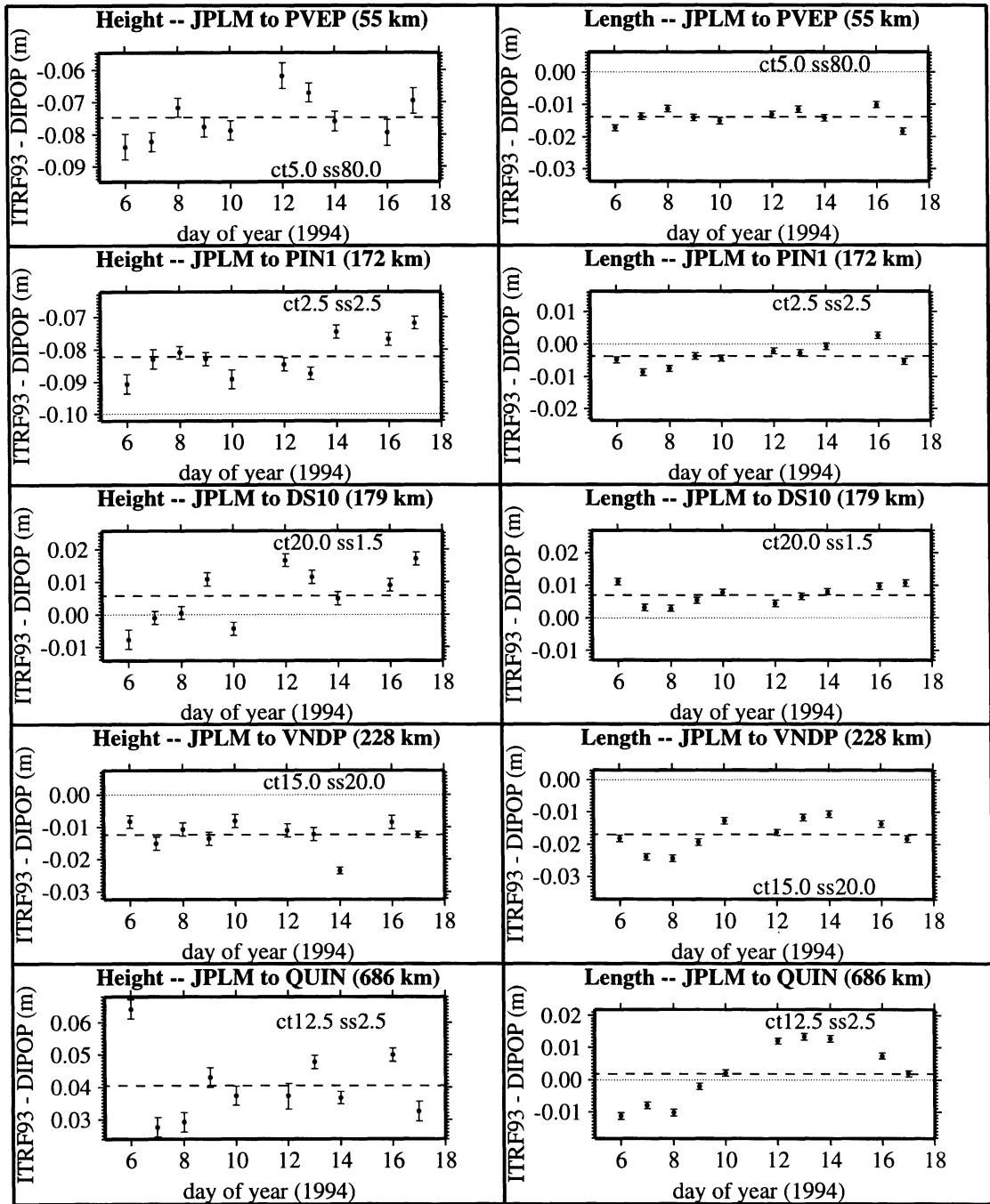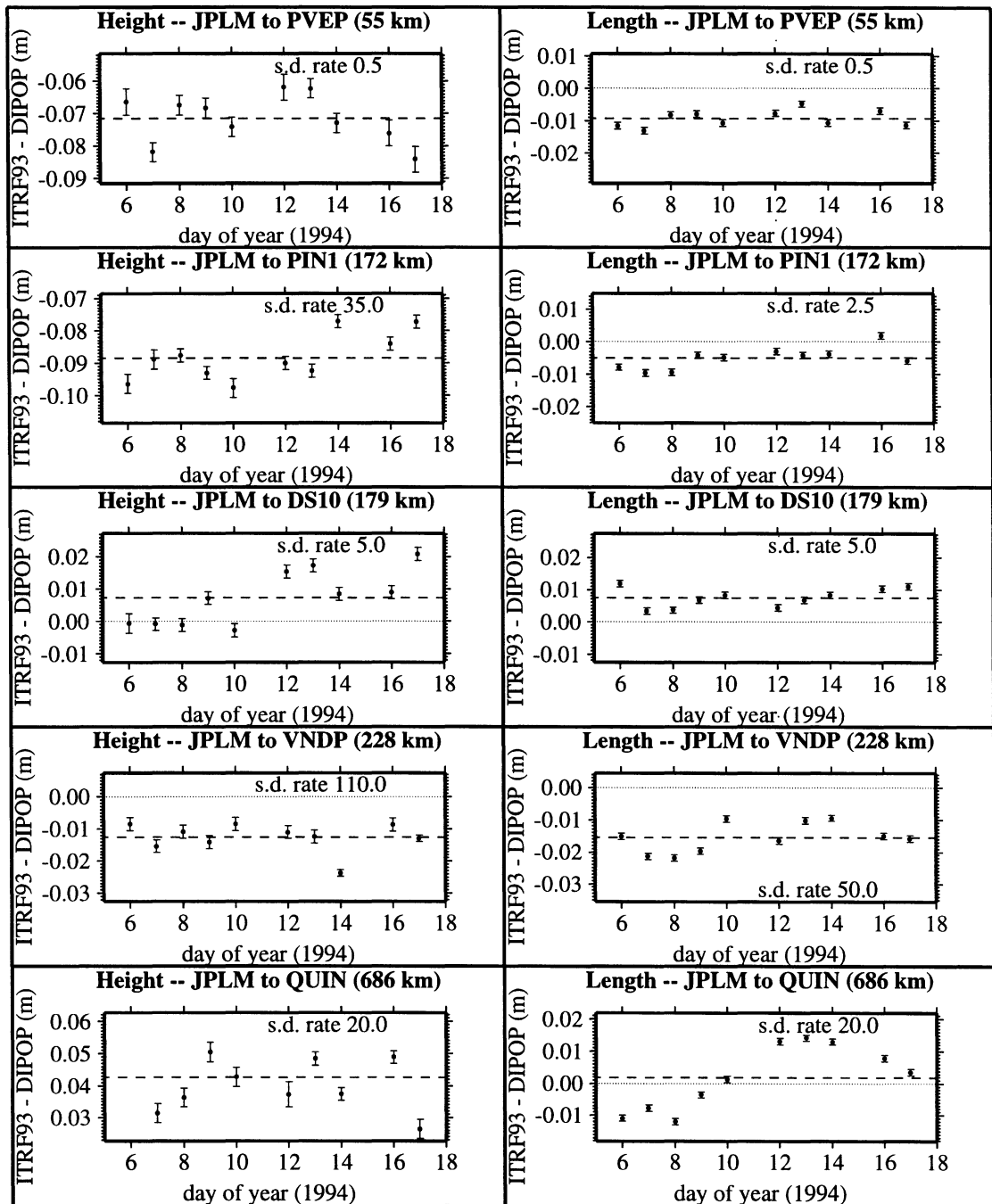**Figure 4.8** -- Kalman filter (random walk) residual neutral-atmosphere delay estimation discrepancy between DIPOP and IGS-ITRF93 estimates of height and length for the five test baselines. The dashed line represents the 10 day DIPOP solution mean value.

4.4 Sequential Weighted Least Squares

The evaluation of the sequential weighted least squares technique as described in section 2.4.3.3 is based on the similarities between it and the Kalman filtering technique. Hence, the conclusions drawn from the Kalman filter investigation are applied to the sequential weighted least squares technique. The sequential weighted least squares algorithm provides the same estimates of states and their covariances as does the Kalman filter for the random walk stochastic process. But, the formal equality breaks down when comparing the two strategies under the assumption that the neutral-atmosphere delay is a first order Gauss-Markov process. However, as will be shown, the differences of the two techniques under the Gauss-Markov process are at an apparently insignificant level for the applications in this analysis.

The inequality for the Gauss-Markov case occurs because the state covariance update, eqn. (2.30), requires information about the stochastic process through the transition matrix. In the random walk case, the transition matrix is an identity matrix; hence, the state covariance update is not affected. For the Kalman filter Gauss-Markov process, the transition matrix contains the exponential correlation (m) components of the Gauss-Markov stochastic process. In the sequential weighted least squares method, where the transition matrix is identity and the design matrix coefficients are multiplied by the exponential correlation, eqn. (2.30) becomes:

$$\underline{C}_k^x(-) = \underline{I}\,\underline{C}_{k-1}^x\,\underline{I}^T + \underline{\sigma}_{rw}^2 \cdot (t_k - t_{k-1}). \qquad (4.1)$$

This form holds true for the random walk case where the transition matrix is the identity matrix. However, in the case of the Gauss-Markov process, the Kalman filter and sequential weighted least squares algorithms differ.

Fortunately, in the residual neutral atmosphere delay application of this study, the correlation times are large in comparison to the update times; hence, the exponential correlation function for the Gauss-Markov process is close to unity. In the range of correlation times assessed in this analysis, the squared

value of m is in the range of 0.920 to 0.996. Such values would increase the estimate of the first part of the right hand side of eqn. (4.1) by 0.4 to 8% as compared to the optimal estimate of state covariance update given in eqn. (2.30). This decrease causes a pessimistic variance of the predicted neutral-atmosphere delay state, which will affect the Kalman gain value, which in turn will place more weight on the observations than would have been applied in the optimal Kalman filter method.

Figure 4.21 displays a test case of the Kalman filter and sequential weighted least squares adjustment where the residual neutral-atmosphere delay is estimated as a first order Gauss-Markov process. The two solutions differ at the sub-millimetre to single millimetre level for the worst case scenario in this study of a 1 hour correlation time. Figure 4.22 shows the same test case for the random walk process. As expected, the two solutions are exactly identical. Figure 4.23 shows the Gauss Markov case estimates of residual neutral-atmosphere delay variance for the Kalman filter and sequential least squares methods. The first order Gauss-Markov variances are larger (up to a factor of 2 times) in the sequential weighted least squares case than the Kalman filtering case.

Figure 4.9 -- Kalman filter (panel A) and sequential weighted least squares (panel B) estimates of residual zenith delay and baseline components for JPL1 to QUIN (686 km). Residual neutral-atmosphere delay estimated as a first order Gauss-Markov stochastic process. The vertical scale represents the difference between the estimates from DIPOP and the a priori values.
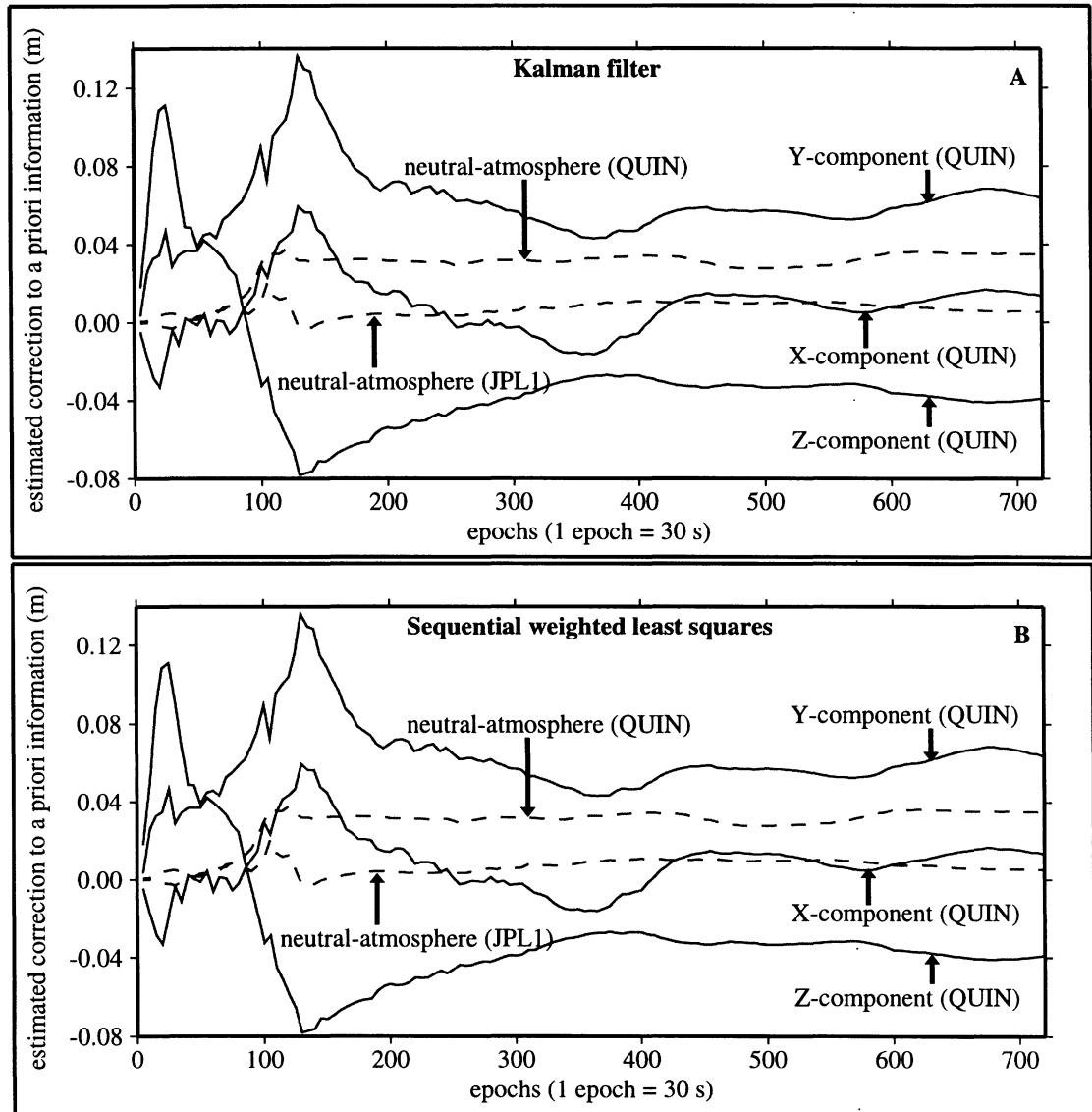
Figure 4.10 -- Kalman filter (panel A) and sequential weighted least squares (panel B) estimates of residual zenith delay and baseline components for JPL1 to QUIN (686 km). Residual neutral-atmosphere delay estimated as a random walk stochastic process. The vertical scale represents the difference between the estimates from DIPOP and the a priori values.
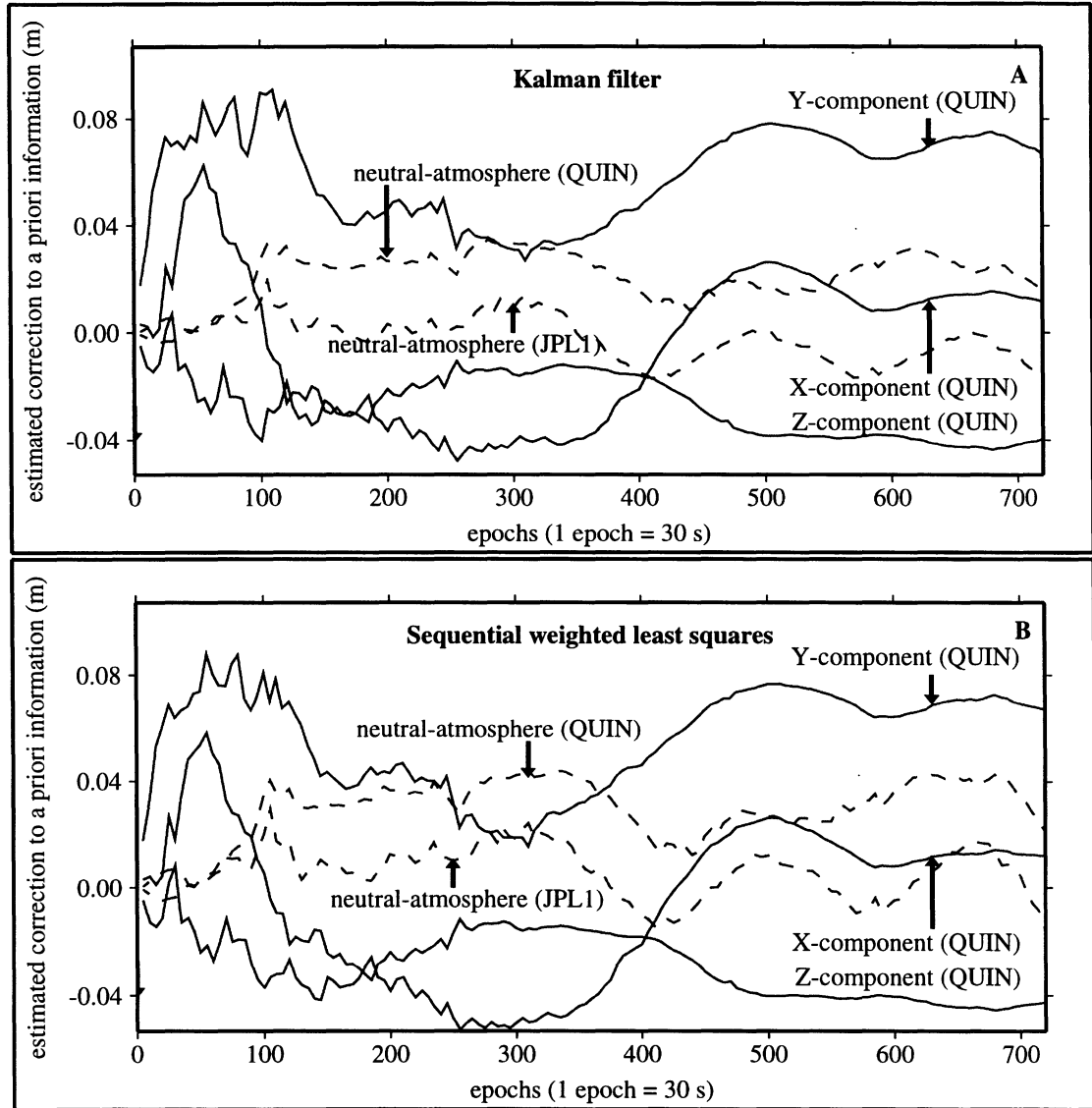
80
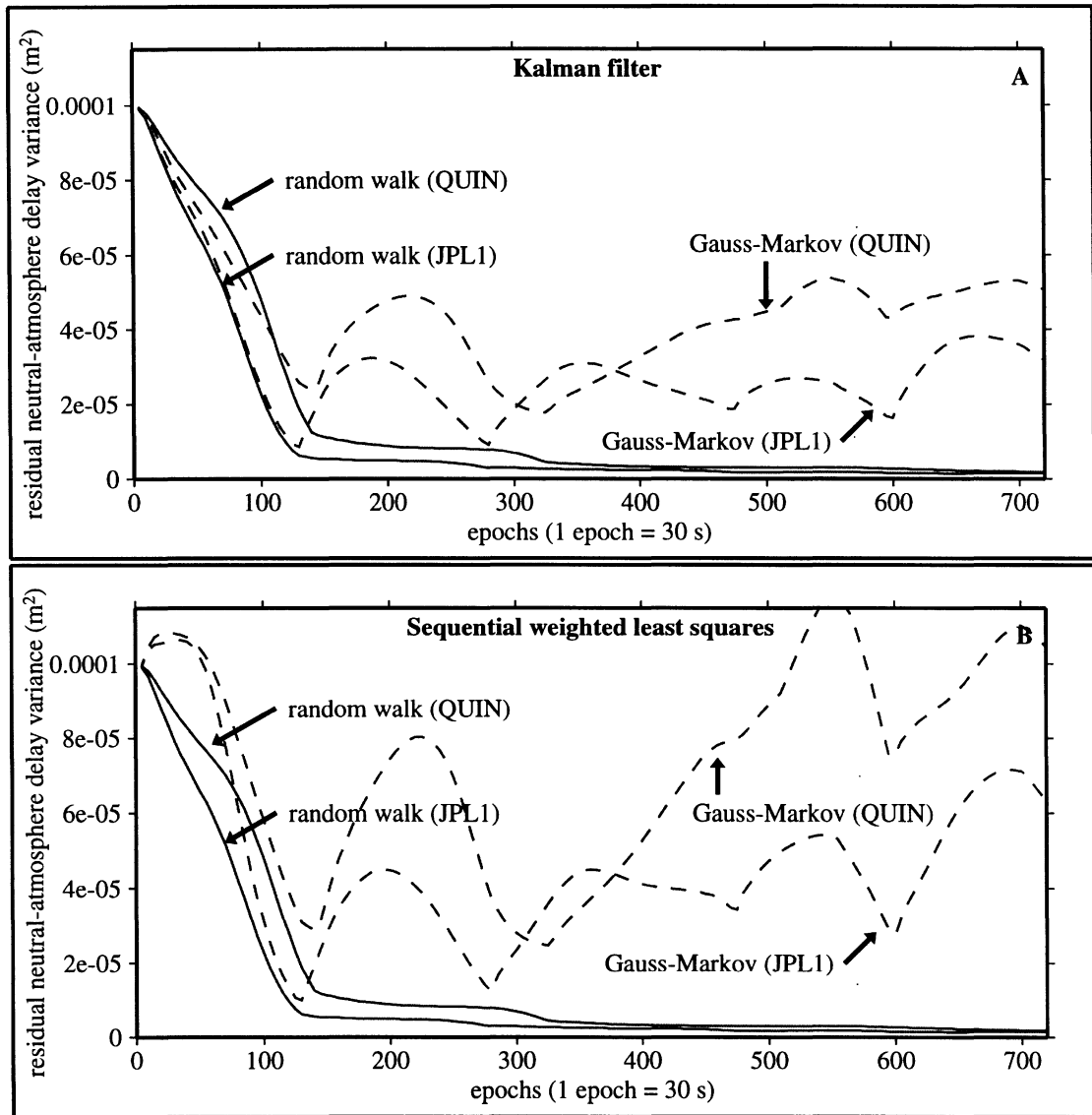
Figure 4.11 -- Kalman filter (panel A) and sequential weighted least squares (panel B) estimates of residual neutral atmosphere delay variance for JPL1 to QUIN (686 km). Residual neutral-atmosphere delay estimated as a first order Gauss-Markov stochastic process.

4.5 Solid Earth Tides

Upon first inspection of the accuracy analysis plots a systematic trend was evident. The approximately 14 day period sinusoid, most noticeable in the length of the longest baseline, pointed towards tidal effects not modelled in DIPOP. Solid earth tide effects are described by Lambeck [1988] and Sovers and Border [1988]. A solid earth tide model was implemented in DIPOP to confirm that the large systematic trends were in fact due to solid earth tides. The results of reprocessing the accuracy analysis data with the solid earth tide model are presented in Figures 4.12 to 4.15. Significant improvements in the length repeatability of the order of a factor of 2 are evident for the longer baselines as compared to the solutions without the tide model. For example, the JPL to QUIN baseline length repeatability improves from 9.6 to 4.5 mm for the random walk case. The height repeatability is virtually unaffected after the inclusion of the earth tide model for all baselines. This would suggest other unmodelled effects are still present in the solutions. The impact of this effect on the final conclusions of this study are hard to assess without further investigation. Reprocessing of the entire data set with the earth tide model, and possibly an ocean loading model, would be required to quantify the impact of this error on the outcome of this study. However, by comparing the results of the accuracy analysis for the cases of including and excluding solid earth tide effects it is apparent that the effect is negligible, i.e. less than a few millimetres, for the three shortest baselines.

82
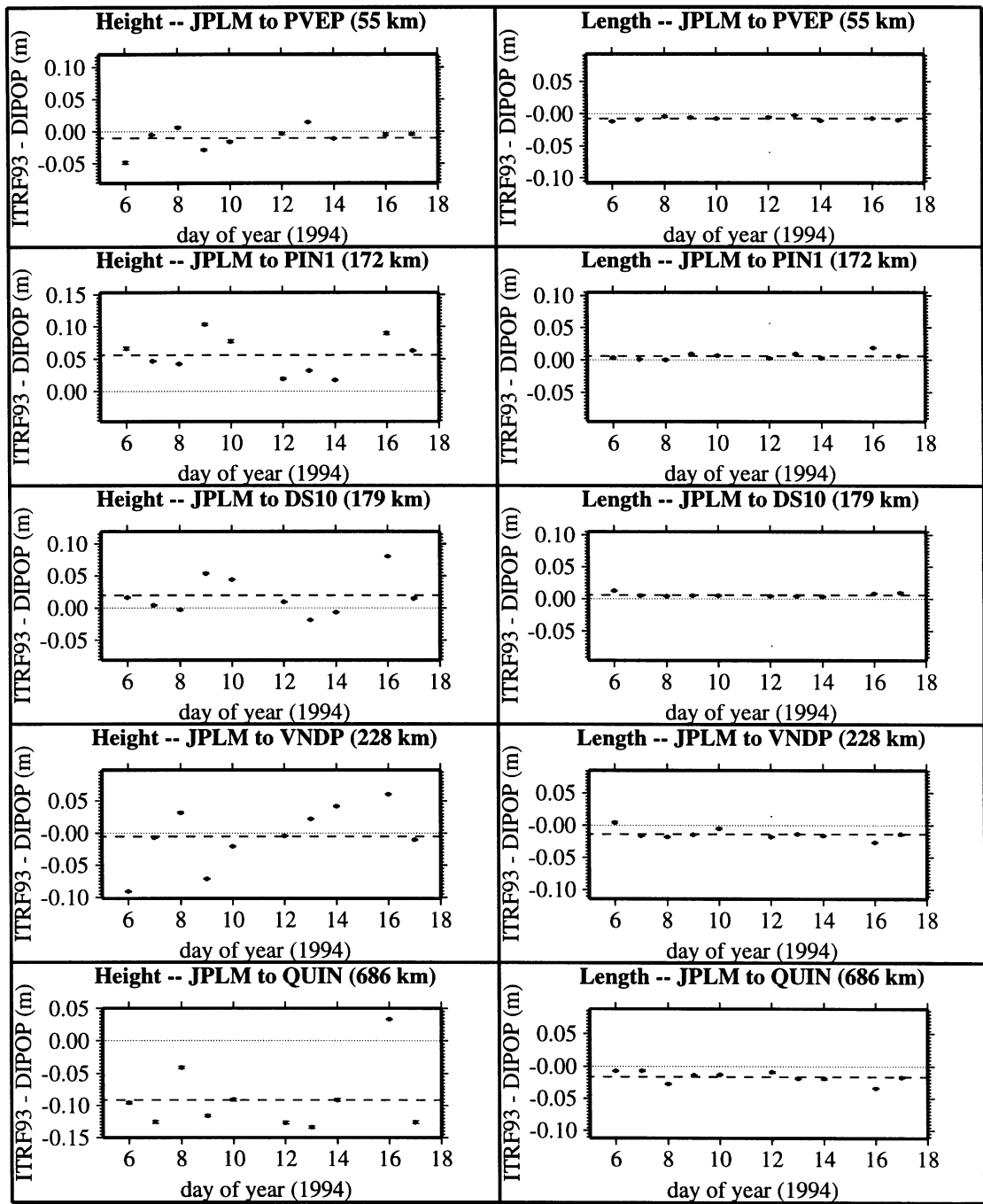
Figure 4.12 -- No residual neutral-atmosphere delay, with solid earth tide model, estimation discrepancy between DIPOP and IGS-ITRF93 estimates of height and length for the five test baselines. The dashed line represents the 10 day DIPOP solution mean value.
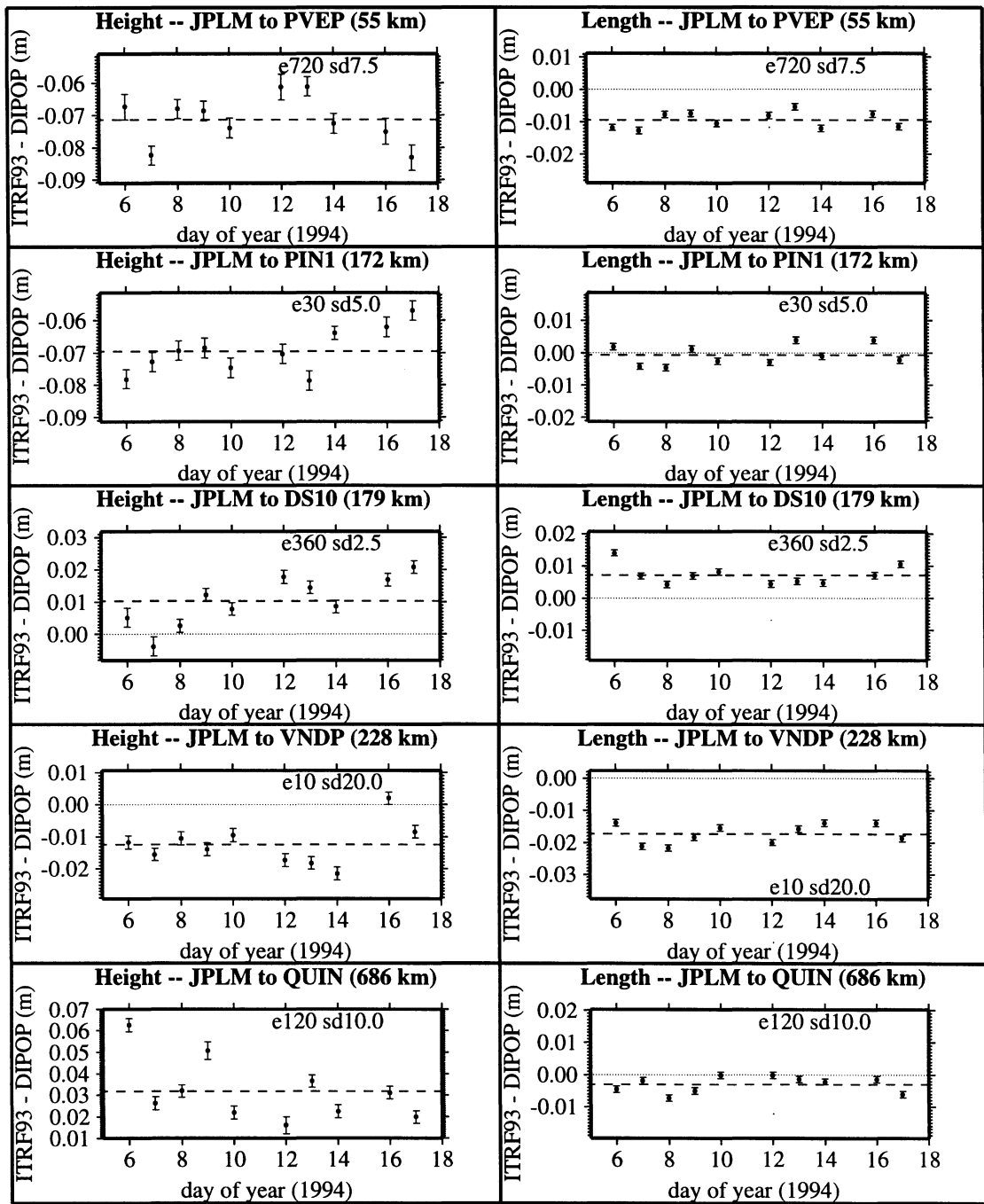
Figure 4.13 -- Conventional weighted least squares, with solid earth tide, model residual neutral-atmosphere delay estimation discrepancy between DIPOP and IGS-ITRF93 estimates of height and length for the five test baselines. The dashed line represents the 10 day DIPOP solution mean value.
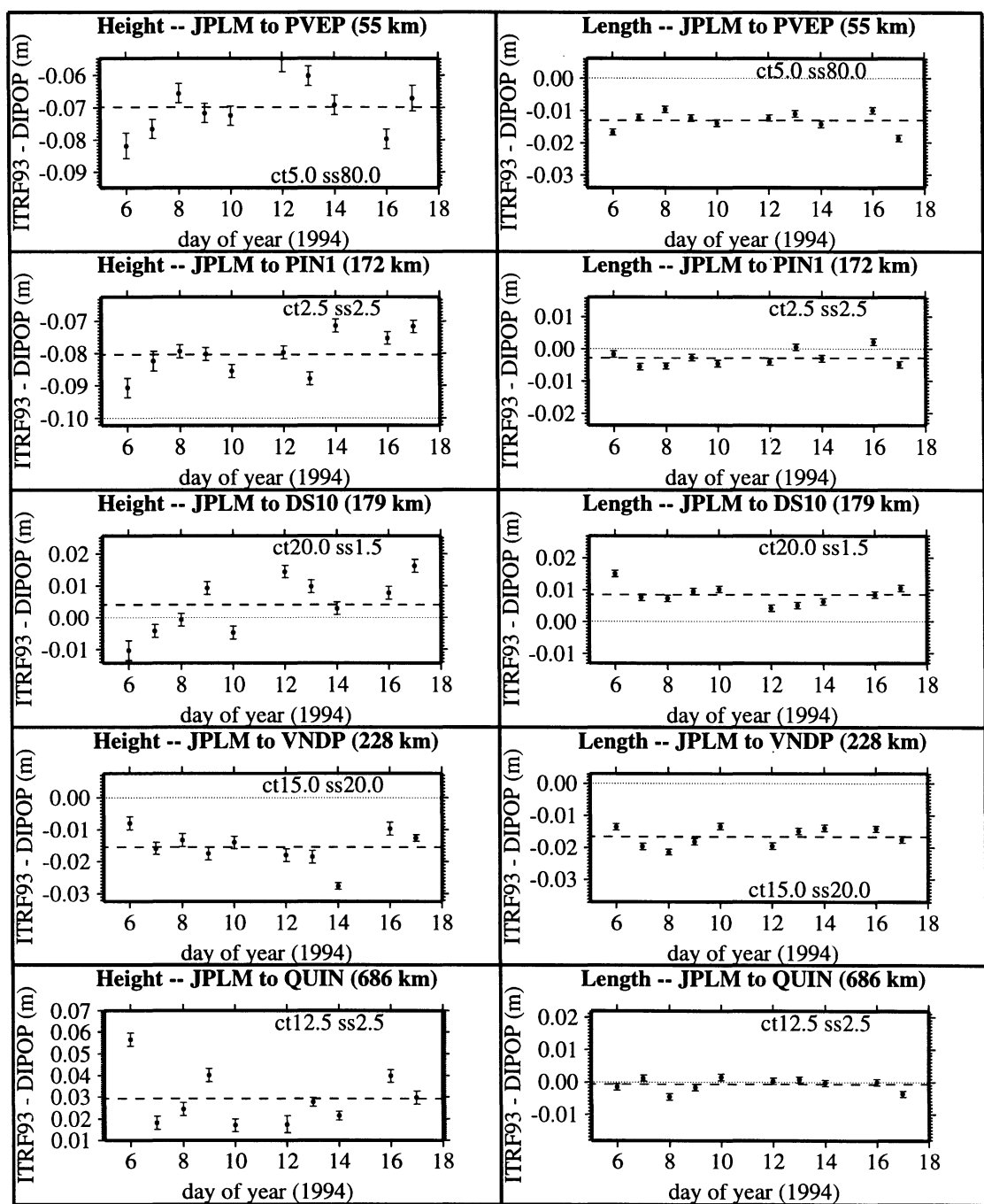
Figure 4.14 -- Kalman filter with solid earth tide model (Gauss-Markov) residual neutral-atmosphere delay estimation discrepancy between DIPOP and IGS-ITRF93 estimates of height and length for the five test baselines. The dashed line represents the 10 day DIPOP solution mean value.
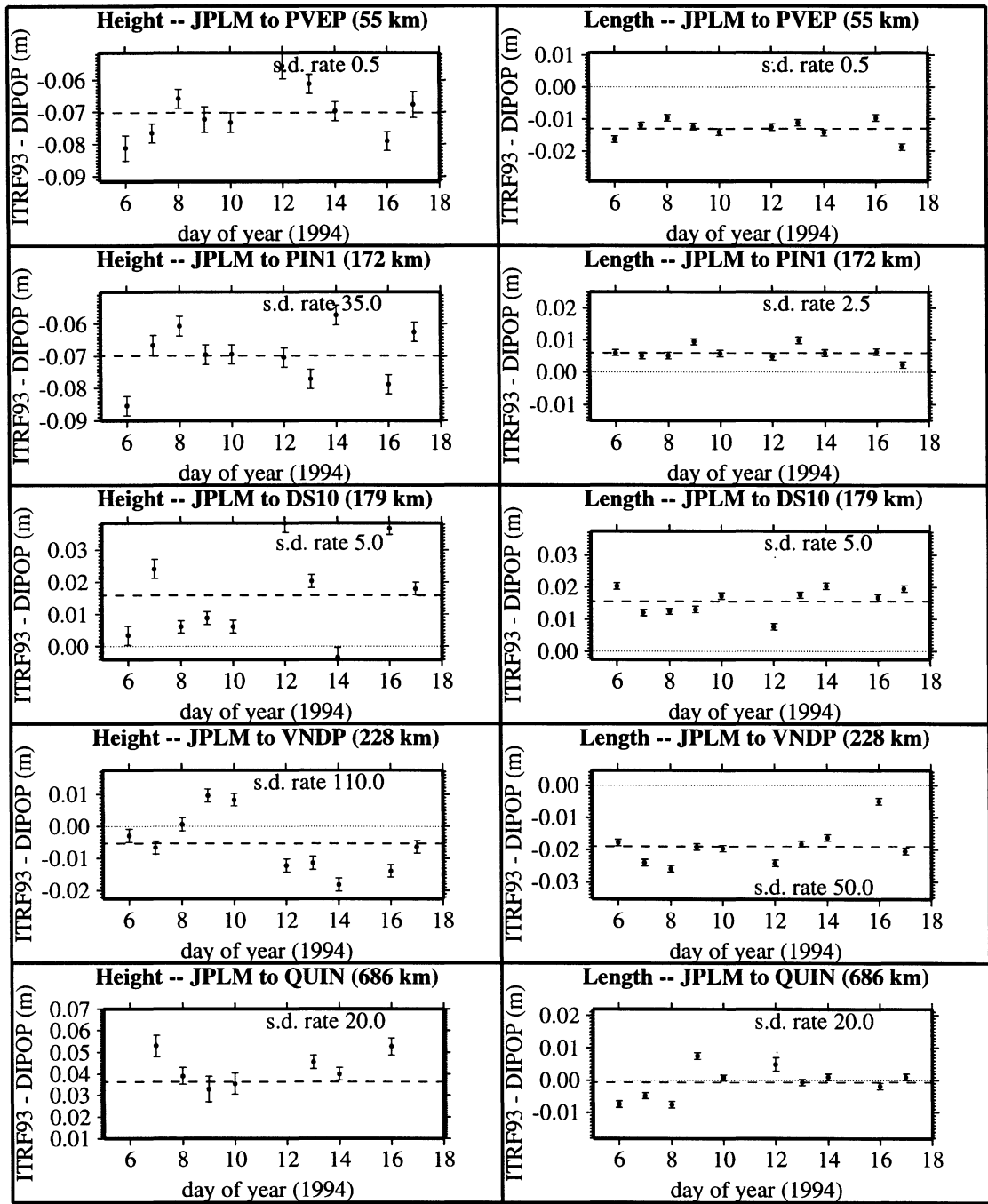
Figure 4.15 -- Kalman filter with solid earth tide model (random walk) residual neutral-atmosphere delay estimation discrepancy between DIPOP and IGS-ITRF93 estimates of height and length for the five test baselines. The dashed line represents the 10 day DIPOP solution mean value.

4.6 Summary and Comparison

In this section, a discussion of the anomalies and expected trends for the conventional weighted least squares, Kalman filter, and sequential weighted least squares strategies is given for the analysis without the solid earth tide effects since not all of the data was reprocessed with the tide model. The results from the individual trials is brought together and compared. Precision has been gauged using the day-to-day scatter (short-term repeatability) of the estimated height and length components of five regional scale baselines in California. Accuracy has been gauged by comparison with IGS-ITRF93 coordinate solution, which is a combined solution of 3 relatively independent techniques.

Overall, height and length precision was of the order of 5 to 15 mm and 2 to 8 mm respectively for the solutions displaying the minimum short-term repeatability. Within the limits of this analysis, the precision can be degraded by a factor of approximately 2 to 3 if depending on the a priori constraints chosen. Table 4.4 summarises the precision for the solutions with the lowest short-term repeatability for the conventional weighted least squares, Kalman filter Gauss-Markov, and Kalman filter random walk strategies. Table 4.4 also shows the relative effect of ignoring the neutral-atmosphere delay.

Table 4.4 -- Precision summary.

| Strategy | Component | Short-term repeatability (mm) | | | | |
		PVEP	PIN1	DS10	VNDP	QUIN
Ignore	height	15.5	25.7	29.2	44.7	72.8
	length	3.1	6.0	3.4	7.2	10.7
Conv. W.L.S.	height	6.8	6.7	6.8	5.6	13.0
	length	2.4	3.3	3.3	4.7	9.5
Kalman (GM)	height	6.2	5.8	7.8	6.0	9.8
	length	2.4	3.1	2.8	4.6	9.0
Kalman (rw)	height	6.9	6.7	8.2	5.9	10.1
	length	2.4	3.2	2.9	4.4	9.6

The results summarised in Table 4.4 are consistent with other studies of this nature, for example those of Tralli and Dixon [1988] and Dixon et al. [1991]. Ignoring the residual neutral-atmosphere delay clearly results in a significant deterioration of the height and length precision. Precision is generally worse for all height components as compared to length components by a factor of 2 to 3. There is no apparent systematic trend as to the choice of a priori coefficients, i.e. there is no apparent height or length dependence on the choice of optimum a priori constraints. Which emphasises the non-deterministic nature of the delay variability.

Height and length accuracy in the range of a few millimetres to nearly ten centimetres were observed for the DIPOP solutions with the lowest short-term repeatability. Table 4.5 summarises the accuracy investigation for height and length.

Table 4.5 -- Accuracy summary.

Strategy	Component	Differences between IGS-ITRF93 and DIPOP estimates (mm)
		PVEP	PIN1	DS10	VNDP	QUIN
Ignore	height	-10.7	53.2	19.1	-1.7	-83.5
	length	-7.7	5.2	5.1	-14.3	-11.5
Conv. W.L.S.	height	-71.6	-71.3	11.9	-9.3	43.2
	length	-9.3	-1.4	7.8	-17.7	0.2
Kalman (GM)	height	-74.8	-82.2	5.7	-12.3	40.5
	length	-13.9	-3.7	7.0	-16.9	1.8
Kalman (rw)	height	-71.5	-88.5	7.3	-12.5	42.7
	length	-9.4	-5.1	7.4	-15.5	1.9

Length accuracy is consistent with previous studies such as those of Tralli and Dixon [1988] and Dixon et al. [1991]. Two of the five adjusted stations displayed a close height agreement with the IGS-ITRF93 values, agreeing at approximately the same level of accuracy as the length components.

However, the accuracy of the remaining three heights does not reflect the level of precision or accuracy attained in this analysis and in some previous studies. The discrepancies are puzzling and hence some hypotheses are proposed for their explanation: (1) the local survey ties between the co-located GPS, VLBI, and SLR antennae could be incorrect; (2) incorrect antenna heights were used in this analysis; (3) incorrect antenna phase centre offset information was used in this analysis; or (4) differences between the physical models used in DIPOP and those used to establish the benchmark reference frame. Larson and Agnew [1991] have reported similar discrepancies for GPS/VLBI comparisons without a significantly plausible explanation.

All three techniques evaluated show similar levels of precision and accuracy. An advantage of the stochastic over the conventional weighted least squares method is that the burden of the extra parameters is not a factor in the computational efficiency of the algorithms. Computer run times are essentially the same for all three techniques. However, when more than approximately 20 residual delay parameters are being estimated in the conventional weighted least squares approach the run times start to differ significantly. For example, the run time for the Kalman filter to process a data set of roughly 6000 observations is approximately 30 to 40 seconds (on a SPARCstation 5) which is the same for the conventional weighted least squares case when estimating one residual delay parameter per site and session; contrast this to a run time of nearly 2 minutes for the conventional least squares when estimating residual delay parameters every 15 minutes for the same data set (24 additional parameters over a 6 hour observation session). The lack of correlation between the a priori constraints of the solution exhibiting the lowest short-term repeatability and the height and/or length of the baseline vectors highlights the essentially non-deterministic nature of the residual neutral-atmosphere delay. Hence, until an efficient (precise, accurate, and economical) method of calibration is available, empirical sensitivity tests of this nature will continue to be performed in the search for the optimum precision and accuracy of baseline component estimates. The results of this analysis are limited by the

89

undefined effects of not accounting for the solid earth tide. This limitation applies mainly to the longer

baselines since the solid earth tide effect is barely distinguishable for the shorter baselines.

CHAPTER 5

CONCLUSIONS AND RECOMMENDATIONS

Three strategies for estimating residual neutral-atmosphere propagation delay in high precision GPS data analysis have been evaluated. The strategies are: (1) conventional weighted least squares, (2) Kalman filtering, and (3) sequential weighted least squares. The evaluation was performed with a modified version of the UNB DIPOP software and ten days of data from a permanent tracking network in California.

The DIPOP software was extensively modified to incorporate a Kalman filter algorithm. The filter algorithm is also used, with minor modifications, as a sequential weighted least squares algorithm. The new DIPOP software (version 3.0) is capable of estimating geodetic GPS baseline components in the above three modes. Residual neutral-atmosphere propagation delay parameters have been incorporated in each of the three methods. Additionally, L1 and L2 phase centre offsets for many models of geodetic GPS antennae are accounted for by the inclusion of the HISUB subroutine. An investigation was conducted into the sensitivity of geodetic parameters to realistic variations in a priori conditions such as: (1) the number of delay parameters estimated, and their a priori standard deviation, for the conventional weighted least squares approach; (2) a priori stochastic process coefficients for the first order Gauss-Markov and random walk processes for the Kalman filtering approach. A comparison in order to determine the level of accuracy of the DIPOP solutions exhibiting the lowest short-term repeatability was made. The comparison was made with the IGS-ITRF93 values of the sites under investigation. In total, the sensitivity analysis required that 10 days of data for 5 baselines be processed with 209 sets of a priori coefficients, i.e. 10,450 baseline vectors were analysed.

The evaluation of the sequential weighted least squares technique is based on the conclusions of the Kalman filtering analysis. The sequential weighted least squares technique was found to be equivalent

to the Kalman filter technique for this application when the random walk model was used. However, the equivalence breaks down when a stochastic process with time correlated states is used in the sequential weighted least squares technique. Fortunately, for this application, typical correlation times are much larger (by more than 2 orders of magnitude) than the update rates used. The differences in the two formulations results in discrepancies of geodetic coordinates at the single millimetre level and pessimistic variance estimates for time correlated processes (e.g. first order Gauss-Markov process).

Investigation into some systematic trends in the accuracy analysis time series revealed that solid earth tide effects were significant in the longer baselines (JPL to VNDP and JPL to QUIN). The effect on the shorter baselines was negligible, and hence limitations on the conclusions drawn from only the longer baselines are necessary. The full impact of the solid earth tide effect can only be realised if the whole data set is reprocessed.

The precision analysis revealed: (1) baseline component estimates are significantly sensitive to the a priori constraints placed on the estimated delay parameters; (2) the three techniques are capable of operating at the same level of precision; (3) empirical determination (sensitivity testing) of a priori coefficients is necessary due to a lack of correlation between coefficients and baseline vector components (height and length); (4) precision for the conventional weighted least squares case ranged in magnitude from 5.6 mm to 13.0 mm in the height component, and 2.4 mm to 9.5 mm in the length component; (5) precision for the Kalman filter Gauss-Markov case ranged in magnitude from 5.8 mm to 9.8 mm in the height component, and 2.4 mm to 9.0 mm in the length component; and (6) precision for the Kalman filter random walk case ranged in magnitude from 5.9 mm to 10.1 mm in the height component, and 2.4 mm to 9.6 mm in the length component.

The accuracy assessment revealed: (1) all three techniques are capable of estimating baseline components at approximately the same level of accuracy; (2) two of the five estimated baseline vectors

agree well (within a factor of 2 times their short-term repeatability) in terms of height and length with the IGS-ITRF93 coordinates; (3) three of the five baseline vectors showed large (in some cases up to a factor of 8 times their short-term repeatability) height discrepancies; however, they agree well in the length component estimates. The source of the height discrepancy could not be isolated. It is presumed that either incorrect local survey ties between GPS and VLBI antenna, or incorrect antenna height values may have corrupted one or both of the solutions, or that the DIPOP software does not have the appropriate physical models for this application, for example ocean loading and high order ionosphere effects are not accounted for in DIPOP which are potentially centimetre level errors.

The non-deterministic nature of the neutral-atmosphere delay is highlighted by the lack of correlation between the short-term repeatability of a set of a priori constraints and the height and/or length of the baseline vectors. Hence, until an efficient (precise, accurate, and economic) method of calibration is available, empirical sensitivity tests will continue to be needed in the search for the optimum precision and accuracy of baseline component estimates for regional scale geodetic investigations. One possibility of such an efficient calibration tool may come in the form of more reliable and inexpensive WVRs. If the technology of water vapour radiometry follows a similar path to that of the geodetic precision GPS receiver, then it can be expected that the cost of WVRs will decrease by an order of magnitude over the next decade and greatly improve in precision and reliability.

Considering that all procedures perform at roughly the same level of accuracy and precision, the choice of which technique to employ in practice will be governed mainly by practical issues, such as simplicity and computational efficiency. This would point towards the Kalman filter with a random walk stochastic process defining the residual delay variability. If redundant data in the form of repeated baselines is available the optimisation of the a priori coefficients for the residual delay parameters is performed quickest using the random walk stochastic process since there is only one coefficient to optimise. However, if redundant observations are not available the Kalman filter random walk

procedure should still be used since it is, in the author's opinion, conceptually the easiest method to implement in a GPS observation processing scheme. The process noise variance rate of change should be set to somewhere near 0.2 mm/√s. This value, apart from being the recommended IERS standard value [International Earth Rotation Service, 1992], fits best within the limits of this study, i.e. inspection of Figures 4.4 (a) to (e) would show that a value between 0.2 and 0.4 mm/√s will provide near optimal results for the baselines investigated in this study.

The choice of mapping function for which the residual delay's elevation angle dependence is determined may be a future area for improvements in the estimation of (residual) neutral-atmosphere delay. However, any benefits gained by choosing a "superior" mapping function to use as the elevation angle dependence model would only be significant for very low elevation angle observations, say below 10° where most "ordinary" mapping functions start to deteriorate, and applications where precision is of utmost importance. A quick glance at the order of magnitude differences between using different mapping functions (Hopfield-Moffet, Herrring-MTT, and Ifadis) for the residual delay model show that baseline component estimates vary due to the change in mapping function at the sub to single millimetre level for a 700 km baseline using a 15° elevation angle mask.

Recommendations for future analysis of residual neutral-atmosphere delay estimation procedures to emerge from this study in order of priority are: (1) reprocessing of the complete data set with solid earth tide model incorporated in DIPOP; (2) sensitivity analysis of a priori constraints for various geographic locations; (3) implementation of a carrier phase cycle ambiguity resolution technique for long baselines in DIPOP; (4) investigation of the influence of mapping function errors in residual delay estimation; (5) investigation into the source of the height discrepancies; (6) investigation into the modelling of neutral-atmosphere delays using other than Gauss-Markov or random walk stochastic processes, such as physical modelling using Kolmogorov turbulence; (7) investigation of methods for estimating azimuthally asymmetric neutral-atmosphere delays; (8) an empirical investigation into the effects on

94

baseline component variance estimates of the number of unknown parameters in the estimated a posteriori variance factor for a digital filter; and (9) an empirical study into the definition of "strong" and "weak" constraints between successive process noise states in a digital filter. Some comments on the main items in this list are presented below.

To be able to fully quantify the effect that the solid earth tide has had on the interpretation of the results in this study it would be necessary to reprocess the complete data set (all 10,450 baselines) with the incorporation of the earth tide effect (possibly ocean loading effects too). In particular it is hard to determine what affect the tide has had on the results of the two longest baselines (JPL to VNDP and JPL to QUIN). However, it is evident from the comparison of the figures in sections 4.3 and 4.5 that the conclusions drawn from the results of the three shortest baselines are insignificantly influenced by the earth tide. The fact that the earth tide affects station positions predominantly in the vertical component and that the neutral atmosphere delay is also highly correlated with the vertical component of position makes this a very important issue that needs to be quantified in relation to this analysis.

This type of analysis should be conducted over a broad range of geographic locations covering different climatic regions so that a more general form of conclusion can be drawn with regards to the comparison of different (residual) neutral-atmosphere delay estimation procedures. This type of study will help to determine if the current practice of fixing the a priori constraints of (residual) delay parameters to some "standard" value (such as the IERS value) is an acceptable practice globally, or would the geoscience community benefit from some form of region-dependent "standard". For example, the contrast between desert and tropical regions is considerable in terms of water vapour content, thus, is it wise to use the same constraints for desert and tropical regions where one region would be susceptible to the relatively larger amounts of the highly unpredictable water vapour? Should the same constraints be applied to these two regions? Remembering that all of the estimation techniques

in this study are significantly sensitive, as can be witnessed by the results of Chapter 4, to the constraints placed on the residual delay parameters.

Carrier phase ambiguity resolution should be seriously considered for further analysis of GPS error models such as this. Although it was pointed out that the correlation between the estimated (real-valued) ambiguities and the residual delay estimates was insignificant, i.e. generally below the 10% level, future refinements to the GPS error model may be influenced by such correlations, especially when error model refinements are being made at the single millimetre level, such as high order ionospheric effects, ocean loading effects, and relativistic effects. All of which are not (currently) considered in DIPOP.

The analsysis of mapping function errors in relation to their use in residual neutral-atmosphere delay estimation would be of particular benefit to very high precision applications of GPS surveying. To improve the geometry of the trilateration technique used in GPS positioning it is important to have observations at low elevation angles. Unfortunately, this is where mapping functions start to lose accuracy. Hence, a study to determine if there is a significant effect on GPS baseline component estimates when using different mapping functions for the elevation dependence of the residual delay would be beneficial to users of high precision GPS techniques.

REFERENCES

Agrotis, L.G. (1988). "Near-earth satellite orbit determination and its applications." *ESA Journal*, Vol. 12, pp. 441-453.

Allnutt, J.E. (1989). *Satellite-to-Ground Radiowave Propagation: Theory, Practice and System Impact at Frequencies Above 1 GHz*. P. Peregrinus on behalf of the Institution of Electrical Engineers, London.

Argus, D.F. and R.G. Gordon (1991). "No-net-rotation model of current plate velocities incorporating plate motion model NUVEL-1." *Geophysical Research Letters*, Vol. 18, No. 11, pp. 2039-2042.

Ashjaee, J. and R. Lorenz (1992). "Precision GPS surveying after Y-code." *ION GPS-92, Proceedings of Fifth International Technical Meeting of the Satellite Division of The Institute of Navigation*, The Institute of Navigation, Albuquerque, N. Mex., 16-18 September, The Institute of Navigation, Alexandria, Va., pp. 657-659.

Bagley, L.C. and J.W. Lamons (1992). "NAVSTAR Joint Program Office and a status report on the GPS program." *Proceedings of Sixth International Geodetic Symposium on Satellite Positioning*, IAG, AGU, ACSM, NOAA, USGS, Columbus, Ohio, 17-20 March, Columbus, Ohio, Volume I, pp. 21-30.

Barry, R.G. and R.J. Chorley (1987). *Atmosphere, Weather and Climate*. 5th ed., Methuen, New York.

Bean, B.R. and E.J. Dutton (1966). "Radio meteorology." Central Radio Propagation Laboratory, National Bureau of Standards, Monograph No. 92, U.S. Government Printing Office, Washington, D.C.

Beutler, G., A. Davidson, R.B. Langley, R. Santerre, P. Vanicek, and D.E. Wells (1984). "Some theoretical and practical aspects of geodetic positioning using carrier phase difference observations of GPS satellites." Department of Surveying Engineering Technical Report No. 109, University of New Brunswick, Fredericton, N.B., Canada.

Bierman, G.J. (1977). *Factorization Methods for Discrete Sequential Estimation*. Academic Press, Orlando, Florida.

Bilham, R. (1991). "Earthquakes and sea level: space and terrestrial metrology on a changing planet." *Reviews of Geophysics*, Vol. 29, No. 1, pp. 1-29.

Black, H.D. (1978). "An easily implemented algorithm for tropospheric range correction." *Journal of Geophysical Research*, Vol. 38, No. B4, pp. 1825-1828.

Black, H.D. and A. Eisner (1984). "Correcting satellite Doppler data for tropospheric effects." *Journal of Geophysical Research*, Vol. 89, No. D2, pp. 2616-2626.

Blewitt, G. (1989). "Carrier phase ambiguity resolution for the Global Positioning System applied to geodetic baselines up to 2000 km." *Journal of Geophysical Research*, Vol. 94, No. B8, pp. 10187-10203.

Blewitt, G. (1993). "Advances in Global Positioning System technology for geodynamics investigations: 1978-1992." *Contributions of Space Geodesy to Geodynamics: Technology,* D.E. Smith and D.L. Turcotte (Eds.), American Geophysical Union, Washington, D.C., Geodynamics Series, Vol. 25, pp. 195-213.

Bock, Y. (1991). "Continuous monitoring of crustal deformation." *GPS World,* Vol. 2, No. 6, June, 7 pp. 40-47.

Bock, Y. and M.H. Murray (1988). "Assessing the long-term repeatability and accuracy of GPS: Analysis of three campaigns in California." In *Proceeding of 5th International (FIG) symposium on Deformation Measurement and 5th Canadian Symposium on Mining Surveying and Rock Deformation Measurements,* A. Chrzanowski and W. Wells (Eds.), 6-9 June, UNB, Dept. Surv. Eng., Fredericton, N.B., Canada. pp. 91-102.

Braun, J., C. Rocken, and J. Johnson (1994). "Consistency of high precision GPS antennas." Abstract in: *EOS Transactions of the American Geophysical Union,* Vol. 75, No. 44, Supplement, p. 172.

Brown, R.G. (1994). Personal communication. Navigation Specialist, Clear Lake, Iowa, November.

Brown, R.G. and P.Y. Hwang (1992). *Introduction to Random Signals and Applied Kalman Filtering.* John Wiley and Sons, Toronto, Canada.

Brunner, F.K. (Ed.) (1984). *Geodetic Refraction: Effects of Electromagnetic Wave Propagation Through the Atmosphere.* Springer-Verlag, New York, N.Y.

Brunner, F.K. and P. Tregoning (1994a). "Investigation of height repeatability from GPS measurements." *Australian Journal of Geodesy, Photogrammetry, and Surveying,* June, No. 60, pp. 33-48.

Brunner, F.K. and P. Tregoning (1994b). "Tropospheric propagation effects in GPS height results using meteorological observations." *Australian Journal of Geodesy Photogrammetry and Surveying,* June, No. 60, pp. 49-65.

Brunner, F.K., and W.M. Welsch (1993). "Effect of the troposphere on GPS measurements." *GPS World,* Vol. 4, No. 1, pp. 42-51.

Champion, K.S., A.E. Cole, and A.J. Cantor (1985). "Standard and reference atmospheres." Chapter 14 of the *Handbook of Geophysics and the Space Environment,* A.S. Jursa (Ed.), Air Force Geophysics Laboratory, Air Force Systems Command, United States Air Force, pp. 14-1 to 14-43.

Chen, D.S. (1991). *A long arc approach to GPS satellite orbit improvement.* M.Sc.E. thesis, Department of Surveying Engineering Technical Report No. 154, University of New Brunswick, Fredericton, N.B., Canada.

Chen, D. and R.B. Langley (1990). "A geometrical analysis of the effect of satellite orbit error on GPS relative positioning." In *Proceedings of GPS '90, Second International Symposium on Precise Positioning with the Global Positioning System,* 3-7 September, Ottawa, Canada, pp. 757-771.

Chen, X. (1994). "Analysis of continuous GPS data from the Western Canada Deformation Array." *ION GPS-94, Proceedings of Seventh International Technical Meeting of the Satellite Division of The Institute of Navigation*, The Institute of Navigation, Salt Lake City, Utah, 20-23 September, The Institute of Navigation, Alexandria, Va., pp. 1339-1348.

Coates, R.J., H. Frey, G.D. Mead, and J.M. Bosworth (1985). "Space-age Geodesy : The NASA Crustal Dynamic Project." *IEEE Transactions on Geoscience and Remote Sensing*, Vol. GE-23, No. 4, pp. 360-368.

Coco, D. (1991). "GPS-satellites of opportunity for ionospheric monitoring." *GPS World*, Vol. 2, No. 9, October, pp. 47-50.

Davis, J.L. (1986). "Atmospheric propagation effects on radio interferometry." AFGL Technical Report 86-0243, US Air Force Geophysics Laboratory, Hanscomm AFB, Mass.

Davis, J.L., T.A. Herring, I.I. Shapiro, A.E. Rogers, and G. Elgered (1985). "Geodesy by radio interferometry: effects of atmospheric modeling errors on estimates of baseline lengths." *Radio Science*, Vol. 20, No. 6, pp. 1593-1607.

Davis, J.L., W.H. Prescott, J.L. Svarc, and K.J. Wendt (1989). "Assessment of Global Positioning System measurements for studies of crustal deformation." *Journal of Geophysical Research*, Vol. 94, No. B10, pp. 13635-13650.

de Jong, C.D. (1991). "GPS - satellite orbits and atmospheric effects." Faculty of Geodetic Engineering Report No. 91.1, Delft University of Technology, Delft, The Netherlands.

Delikaraoglou, D. (1989). "On principle methods and recent advances in studies towards a GPS-based control system for geodesy and geodynamics." NASA Technical Memorandum 100716, Goddard Space Flight Center (GSFC), Greenbelt, Md., 105 pp.

Dixon, T.H. (1991). "An introduction to the Global Positioning System and some geological applications." *Reviews of Geophysics*, Vol. 29, No. 2, pp. 249-276.

Dixon, T.H., G. Gonzalez, S.M. Lichten, and E. Katsigris (1991). "First epoch geodetic measurements with the Global Positioning System across the Northern Caribbean Plate boundary zone." *Journal of Geophysical Research*, Vol. 96, No. B2, pp. 2397-2415.

Dixon, T.H. and S. Kornreich Wolf (1990). "Some tests of wet tropospheric calibration for the CASA Uno Global Positioning System experiment." *Geophysical Research Letters*, Vol. 17, No. 3, pp. 203-206.

Dong, D. and Y. Bock (1989). "Global Positioning System network analysis with phase ambiguity resolution applied to crustal deformation studies in California." *Journal of Geophysical Research*, Vol. 94, No. B4, pp. 3949-3966.

Dutton, J.A. (1986). *The Ceaseless Wind: An Introduction to the Theory of Atmospheric Motion.* Dover Publications, New York.

Elgered, G. (1992). "Refraction in the troposphere." *Proceedings of the Symposium on Refraction of Transatmospheric Signals in Geodesy*, J.C. de Munck and T.A. Spoelstra (Eds.), Netherlands Geodetic Commission, Publications in Geodesy, New Series No. 36, The Hague, Netherlands, 19-22 May, pp. 13-19.

Elgered, G., J.L. Davis, T.A. Herring, and I.I. Shapiro (1991). "Geodesy by radio interferometry: Water vapour radiometry for estimation of the wet delay." *Journal of Geophysical Research*, Vol. 96, No. B4, pp. 6541-6555.

Elósegui, P., J.L. Davis, I.I. Shapiro, R.T.K. Jaldehag, J.M. Johansson, and A.E. Niell (1994). "Effects of signal multipath on GPS estimates of the atmospheric propagation delay." Abstract in: *EOS Transactions of the American Geophysical Union*, Vol. 75, No. 44, Supplement, p. 173.

Fliegel, H.F. and T.E. Gallini (1992). "Global Positioning System radiation force model for geodetic applications." *Journal of Geophysical Research*, Vol. 97, No. B1, pp. 559-568.

Gallini, T.E. (1994). "A survey of tropospheric refraction models." Contract report for Space and Missile Systems Center, Air Force Material Command, Los Angeles, Calif., by Satellite Navigation Department, Systems Engineering Division, The Aerospace Corporation, El Segundo, Calif., 20 April, Aerospace Report No. TOR-94(4488)-11, 32 pp.

Gardner, C.S. (1976). "Effects of horizontal refractivity gradients on the accuracy of laser ranging to satellites." *Radio Science*, Vol. 11, No. 12, pp. 1037-1044.

Gelb, A. (1974). *Applied Optimal Estimation*. The MIT Press, Massachusetts Institute of Technology, Cambridge, Mass., 374 pp.

Genrich, J.F. and Y. Bock (1992). "Rapid resolution of crustal motion at short ranges with the Global Positioning System." *Journal of Geophysical Research*, Vol. 97, No. B3, pp. 3261-3269.

Goad, C.C. and L. Goodman (1974). "A modified Hopfield tropospheric refraction correction model." Paper presented at the American Geophysical Union Fall Annual Meeting, 12-17 December, San Francisco, Ca., 28 pp.

Gourevitch, S.A., R.G. Lorenz, and J.M. Nolan (1993). "Z-tracking™ results: implications to precision civilian applications." Presented at *ION GPS-93*, Ashtech Inc., 14 pp.

Gurtner, W., G. Beutler, and R. Weber (1994). "The use of meteorological data in large scale GPS networks." Presented at American Geophysical Union Spring Meeting, Baltimore, Md., 24 May, 18 pp. (overheads).

Halliday, D. and R. Resnick (1981). *Fundamentals of Physics*. 2nd ed., John Wiley and Sons, New York, N.Y.

Hall, M.P. and L.W. Barclay (Eds.) (1989). *Radiowave Propagation*. P. Peregrinus on behalf of the Institution of Electrical Engineers, London.

Herring, T.A. (1992). "Modeling atmospheric delays in the analysis of space geodetic data." *Proceedings of the Symposium on Refraction of Transatmospheric Signals in Geodesy*, J.C. de Munck and T.A. Spoelstra (Eds.), Netherlands Geodetic Commission, Publications in Geodesy, New Series No. 36, The Hague, Netherlands, 19-22 May, pp. 157-164.

Herring, T.A. (1994). Personal communication. Massachusetts Institute of Technology, Cambridge, Mass., November

Herring, T.A., J.L. Davis, and I.I. Shapiro (1990). "Geodesy by radio interferometry: the application of Kalman filtering to the analysis of very long baseline interferometry data." *Journal of Geophysical Research*, Vol. 95, No. B8, pp. 12561-12581.

Hofmann-Wellenhof, B., H. Lichtenegger, and J. Collins (1993). *GPS Theory and Practice*. 2nd ed., Springer-Verlag, Wien, Austria.

Hopfield, H.S. (1969). "Two-quartic tropospheric refractivity profile for correcting satellite data." *Journal of Geophysical Research*, Vol. 74, No. 18, pp. 4487-4499.

Hopfield, H.S. (1971). "Tropospheric effect on electromagnetically measured range: Prediction from surface weather data." *Radio Science*, Vol. 6, No. 3, pp. 357-367.

Ifadis, I.I. (1986). "The atmospheric delay of radio waves: modeling the elevation angle dependence on a global scale." Technical Report 38L, Chalmers University of Technology, Göteborg, Sweden.

International Association of Geodesy (1963). "Resolutions." *Bulletin Geodesique*, Vol. 70, pp. 389-415.

International Earth Rotation Service (1992). *IERS Standards*, International Earth Rotation Service (IERS) Technical Note 13, D.D. McCarthy (Ed.), Central Bureau of IERS, Paris, France.

Janes, H.W., R.B. Langley, and S.P. Newby (1991). "Analysis of tropospheric delay prediction models: comparisons with ray tracing and implications for GPS relative positioning." *Bulletin Geodesique*, Vol. 65, No. 3, pp. 151-161.

Janssen, M.A. (1985). "A new instrument for the determination of radio path delay due to atmospheric water vapor." *IEEE Transactions on Geosciences and Remote Sensing*, Vol. GE-23, No. 4, pp. 485-490.

King, R.W. and G. Blewitt (1990). "Present capabilities of GPS for high-precision regional surveys." In *Proceedings of the International Association of Geodesy Symposia 102*, Y. Bock and N. Leppard (Eds.). Edinburgh, Scotland, 7-8 August, 1989. Springer-Verlag, New York, N.Y., pp. 24-39.

Kleusberg, A. (1986). "Ionospheric propagation effects in geodetic relative GPS positioning." *Manuscripta Geodaetica*, Vol. 11, No. 4, pp. 256-261.

Kleusberg, A., Y. Georgiadou, F. van den Heuvel, and P. Heroux (1989). "Single and dual frequency GPS data preprocessing with DIPOP 2.1." Department of Surveying Engineering Technical Memorandum TM-21, University of New Brunswick, Fredericton, N.B., Canada.

Klobuchar, J.A. (1991). "Ionospheric effects on GPS." *GPS World*, Vol. 2, No. 4, April, pp. 48-51.

Kouba, J. (1979). "Improvements in Canadian geodetic Doppler programs." *Proceedings of the Second International Geodetic Symposium on Satellite Doppler Positioning*. Applied Research Laboratories, University of Texas at Austin, Austin, Texas, January, pp. 63-82.

Krakiwsky, E.J. and P. Gagnon (1987). "Least squares adjustment." *Papers for the CISM Adjustment and Analysis Seminars*, 2nd ed., The Canadian Institute of Surveying and Mapping, Ottawa, Ontario, Canada, pp. 108-149.

Kroger, P.M., J.M. Davidson, and E.C. Gardner (1986). "Mobile very long baseline interferometry and Global Positioning System measurement of vertical crustal motion." *Journal of Geophysical Research*, Vol. 91, No. B9, pp. 9169-9176.

Lambeck, K. (1988). *Geophysical Geodesy - the Slow Deformations of the Earth.* Oxford University Press, Oxford.

Langley, R.B. (1992). "The effect of the ionosphere and troposphere on satellite positioning systems." *Proceedings of the Symposium on Refraction of Transatmospheric Signals in Geodesy,* J.C. de Munck and T.A. Spoelstra (Eds.), Netherlands Geodetic Commission, Publications in Geodesy, New Series No. 36, The Hague, The Netherlands, 19-22 May, p. 97 (abstract only). Paper available on the University of New Brunswick's gopher server, gopher://unbmvs1.csd.unb.ca:1570/1EXEC%3aCANSPACE/UNB.DENHAAG.ATMOS.PAPER.PS.Z.

Langley, R.B. (1993). "The GPS observables." *GPS World,* Vol. 4, No. 4, April, pp. 52-59.

Langley, R.B., G. Beutler, D. Delikaraoglou, B. Nickerson, R. Santerre, P.Vanicek, and D.E. Wells (1984). "Studies in the application of the Global Positioning System to differential positioning." Department of Surveying Engineering Technical Report No. 108, University of New Brunswick, Fredericton, N.B., Canada.

Lanyi, G. (1984). "Tropospheric delay effects in radio interferometry." *Telecommunications and Data Acquisition Progress,* JPL Technical Report 42-78, Jet Propulsion Laboratory, Pasadena, California, pp. 152-159.

Larson, K.M. and D.C. Agnew (1991). "Application of the Global Positioning System to crustal deformation measurement 1. Precision and accuracy." *Journal of Geophysical Research,* Vol. 96, No. B10, pp. 16547-16565.

Larson, K.M., F.H. Webb, and D.C. Agnew (1991). "Application of the Global Positioning System to crustal deformation measurement 2. The influence of errors in orbit determination networks." *Journal of Geophysical Research,* Vol. 96, No. B10, pp. 16567-16584.

Li, P. (1994). *Determination of earth rotation parameters and adjustment of a global geodetic network using the Global Positioning System.* M.Sc.E. thesis, Department of Surveying Engineering, University of New Brunswick, Fredericton, N.B., Canada.

Lichten, S.M. (1990a). "Estimation and filtering for high-precision GPS positioning applications." *Manuscripta Geodaetica,* Vol. 15, pp. 159-176.

Lichten, S.M. (1990b). "Precise estimation of tropospheric path delays with GPS techniques." Telecommunications and Data Acquisition Progress Report (in press), Jet Propulsion Laboratory, Pasadena, California, U.S.A., 19 pp.

Lichten, S.M. (1994). Personal communication. Jet Propulsion Laboratory, Pasadena, California, November.

Lichten, S.M. and J.S. Border (1987). "Strategies for high-precision Global Positioning System orbit determination." *Journal of Geophysical Research,* Vol. 92, No. B12, pp. 12751-12762.

Lindqwister, U.J., J.F. Zumberge, G. Blewitt, and F. Webb (1990). "Application of stochastic troposphere modeling to the California permanent GPS geodetic array." Presented at the American Geophysical Union Fall Meeting, San Francisco, California, 6 December, 14 pp.

Lutgens, F.K. and E.J. Tarbuck (1986). *The Atmosphere: An Introduction to Meteorology.* 3rd ed., Prentice-Hall, Englewood Cliffs, New Jersey.

Marini, J.W. (1972). "Correction of satellite tracking data for an arbitrary tropospheric profile." *Radio Science*, Vol. 7, No. 2, pp. 223-231.

Meehan, T.K., J.M. Srinivasan, D.J. Spitzmesser, C.E. Dunn, J.Y. Ten, J.B. Thomas, T.N. Munson, C.B. Duncan (1992). "The TurboRogue receiver." *Proceedings of Sixth International Geodetic Symposium on Satellite Positioning*, IAG, AGU, ACSM, NOAA, USGS, Columbus, Ohio, 17-20 March, Columbus, Ohio, Volume I, pp. 209-218.

Mendes, V.B. (1995). Personal communication. Geodetic Research Laboratory, University of New Brunswick, Fredericton, New Brunswick, Canada, September.

Mendes, V.B. and R.B. Langley (1994). "A comprehensive analysis of mapping functions used in modeling tropospheric propagation delay in space geodetic data." In proceedings of KIS94, International Symposium on Kinematic Systems in Geodesy, Geomatics and Navigation, Banff, Canada, 30 August - 2 September, pp. 87-98.

Mendes, V.B., and R.B. Langley (1995). "Zenith wet tropospheric delay determination using prediction models: accuracy analysis." *Cartografia e Cadastro*, No. 2, June, pp. 41-47.

Muellerschoen, R. (1994). Personal communication. Jet Propulsion Laboratory, Pasadena, California, November.

Müller, A., J. Campbell, and F.J. Lohmar (1989). "Analysis of multipath effects in GPS data from European fiducial stations." *Proceedings of the Fifth International Geodetic Symposium on Satellite Positioning*, DMA, NGS, Las Cruces, New Mexico, March 13-17, Physical Science Laboratory, New Mexico State University, Las Cruces, New Mexico, Vol. II, pp. 832-841.

Neill, A.E. (1993a). "A new approach for the hydrostatic mapping function." *Proceedings of the International Workshop for Reference Frame Establishment and Technical Development in Space Geodesy*, Communications Research Laboratory, Koganei, Tokyo, Japan, 18-21 January, pp. 61-68.

Neill, A.E. (1993b). "Improved global atmospheric mapping functions for VLBI and GPS." *URSI/IAU Symposium on VLBI Technology - Progress and Future Observational Possibilities*, Kyoto, Japan, 6-10 September, (abstract).

Niell, A.E., P. Elósegui, J.L. Davis, I.I. Shapiro, R.T.K. Jaldehag, and J.M. Johansson (1994). "Reduction of signal multipath effects on GPS estimates of site position." Abstract in: *EOS Transactions of the American Geophysical Union*, Vol. 75, No. 44, Supplement, p. 171.

Prescott, W.H., J.L. Davis, and. Svarc (1989). "Global Positioning System measurements for crustal deformation: Precision an accuracy." *Science*, Vol. 244, pp. 1337-1340.

Remondi, B.W. (1985). "Global Positioning System carrier phase: description and use." *Bulletin Geodesique*, Vol. 59, No. 4, pp. 361-377.

Robinson, S.E. (1988). "The profile algorithm for microwave delay estimation from water vapor radiometer data." *Radio Science*, Vol. 25, No. 3, pp. 401-408.

Rocken, C., F. Solheim, R.H. Ware, M. Exner, D. Martin, and M. Rothacher (1995). "Application of IGS data to GPS sensing of the atmosphere for weather and climate research." Paper on the UNAVCO World Wide Web site, http://www.unavco.ucar.edu/articles/pots_pap.html, UNAVCO, Boulder Colorado, U.S.A., retrieved: August 1995, 11 pp.

Rothacher, M. (1992). "Orbits of satellite systems in space geodesy." Volume 46, Swiss Geodetic Commision (SGK), Zurich, Switzerland.

Saastamoinen, J. (1973). "Contributions to the theory of atmospheric refraction." In three parts. *Bulletin Geodesique*, No. 105, pp. 279-298; No. 106, pp. 383-397; No. 107, pp. 13-34.

Santerre, R., A. Kleusberg, and G. Beutler (1985). "DIPOP software documentation." Department of Surveying Engineering Technical Memorandum TM-6, University of New Brunswick, Fredericton, N.B., Canada.

Santos, M.C. (1995a). Personal communication. Geodetic Research Laboratory, University of New Brunswick, Fredericton, N.B., Canada, February.

Santos, M.C. (1995b). *On Real-time Orbit Improvement for GPS Satellites*. Ph.D. dissertation, Department of Geodesy and Geomatics Engineering, University of New Brunswick, Fredericton, N.B., Canada, 125 pp.

Schupler, B.R., R.L. Allshouse, and T.A. Clark (1994). "Signal characterisitics of GPS user antennas." *Navigation*, Vol. 41, No. 3, pp. 277-295.

Schwarz, K.P. (1987). "Kalman filtering and optimal smoothing." *Papers for the CISM Adjustment and Analysis Seminars*, 2nd ed., The Canadian Institute of Surveying and Mapping, Ottawa, Ontario, Canada, pp. 230-264.

Seeber, G. (1993). *Satellite Geodesy: Foundations, Methods, and Applications*. Walter de Gruyter, New York, N.Y.

Solheim, F.S. (1993). "Use of pointed water vapor radiometer observations to improve vertical GPS surveying accuracy." Ph.D. dissertation, Department of Physics, University of Colorado, Boulder, Colorado.

Sovers, O.J., and J.S. Border (1988). "Observation model and parameter partials for the JPL geodetic GPS modeling software "GPSOMC"." Jet Propulsion Laboratory, California Institute of Technology, Pasadena, California, JPL Publication 87-21, Rev. 1, 37 pp.

Thayer, G.D. (1974). "An improved equation for the radio refractive index of air." *Radio Science*, Vol. 9, No. 10, pp. 803-807.

Tralli, D.M. and T.H. Dixon (1988). "A few parts in 10^8 geodetic baseline repeatability in the Gulf of California using the Global Positioning System." *Geophysical Research Letters*, Vol. 15, No. 4, pp. 353-356.

Tralli, D.M. and S.M. Lichten (1990). "Stochastic estimation of tropospheric path delays in Global Positioning System geodetic measurements." *Bulletin Geodesique*, Vol. 64, No. 2, pp. 127-159.

Tralli, D.M., T.H. Dixon, and S.A. Stephens (1988). "Effect of wet tropospheric path delays on estimation of geodetic baselines in the Gulf of California using the Global Positioning System." *Journal of Geophysical Research*, Vol. 93, No. B6, pp. 6545-6557.

Tranquilla, J.M. (1986). "Multipath and imaging problems in GPS receiver antennas." *Proceedings of the Fourth International Geodetic Symposium on Satellite Positioning*, Austin, Texas, 28 April-2 May, University of Texas at Austin, Austin, Texas, Vol. I, pp. 557-571.

Trehauft, R.N. (1992). "Tropospheric and charged particle propagation errors in very long baseline interferometry." *Proceedings of the Symposium on Refraction of Transatmospheric Signals in Geodesy*, J.C. de Munck and T.A. Spoelstra (Eds.), Netherlands Geodetic Commission, Publications in Geodesy, New Series No. 36, The Hague, The Netherlands, 19-22 May, pp. 45-53.

Trimble Navigation (1992). "Recent advances in GPS hardware and software." Trimble Navigation, Sunnyvale, Ca., 9 pp.

UNAVCO (1994). "QC v3 users guide." Software documentation, University NAVSTAR Consortium, Boulder, Colorado, document prepared: March 1994, 30 pp.

Vanicek, P., and E. Krakiwsky (1986). *Geodesy: The Concepts*, 2nd Ed., Elsevier, New York, N.Y., 697 pp.

Vanicek, P., G. Beutler, A. Kleusberg, R.B. Langley, R. Santerre, and D.E. Wells (1985). "DIPOP differential positioning program package for the Global Positioning System." Department of Surveying Engineering Technical Report No. 115, University of New Brunswick, Fredericton, N.B., Canada.

Wells, D.E., N. Beck, D. Delikaraoglou, A. Kleusberg, E.J. Krakiwsky, G. Lachapelle, R.B. Langley, M. Nakiboglou, K.P. Schwarz, J. Tranquilla, and P. Vaníček (1986). *Guide to GPS Positioning*. Canadian GPS Associates, Fredericton, N.B., Canada.

Wells, D.E., R.B. Langley, A. Komjathy, and D. Dodd (1995). "Acceptance tests on Ashtech Z-12 receivers." Final report for Public Works and Government Services Canada, February, 149 pp.

Wessel, P. and W.H. Smith (1991). "Free software helps map and display data." *EOS, Transactions of the AGU*, Vol. 72, page 441.

Wu, S.C. (1979). "Optimum frequencies of a passive microwave radiometer for tropospheric path-length correction." *IEEE Transactions on Antennas and Propagation*, Vol. AP-27, No. 2, pp. 233-239.

Yionoulis, S.M. (1970). "Algorithm to compute refraction effects on range measurements." *Journal of Geophysical Research*, Vol. 75, No. 36, pp. 7636-7637.

Yunck, T.P. (1993). "Coping with the atmosphere and ionosphere in precise satellite and ground positioning." Paper in *Environmental Effects on Spacecraft Positioning and Trajectories*, A. Vallance Jones (Ed.), Geophysical Monograph 73, IUGG Volume 13, International Union of Geodesy and Geophysics and the American Geophysical Union, pp. 1-16.

Zumberge, J.F. (1994). "Impact of AS". IGS electronic mail message No. 0511, 25 February, International GPS Service for Geodynamics.

VITA

Candidate's full name: Anthony David van der Wal

Place and date of birth: Perth, Western Australia
18 January 1969

Permanent address: 11 Justin Drive
Sorrento, W.A.
6020
Australia

Schools attended: Sacred Heart College
Sorrento, Western Australia
1982 to 1986

Universities attended: Curtin University of Technology
Perth, Western Australia
1987 to 1990
Degree: Ba.Surv. (Hons)

Publications:
van der Wal, A.D. and R.B. Langley (1995). "Evaluation of residual neutral-atmosphere delay estimation techniques in the analysis of Global Positioning System data." Paper presented at the XXI General Assembly of IUGG, Boulder, Colorado, 2-14 July, American Geophysical Union, Washington, DC.